AFRL-VA-WP-TR-2004-3057

EFFECT OF PREEXISTING CORROSION ON FATIGUE CRACKING OF ALUMINUM ALLOYS 2024-T3 AND 7075-T6

Gerhardus H. Koch and Elise L. Hagerdorn

CC Technologies Laboratories, Inc.
2704 Sawbury Boulevard
Columbus, OH 43235

Alan P. Berens

The University of Dayton Research Institute
300 College Park
Dayton, OH 45469

AUGUST 1995

Final Report for 01 February 1993 – 01 August 1995

STINFO FINAL REPORT

AIR VEHICLES DIRECTORATE
AIR FORCE MATERIEL COMMAND
AIR FORCE RESEARCH LABORATORY
WRIGHT-PATTERSON AIR FORCE BASE, OH 45433-7542

NOTICE

Using government drawings, specifications, or other data included in this document for any purpose other than government procurement does not in any way obligate the U.S. Government. The fact that the government formulated or supplied the drawings, specifications, or other data does not license the holder or any other person or corporation; or convey and rights or permission to manufacture, use, or sell any patented invention that may relate to them.

This report has been reviewed by the Air Force Research Laboratory Wright Site Office of Public Affairs (AFRL/WS/PA) and is releasable to the National Technical Information Service (NTIS). At NTIS, it will be available to the general public, including foreign nationals.

This technical report has been reviewed and is approved for publication.

Copies of this report should not be returned unless return is required by security considerations, contractual obligations, or notice on a specific document.

REPORT DOCUMENTATION PAGE

Form Approved
OMB No. 0704-0188

1. REPORT DATE *(DD-MM-YY)*	2. REPORT TYPE	3. DATES COVERED *(From - To)*
August 1995	Final	02/01/1993 – 08/01/1995

4. TITLE AND SUBTITLE

EFFECT OF PREEXISTING CORROSION ON FATIGUE CRACKING OF ALUMINUM ALLOYS 2024-T3 AND 7075-T6

5a. CONTRACT NUMBER
F33615-93-C-3201

5b. GRANT NUMBER

5c. PROGRAM ELEMENT NUMBER
62201F

6. AUTHOR(S)

Gerhardus H. Koch and Elise L. Hagerdorn (CC Technologies Laboratories, Inc.)
Alan P. Berens (The University of Dayton Research Institute)

5d. PROJECT NUMBER
A04Z

5e. TASK NUMBER

5f. WORK UNIT NUMBER
0V

7. PERFORMING ORGANIZATION NAME(S) AND ADDRESS(ES)

CC Technologies Laboratories, Inc.
2704 Sawbury Boulevard
Columbus, OH 43235

The University of Dayton Research Institute
300 College Park
Dayton, OH 45469

8. PERFORMING ORGANIZATION REPORT NUMBER

R215-04

9. SPONSORING/MONITORING AGENCY NAME(S) AND ADDRESS(ES)

Air Vehicles Directorate
Air Force Research Laboratory
Air Force Materiel Command
Wright-Patterson Air Force Base, OH 45433-7542

10. SPONSORING/MONITORING AGENCY ACRONYM(S)
AFRL/VAO

11. SPONSORING/MONITORING AGENCY REPORT NUMBER(S)
AFRL-VA-WP-TR-2004-3057

12. DISTRIBUTION/AVAILABILITY STATEMENT
Approved for public release; distribution is unlimited.

13. SUPPLEMENTARY NOTES
Report contains color.

14. ABSTRACT

A significant number of commercial and military aircraft have reached or exceeded their original design life, and fleet surveys have shown that the major problem of corrosion is increasing with the fleet's age. Corrosion can affect an airframe's structural integrity in three different ways. First, corrosion has a direct effect on aircraft structures by causing metal loss, which affects the residual strength, and thereby reduces the structural integrity of aircraft components. Secondly, corrosion can act in conjunction with mechanical stresses, resulting in cracking phenomena such as stress-corrosion cracking (SCC) and corrosion-fatigue cracking (CFC). Thirdly, with the aging of the fleet, the interaction between preexisting corrosion and fatigue cracking may affect safety and durability of structural aircraft components.

15. SUBJECT TERMS
aging aircraft, corrosion, corrosion fatigue, environment, cracks

16. SECURITY CLASSIFICATION OF:

a. REPORT	b. ABSTRACT	c. THIS PAGE
Unclassified	Unclassified	Unclassified

17. LIMITATION OF ABSTRACT:
SAR

18. NUMBER OF PAGES
124

19a. NAME OF RESPONSIBLE PERSON (Monitor)
Clare A. Paul
19b. TELEPHONE NUMBER *(Include Area Code)*
(937) 904-8206

Standard Form 298 (Rev. 8-98)
Prescribed by ANSI Std. Z39-18

TABLE OF CONTENTS

LIST OF FIGURES

LIST OF FIGURES (continued)

LIST OF FIGURES (continued)

LIST OF FIGURES (continued)

LIST OF FIGURES (continued)

LIST OF FIGURES (continued)

LIST OF TABLES

ABSTRACT

A significant number of commercial and military aircraft have reached or exceeded their original design life, and fleet surveys have shown that the major problem of corrosion is increasing with the fleet's age. Laboratory tests and modeling studies were undertaken to ascertain the effects of preexisting corrosion on the fatigue cracking behavior of aircraft aluminum alloys 2024-T3 and 7075-T6. It was determined that preexisting corrosion has a detrimental effect on the fatigue life of aluminum alloys 2024-T3 and 7075-T6. The results of the laboratory studies indicated that the effects depend on alloy composition and grain (boundary) orientation. The effect of pitting and intergranular corrosion is most pronounced in the initiation stage of cracking. The results of the probabilistic study indicate that, when inspection intervals are set by damage tolerance analysis of cracks in a pristine structure, the effects of corrosion may be a safety issue, as well as a durability issue.

FOREWORD

This report presents the results of laboratory and modeling studies of the effects of preexisting corrosion on the fatigue cracking behavior of aircraft aluminum alloys 2024-T3 and 7075-T6. The work was performed by CC Technologies Laboratories, Inc. (CC Technologies) and the Structural Integrity Division of the University of Dayton Research Institute for the Flight Dynamics Directorate of the Air Force Wright Laboratory under Contract F33615-93-C-3201. The work was jointly sponsored by WL/FIBEC, ASC/SDCA and the FAA-Technical Center. The period of performance was from February 1, 1993 through August 1, 1995. Mr. Joseph E. Burns, WL/FIBEC, was the Air Force Project Monitor during the first phase of the program, and Mr. Clare A. Paul, WL/FIBEC, was the Project Monitor during the final stage of the program. The authors further would like to acknowledge Dr. T. Flournoy (FAA-Technical Center) and Mr. D. Nieser (ASC/SDCA) for their support of the program.

This report has been edited by Mr. Clare Paul to remove all data, figures and analysis of crack growth rate data associated with the modified CT specimens and the extended compact tension (ECT) specimens. Additionally, the appendix containing the WINPROF user's guide has been removed.

Error! No table of contents entries found.**EXECUTIVE SUMMARY**

In determining the structural integrity of damage-tolerant aircraft structures, environmental effects have generally not been considered, and in fact, structural integrity assessment and life prediction of critical aircraft structures have until recently only been conducted for dominant cracks in uncorroded structures. However, it has been reported that the presence of corrosive operating environments may reduce the life of and compromise the structural integrity of aircraft components significantly. To account for the effects of corrosion on damage-tolerant structures, realistic data for the effects of fatigue crack initiation and growth in complex built-up structures need to be generated.

In general, the effects of environment on the fatigue and fracture behavior of metals and alloys are assessed in the laboratory by applying load and environment simultaneously. The results of these laboratory experiments indicate that specific corrosive environments have a significant effect on the fatigue and fracture behavior of aircraft aluminum alloys. However, in actual aircraft corrosion and fatigue cracking occur at different times. Specifically while fatigue cracking occurs during flight, corrosion occurs primarily when the aircraft is on the ground. This would lead to the recently recognized phenomenon of fatigue cracking in corroded structures. Thus, an effort was started to investigate the effects of preexisting corrosion on fatigue crack initiation and growth in laboratory sized test panels and specimens as a potential means of obtaining fatigue data for the structural integrity evaluation process.

To achieve the objectives of the project, a three-task program was conducted: Task 1 - Effect of Preexisting Corrosion on Fatigue Crack Propagation, Task 2 - Effect of Preexisting Corrosion on Fatigue Crack Initiation, and Task 3 - Modeling.

In the first task, the effects of different modes and degrees of corrosion on fatigue crack propagation were investigated. Different types of specimens of two typical aircraft aluminum alloys, 2024-T3 and 7075-T6, were used in this task. To fully assess the effect of preexisting corrosion on the fatigue crack propagation behavior, increasing ΔK as well as constant ΔK tests were performed.

The purpose of the second task was to investigate the effects of different modes and degrees of corrosion on fatigue crack initiation of aluminum alloys 2024-T3 and 7075-T6. To study specific aspects of the interaction between crack initiation and preexisting corrosion, slow strain rate experiments also were conducted.

Finally, in Task 3, a methodology was developed, implemented and demonstrated, to quantify the effects of corrosion on the fracture risks in an operational aircraft environment. The resulting model will be incorporated into the Probability Of Fracture (PROF) computer code.

The results of the research presented in this report indicate that preexisting corrosion can have a significant detrimental effect on the fatigue cracking behavior of aircraft aluminum alloys,

depending on alloy composition, heat treatment, and grain orientation. To assess the effects of the different types and degrees of preexisting corrosion, and above mentioned material parameters on the corrosion/fatigue interaction process, the three different phases that determine the fatigue life, namely corrosion, fatigue crack initiation, and fatigue crack propagation, were investigated.

Based on the results of this study, the following conclusions were drawn:

1. Preexisting corrosion has a detrimental effect on the fatigue life of aluminum alloys 2024-T3 and 7075-T6. The results of the laboratory studies indicated that the effects depend on alloy composition and grain (boundary) orientation. The effect of pitting and intergranular corrosion is most pronounced in the initiation stage of cracking.

2. The corrosion morphology has a significant effect on the fatigue crack initiation in both alloys. Fatigue crack nucleation sites appear to be associated with constituent particles, which can act as stress concentrations or as trapping sites for hydrogen, generated during the corrosion process.

3. It was proposed that an initial approach needs to be taken to assign equivalent mechanical damage to the corrosion damage resulting from preexposure to corrosive environments. Based on the assumption that corrosion damage can be treated as a combination of thickness reduction and local stress concentration, fracture mechanics principles can be applied.

4. The interaction between thinning effects and pitting and fatigue cracking on the structural integrity of a representative airframe structure was evaluated in terms of single flight probabilities of fracture as a function of flight hours. The results of this preliminary study indicate that, when the inspection intervals are set by damage tolerance analysis of fatigue cracks in a pristine structure, the effects of corrosion may be a safety issue as well as a durability issue.

Based on the conclusions drawn from the results and analyses of the laboratory work, and the probabilistic analyses of the effect of corrosion on a representative airframe structure, the following recommendations are made:

1. As an initial approach, the corrosion damage should be quantified as simple, mechanical equivalent damage. This would be a first meaningful attempt to deal with the detrimental effects of preexisting corrosion on the structural integrity and durability of aircraft components.

2. In addition to the initial step (Item 1 above), more realistic corrosion geometries should be characterized and the effects of these complex geometries should be incorporated into the geometric approach described above.

The possible role of hydrogen generated by the corrosion process, on the fatigue behavior of the aluminum alloys is not well understood, and, at a minimum, the hydrogen factor should be taken into account by applying some safety factor. However, work needs to be conducted to develop a

better understanding of the role of hydrogen, so that the effects of corrosion on structural integrity and durability of airframe components are better understood and a more reliable assessment of the safety and life of corroded structures can be developed.

1. INTRODUCTION

In determining the structural integrity of damage-tolerant aircraft structures, environmental effects have generally not been considered, and in fact, structural integrity assessment and life prediction of critical aircraft structures have until recently only been conducted for dominant cracks in uncorroded structures. However, it has been reported[1] that the presence of corrosive operating environments may reduce the life of and compromise the structural integrity of aircraft components significantly. The schematic diagram in Figure 1 shows a possible way of accounting for the effects of corrosion on fatigue of damage-tolerant structures.
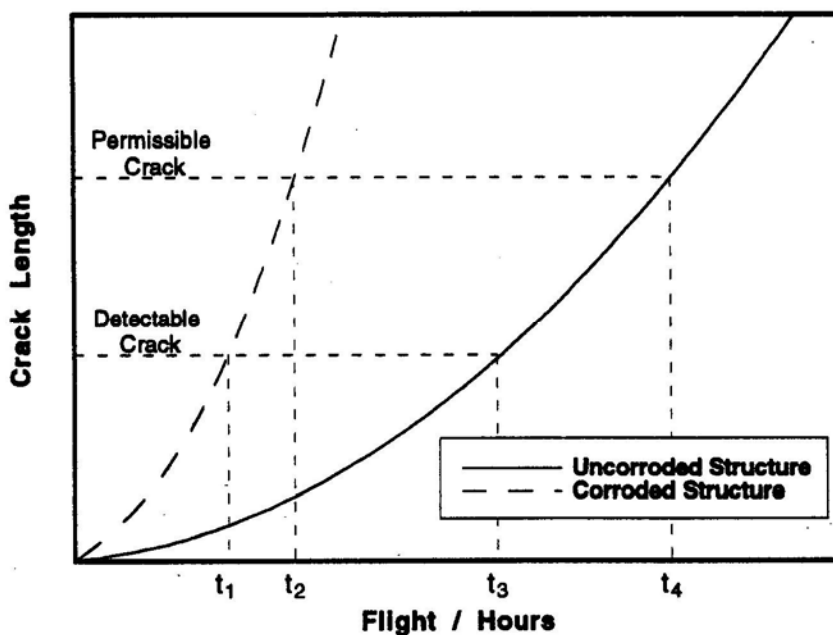
Figure 1. The Effect of Corrosion on Predicted Structural Crack Growth Life Prediction

To account for the effects of corrosion on damage-tolerant structures, realistic data for the effects of fatigue crack initiation and growth in complex built-up structures need to be generated.

In general, the effects of environment on the fatigue and fracture behavior of metals and alloys are assessed in the laboratory by applying load and environment simultaneously. The results of these laboratory experiments indicate that specific corrosive environments have a significant effect on the fatigue and fracture behavior of aircraft aluminum alloys. In service, however, it is most likely that corrosion and fatigue cracking do not occur simultaneously. Thus, an effort was started to investigate the effects of corrosion on fatigue crack initiation and growth in laboratory sized test panels and specimens as a potential means of obtaining material data for the structural integrity evaluation process.

2. OBJECTIVE AND TECHNICAL SCOPE

The objective of this project was to investigate and determine the effects of preexisting corrosion on the fatigue crack initiation and fatigue crack growth behavior of the typical aircraft aluminum alloys 2024-T3 and 7075-T6. To achieve the objectives of the project, a three-task program was conducted: Task 1 - Effect of Preexisting Corrosion on Fatigue Crack Propagation, Task 2 - Effect of Preexisting Corrosion on Fatigue Crack Initiation, and Task 3 - Modeling.

3. BACKGROUND

Most aircraft structures are susceptible to deterioration by corrosion and fatigue. The type of corrosion suffered by these structures depends on the alloy and heat treatment of the material, the structural design, the type of corrosion protection used, and the operating environments. Fatigue damage depends primarily on the structural design details, the design stress levels, the operating cyclic service loads, and the interaction with preexisting corrosion. The presence of corrosive operating environments may reduce the life and significantly compromise the structural integrity of these critical aircraft components. Thus, to more accurately assess the structural integrity and durability of aged aircraft components, the effects of operating environments should be incorporated into the structural integrity and durability assessments.

Corrosion in aircraft aluminum alloys occurs in several different forms.[2-3] Pitting and crevice corrosion are most common in the 2000- and 7000-series aluminum alloys which are the principal materials of construction. Pitting corrosion is a form of localized corrosion that occurs on exposed surfaces of passive metals under relatively stagnant conditions. Pitting may also occur on relatively film free metals at local metallurgical imperfections such as inclusions or constituent particles.[4] Although the mechanism of pit nucleation is not well understood, there is some evidence in aluminum alloys, that constituent particles act as nucleation sites. Wei and coworkers[5] have demonstrated that in 2000-series alloys, pitting nucleates at Al-Cu-Mg- and Al-Cu-Mn-Fe- containing particles, with the former particles acting as anodic sites, and the latter as cathodic sites. Figure 2 shows a typical microstructure of aluminum alloy 2024-T3 showing the elongated grains with a significant number of constituent particles.

Figure 2. Optical Micrograph of Cross Section through Aluminum Alloy 2024-T3 Showing Elongated Grains and Constituent Particles

Particularly, the copper containing particles have a detrimental effect on the pitting behavior of these aluminum alloys. The detrimental effect of copper in aluminum alloys is illustrated in Figure 3 which shows an increase in pitting potential as a function of copper concentration in Al-Cu alloys.[6]
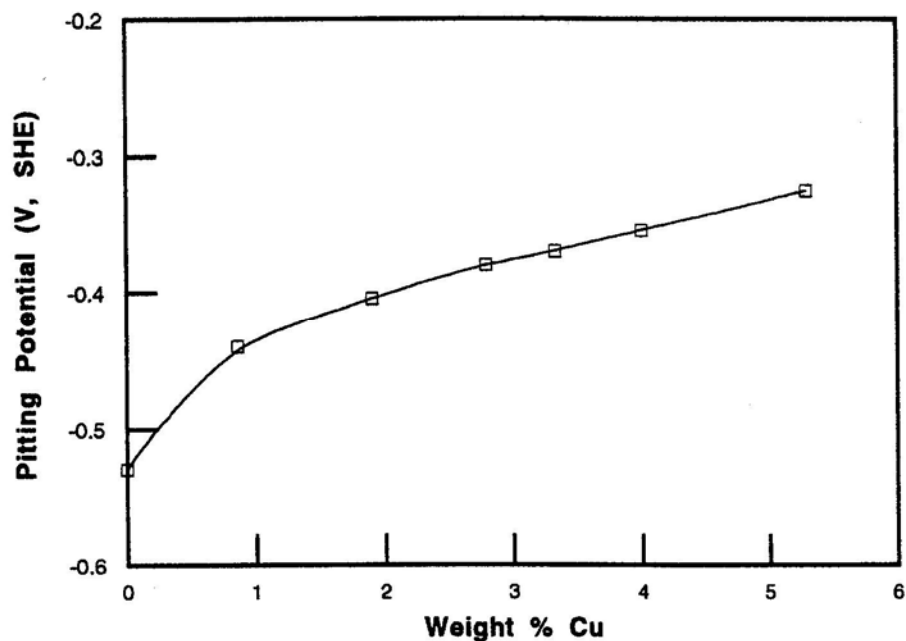
Figure 3. Effect of Cu Content on Pitting Potential of Al-Cu Alloys. Mean Pitting Potentials Measured For Solution Treated Alloys In Deaerated 1M NaCl at 25 °C[6]

The pitting potential shown in Figure 3 is an electrochemical parameter indicating the susceptibility of the alloy to pitting corrosion. The propagation stage of pitting in aluminum alloys consists of metal oxidation within the pit, migration of anions, such as chlorides, into the pit to maintain charge neutrality, acidification in the pit as a result of hydrolysis of the metal ions, and oxygen depletion once an occluded cell has formed.[7] All of these processes tend to further enhance the pitting process, and thus, pitting corrosion is autocatalytic in nature.

Like pitting, crevice corrosion occurs in both passive metals and in relatively film free materials. The presence of a crevice or occluded cell is essential for initiation of crevice corrosion. Alkire[8-9] developed a model for initiation of crevice corrosion of aluminum in dilute chloride solutions, based on the classical mechanism of deaeration within the crevice, followed by a decrease in pH and an increase in chloride concentration, which eventually leads to the complete breakdown of the passive film within the crevice. This model could not, however, be confirmed by experiment, and further work by Alkire[10-12] led to the conclusion that chloride build up does not occur to any great extent in aluminum crevices. Furthermore, the main factor in initiating crevice corrosion is the build up of a critical concentration of Al^{3+} ions in the crevice solution. This mechanism has been confirmed and modeled to the extent that setting a critical Al^{3+} ion concentration of 0.003M brings about agreement between experiment and theory.

Once crevice corrosion has initiated, the complex process of crevice corrosion propagation occurs. Alavi and Cottis[13] discussed some of the complexities of crevice corrosion propagation in aluminum. Micropits form on the crevice walls which can result in hydrogen evolution. This process can cause an increase in pH and affect the various equilibrium reactions. In other parts

5

of the crevice, the pH decreases as a function of hydrolysis of the Al^{3+} ions. Alavi and Cottis observed acidic regions near the mouth of the crevice, while alkaline regions were observed deep inside the crevice. Although crevice corrosion is a common form of corrosion in aircraft structures, for example lap joints, its mechanism is poorly understood. If predictions on the corrosion life of structures subject to crevice corrosion are to be made, a better mechanistic understanding is required.

A third common form of corrosion in susceptible aluminum alloys is exfoliation. Exfoliation corrosion is a particularly severe form of intergranular attack which occurs in wrought high-strength aluminum alloys in the age-hardened condition. Exfoliation corrosion greatly depends on the elongated grain shape and orientation, as well as on the active corrosion paths along the grain boundaries. A considerable amount of research has been conducted on the mechanism of this form of corrosion,[14-16] and there is a consensus that exfoliation corrosion propagates as a result of electrochemical action between age-hardening precipitates and adjacent precipitation free zones. As a result of the corrosion reaction, a corrosion product forms, which is typically $Al_2O_3.nH_2O$ or $Al(OH)_3$. If the volume of the corrosion product exceeds the volume of the alloy, the resulting wedging stresses will lift the grains. Several mechanistic studies have been conducted, which assume that the wedging stresses simply result from the intergranular corrosion process, or in which the wedging stresses are considered essential for the propagation of the intergranular attack by means of stress-corrosion cracking.[17] Although a basic understanding of the mechanism of this severe and common form of corrosion exists, quantitative parameters need to be developed to predict the growth rate of exfoliation corrosion, which then can contribute to durability and integrity considerations.

Corrosion can have a direct detrimental effect on the structural integrity of aircraft components, but the effect of interaction between preexisting corrosion and fatigue cracking may be even worse. Although very little work has been conducted and published on this subject, the available literature[18-22] indicates that corrosion decreases the fatigue life by promoting fatigue crack initiation and propagation. Harmsworth[18] demonstrated that pitting corrosion has a detrimental effect on the fatigue behavior of alloy 2024-T4. The effect of preexisting corrosion on fatigue behavior was largely determined to be that of a stress raiser. In the case of pitting corrosion, calculations were made, based on critical pit measurements, to determine the stress concentration of the corrosion pit.

Work by Person,[19] and by Abramovici and coworkers[20] showed that pitting corrosion in aluminum alloys greatly reduced their fatigue life. This observation was confirmed by Smith and Duquette,[20,22] who found that precorrosion of 7075-T6 test panels greatly reduced their fatigue life. Chubb and coworkers[21] studied the crack propagation behavior of 2000- and 7000-series aluminum alloys through areas with exfoliation corrosion and found that fatigue cracks propagating in the 7000-series alloys accelerated considerably when they reached the exfoliated areas, see Figure 4.

6
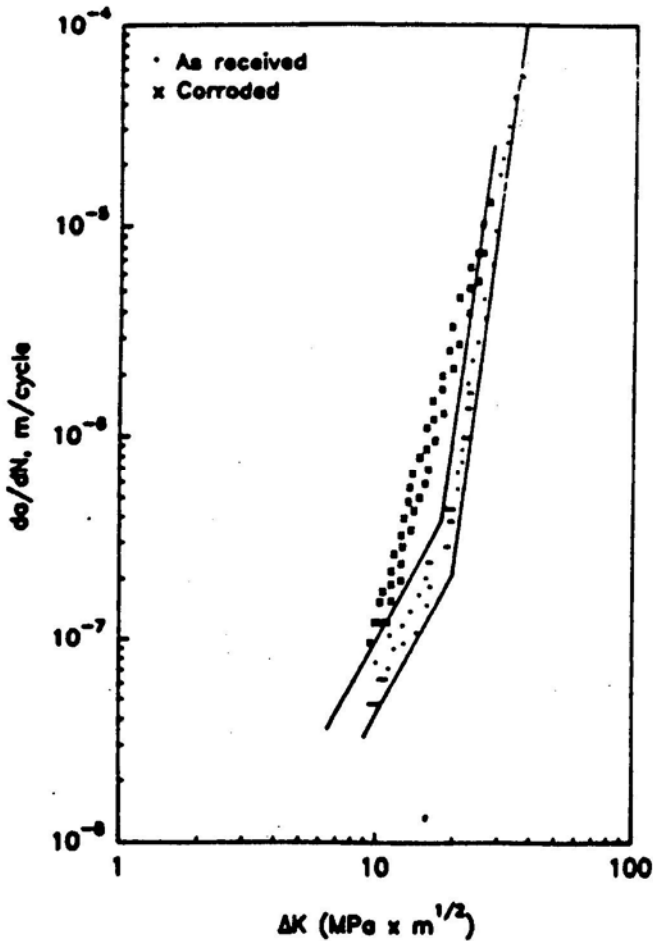
Figure 4. Fatigue Crack Growth Data for Corroded 7178-T6 Compared with As-Received 7178-T6 Tested in Dry Air

However, Figure 5 shows that, in the 2000-series alloys, no noticeable effect of corrosion on fatigue crack propagation was found. It should be noted that the test panels were made from actual aircraft skin corroded in service and that in the calculation of ΔK, no correction was made for the loss in thickness due to corrosion. Smith and coworkers[22] produced multisite fatigue damage initiation and subsequent fatigue cracking in aluminum alloy 2024-T3 and 7075-T6 specimens with a collinear array of open fastener holes. They found that corrosion greatly decreased the fatigue life of the test panels and also observed faster growth rates in the corroded specimens.
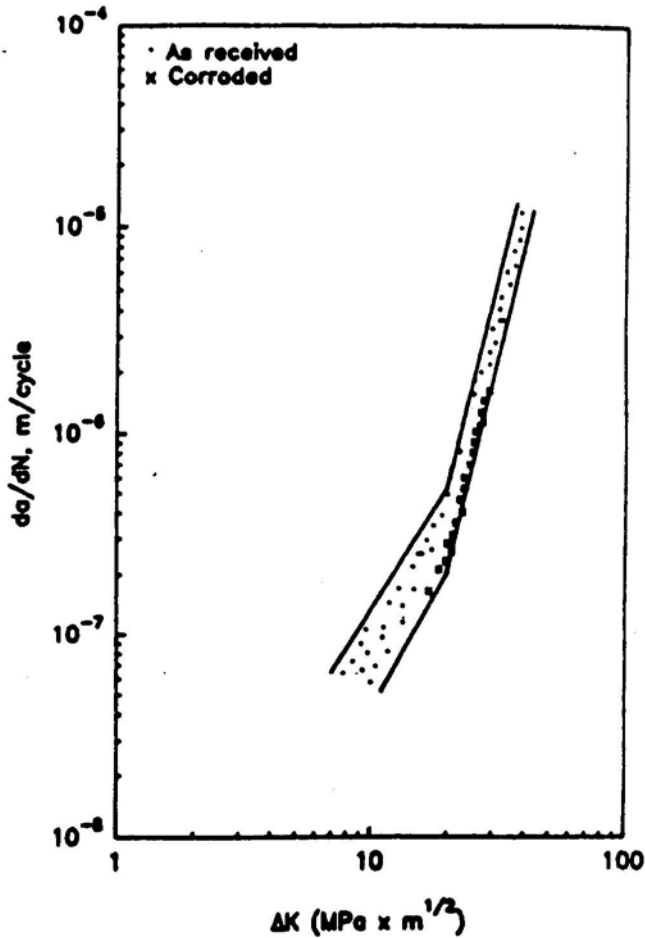
Figure 5. Fatigue Crack Growth Data for Corroded 2024-T351 Compared with As-Received 2024-T351 Tested in Dry Air

A review paper by Koch[23] discusses the implications of the findings in the literature. The paper suggests that the mechanism of interaction between corrosion and fatigue cracking may be different for the 2000- and 7000-series alloys. It was discussed that the main effects of corrosion are mechanical in nature, but that hydrogen may likely be a contributor to the mechanism of corrosion-fatigue interaction in 7000-series alloys. Mechanistic details will be discussed in the Discussion Section of this report.

As a result of the different forms of corrosion described above (pitting, crevice, or exfoliation), damage is created in a structure. This damage can be considered the equivalent to mechanical damage. With this initial approach, fracture mechanics may be applied using equivalent flaw sizes to compute the stress concentrations created by corrosion, or the increased stresses, which result from thickness loss by corrosion.[24]

To evaluate the potential joint effects of fatigue damage and corrosion on safety, an analytical framework for modeling these effects must be established. While fatigue damage can be

8

modeled by fracture mechanics, to date there are no generally accepted metrics for quantifying the extent of corrosion damage or predicting its development. The damage resulting from environmental attack can take many forms, and can lead to enhanced crack growth rates (corrosion fatigue), thickness loss (increased stresses), intergranular corrosion and stress-corrosion cracking (stress risers), pitting (stress risers), and dimensional changes which increase the state of stress in the structure. Since these types of corrosion damage can be incorporated into fracture mechanics concepts, analyses based on fracture mechanics are considered to provide at least first order approximations of the effects of corrosion damage.

However, when localized corrosion occurs, the cathodic reaction typically consists of hydrogen ion reduction, creating hydrogen atoms on the alloy surface. Because of the high fugacity or partial pressure of the hydrogen atoms, it is likely that hydrogen will be absorbed and diffuse into the alloy lattice, possibly resulting in some form of hydrogen embrittlement. In fact, there is literature indicating that hydrogen embrittlement plays a significant role in environmentally induced cracking (SCC and CFC) of aluminum alloys. Particularly, SCC and CFC of the 7000-series aluminum alloys have been attributed to a hydrogen related mechanism.[25-29]

Duquette and coworkers[27-29] have conducted extensive research to demonstrate a hydrogen related mechanism for CFC of 7000-series alloys. They studied the effect of cathodic polarization and catalyst poisoning of the hydrogen recombination reaction. Based on results such as shown in Figures 6 and 7, they concluded that the hydrogen is responsible for the reduction in fatigue strength of 7000-series alloys. Figure 6 shows that cathodic polarization of the aluminum alloy during fatigue cracking in an NaCl solution significantly lowers the fatigue strength.[27] At these cathodic potentials, hydrogen ion reduction is the cathodic reaction, and the hydrogen generated in that reaction can be readily absorbed into the aluminum alloy lattice. Moreover, Figure 7 shows that when arsenic (As) was added to the NaCl solution during fatigue cracking, the fatigue strength was lowered. Jacko and Duquette[28] explained that the As inhibited the hydrogen re-combination reaction to form H_2, thereby facilitating hydrogen absorption into the aluminum alloy lattice. Fractography of specimens which were fatigue fractured under cathodic polarization, further showed that the initial fracture mode was intergranular, but that at longer crack lengths, the fracture became transgranular with significant amounts of cleavage or quasi-cleavage type fracture which is characteristic of hydrogen-induced cracking.
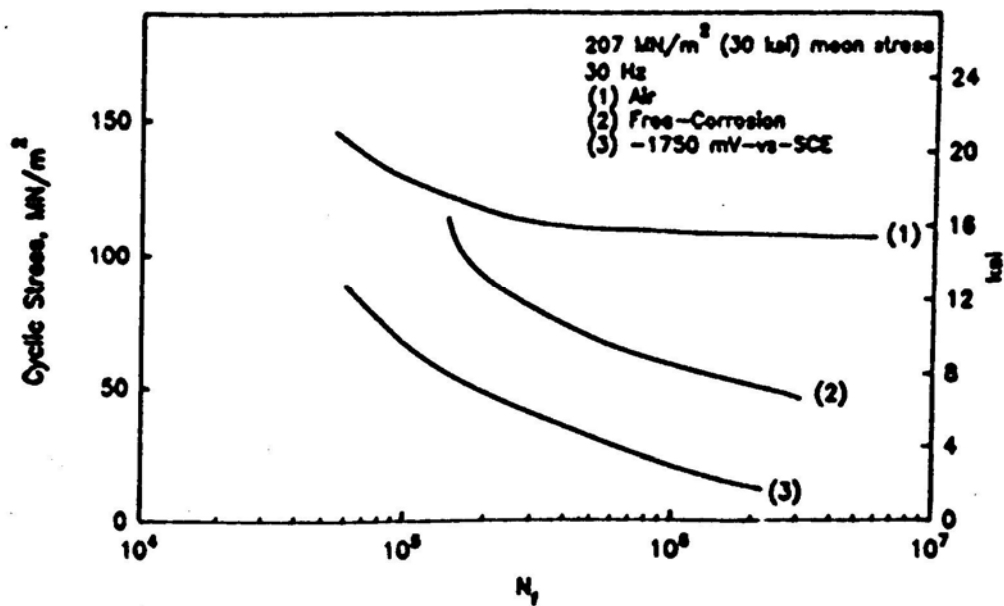
Figure 6. Fatigue Behavior of Al - 5.5 Zn - 2.5 Mg - 1.5 Cu in 0.5 M NaCl at Room Temperature Cathodically Polarized to -1750 mV Versus SCE Compared to Fatigue Behavior in Air and under Free Corrosion Conditions in 0.5 M NaCl
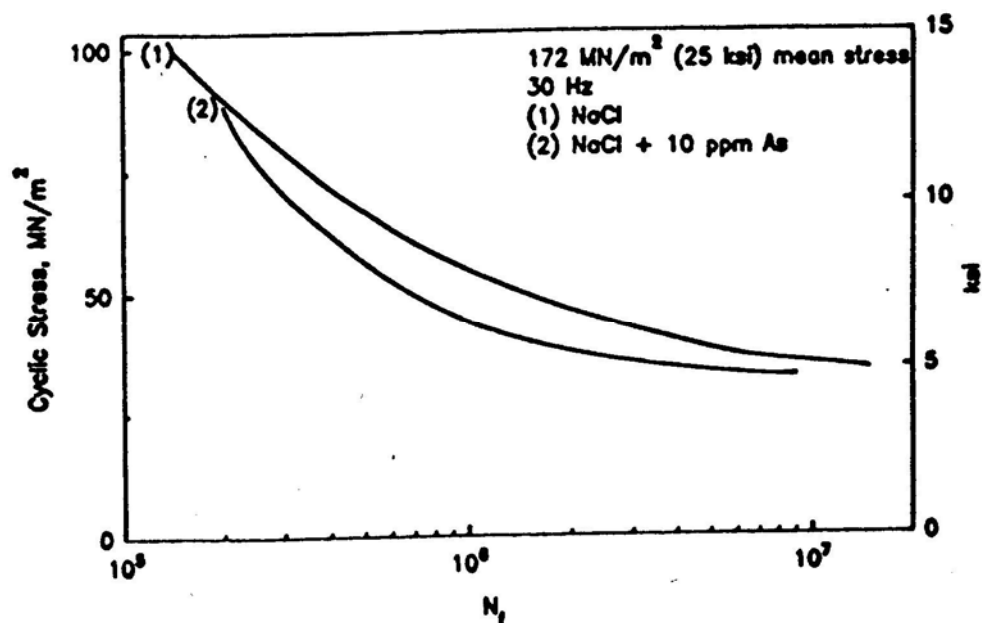
Figure 7. Fatigue Behavior f 7075-T6 in 0.5N NaCl + 10 ppm Arsenic (As) Compared to Fatigue Behavior under Free Corrosion Conditions in 0.5N NaCl

10

4. APPROACH

This project was divided into three individual tasks: Task 1 - Effect of Preexisting Corrosion On Fatigue Crack Propagation, Task 2 - Effect of Preexisting Corrosion On Fatigue Crack Initiation, and Task 3 - Modeling. Prior to starting the laboratory and modeling work, a literature survey was conducted to gain better insight into the current understanding of the effect of corrosion on fatigue cracking of aircraft aluminum alloys. The results of this literature survey, which formed the basis for the experimental and analytical work, were presented in the Background Section of this report.

In the first task, the effects of different modes and degrees of corrosion on fatigue crack propagation were investigated. Different types of specimens of two typical aircraft aluminum alloys, 2024-T3 and 7075-T6, were used in this task. To assess the effect of preexisting corrosion on the fatigue crack propagation behavior, increasing ΔK as well as constant ΔK tests were performed.

The purpose of the second task was to investigate the effects of different modes and degrees of corrosion on fatigue crack initiation of aluminum alloys 2024-T3 and 7075-T6. To study specific aspects of the interaction between crack initiation and preexisting corrosion, slow strain rate experiments also were conducted.

Finally, in Task 3, a methodology was developed, implemented and demonstrated, to quantify the effects of corrosion on the fracture risks in an operational aircraft environment. The resulting model will be incorporated into the PROF computer code.[29,30]

4.1 Task 1 - Effect of Preexisting Corrosion on Fatigue Crack Propagation

In this task, the effects of different types and degrees of corrosion on the propagation of long fatigue cracks in aluminum alloys 2024-T3 and 7075-T6 were investigated. The nominal composition of these alloys is given in Table 1. The different types of corrosion, pitting and exfoliation corrosion were achieved by exposing test panels to specific corrosive environments, for various lengths of time. Details of the test panel configurations and precorrosion, as well as the testing procedures are described in the following sections.

Table 1. Nominal Composition of Aluminum Alloys 2024-T3 and 7075-T6

Composition %							
UNS	**Name**	**Cr**	**Cu**	**Mg**	**Mn**	**Si**	**Zn**
A92024	Al2024	0.1 max	3.8-4.9	1.2-1.8	0.3-0.9	0.5 max	0.25 max
A97075	Al7075	0.18-0.28	1.2-2.0	2.1-2,9	0.3 max	0.4 max	5.1-6.1

4.1.1 Specimen Configuration

For this task two types of specimens were used, namely a compact tension (CT) specimen and a modified CT specimen. The CT specimen, shown in Figure 8 was designed according to ASTM Standard E 647.[31] As indicated in the figure, the CT specimens were machined into 1.5 by 1.44 by 0.125 inch (38.1 by 36.6 by 3.2 mm) coupons. The width of the specimen was oriented in the longitudinal (L) direction of the sheet, and the crack was oriented in the T-L direction.
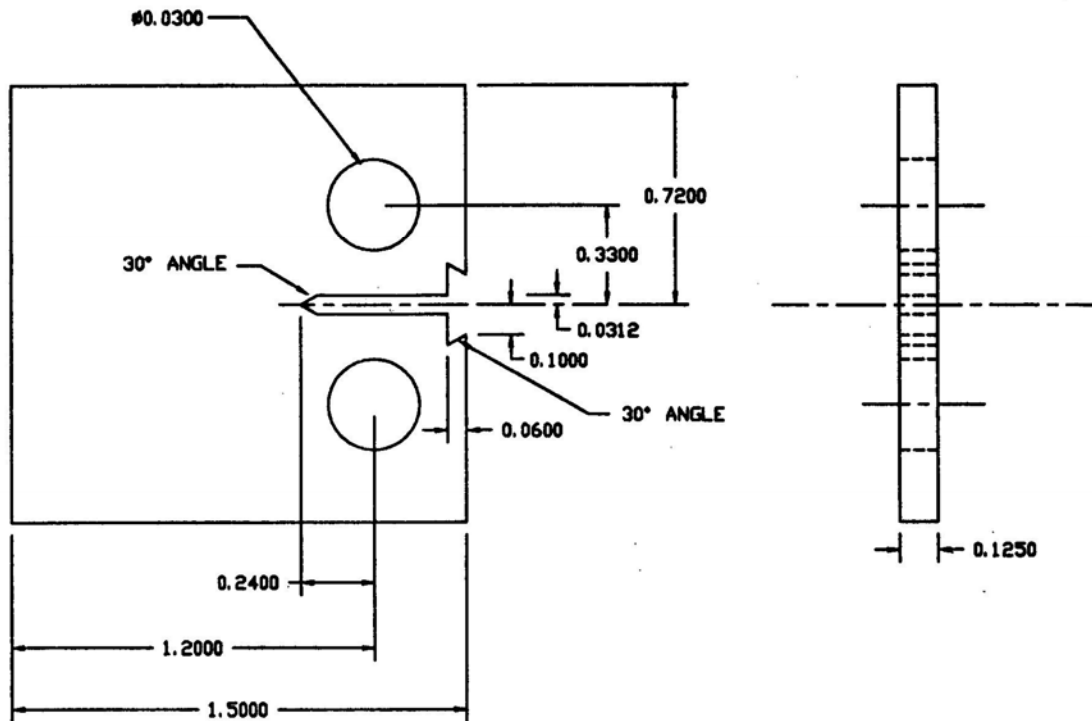
Figure 8. Schematic Drawing of Standard ASTM Compact Tension Specimen

Unfortunately, data from crack opening displacement (COD) tests for the modified CT specimens shown in Figure 9 could not be used to accurately infer crack length; therefore, crack growth data from modified CT specimens were not used to study the effect of precorrosion on crack growth rate (da/dN).
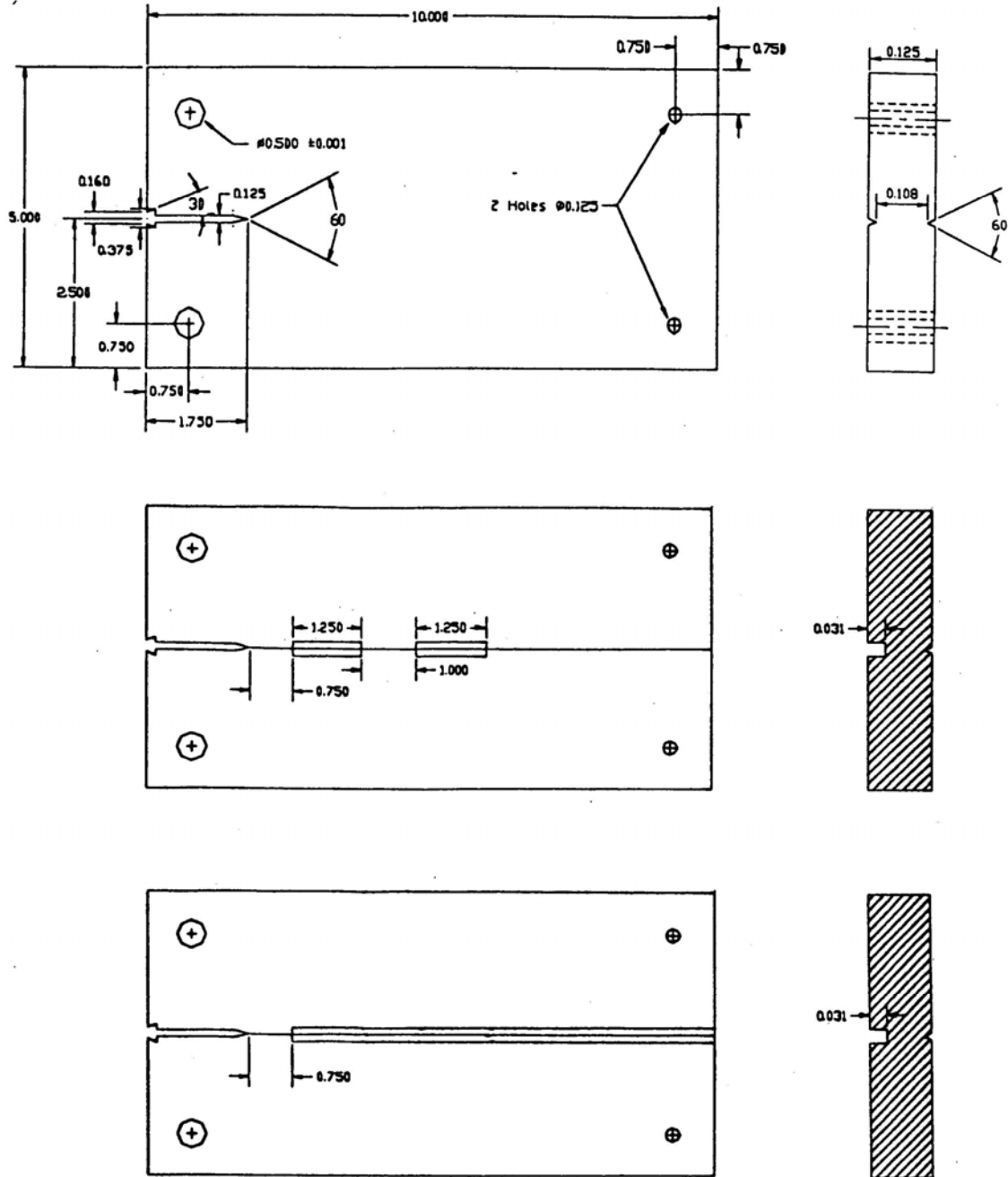
Figure 9. Schematic Drawing of Modified Compact Tension Specimens

4.1.2 Preconditioning of Specimens

To simulate the various types and degrees of corrosion that are observed on aircraft, the test specimens were exposed to different standard corrosion environments for varying lengths of time prior to fatigue testing. The purpose of these preconditioning treatments was to create different levels of pitting and exfoliation corrosion in specific areas of the test specimens.

13

4.1.2.1 Pitting Corrosion

In an attempt to quantify the effects of pitting corrosion, 2 by 4 inch (50.8 by 101.6 mm) test coupons of aluminum alloys 2024-T3 and 7075-T6 were exposed to a Copper Accelerated Acetic Acid Salt Spray (CASS - ASTM B-368)[32] for periods of 1, 4, 7, 14, and 21 days. The composition of the CASS solution is given in Table 2.

Table 2. CASS Solution Composition (ASTM B-368) to Induce Pitting Corrosion

Chemical Compound	Molarity	Weights and Volumes
NaCl	0.90	5 gm/95 gm distilled H_2O (5.0 weight percent)
$CuCl_2$	0.0014	0.197 gm/l solution
Acetic acid	0.025	21.45 ml/l of solution (pH = 3.0 to 3.1)

After exposure to the CASS environment, the coupons were rinsed with tap water and visually inspected and photographed. Optical microscopy on metallographic cross sections through corroded areas of the test coupons was used to measure the pit depth and width, from which the cross-sectional areas of the pits were calculated. After measurement, the pit sizes were ordered and statistically analyzed. Pit nucleation is a random process, which can be described by the Poisson function. Thus, the pit size (depth, width, and cross-sectional area) can be described by lognormal distributions in which the logarithms of the pit sizes are distributed according to the Gaussian normal distribution. The probability distribution function of the lognormal distribution is given by the following equation:

$$P_{(x)} = \frac{1}{2x(2\pi)1/2} \exp\left\{-(\ln x - \lambda)^2 / 22^2\right\} \tag{1}$$

where x is pit depth, pit width, or pit cross-sectional area, and z and λ are parameters with the following definitions:

$$z^2 = \ln(1 + \frac{\sigma^2}{\mu^2}) \tag{2}$$

$$\lambda = \ln u - \frac{z^2}{2} \tag{3}$$

where μ = the sample mean and σ = the sample standard deviation.

14

The cumulative distribution function is the probability that a pit depth x lies between two values x_1 and x_2, and can be obtained by integrating the probability distribution function between these two values. After the pit depths were measured, the logarithms of their values were taken and their mean and standard deviation were calculated. The probability distribution for pit depth at 1,4,7, and 21 days for the alloys 2024-T3 and 7075-T6 are given in Figures 10 and 11, respectively.
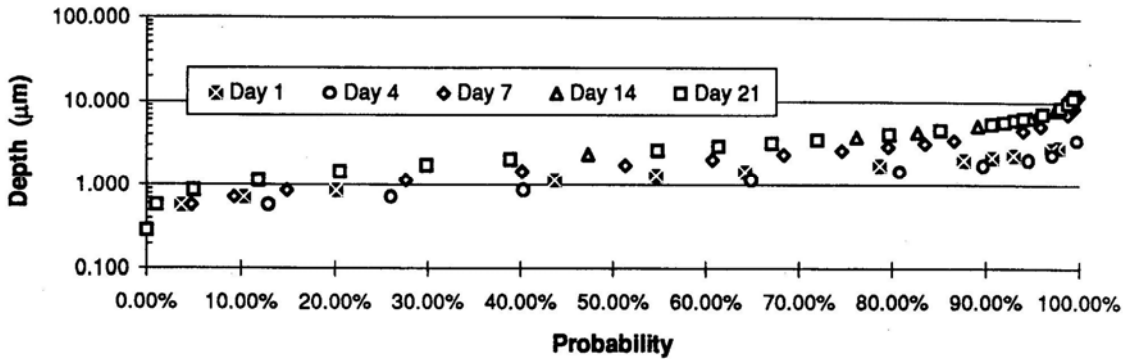
Figure 10. Pit Depth Distributions for Aluminum Alloy 2024-T3 Exposed to the CASS Environment for 1, 4, 7, 14, and 21 Days
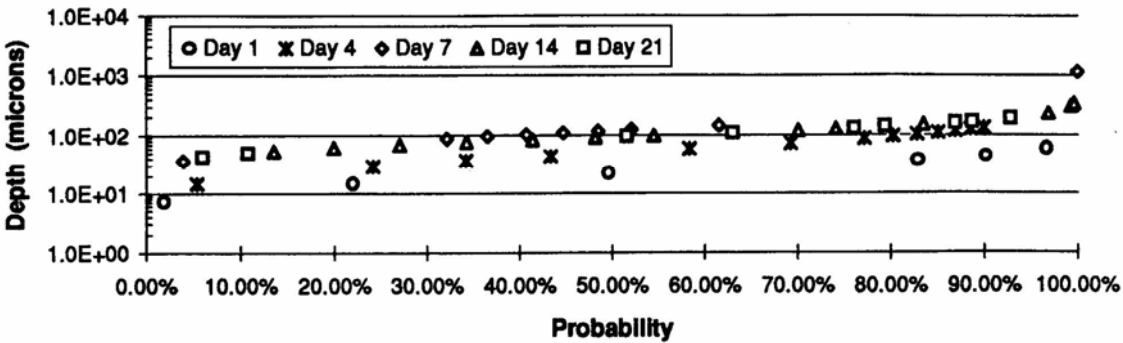
Figure 11. Pit Depth Distributions for Aluminum Alloy 7075-T6 Exposed to the CASS Environment for 1, 4, 7, 14, and 21 Days

Although pitting was initially observed as localized breakdown events in both aluminum alloys 2024-T3 and 7075-T6, propagation of pitting was found to be different for each of these alloys. In the case of aluminum alloy 2024-T3, corrosion pits spread out over the surface, then grew in depth. After a relatively short period of time, the pits started to coalesce, and new pits formed at the bottom of the initial pits. Optical micrographs, shown in Figure 12 demonstrate that the initial pitting occurred within the grains, and that as corrosion progressed, smaller pits formed inside the wide pits. Some intergranular attack also was observed.

15
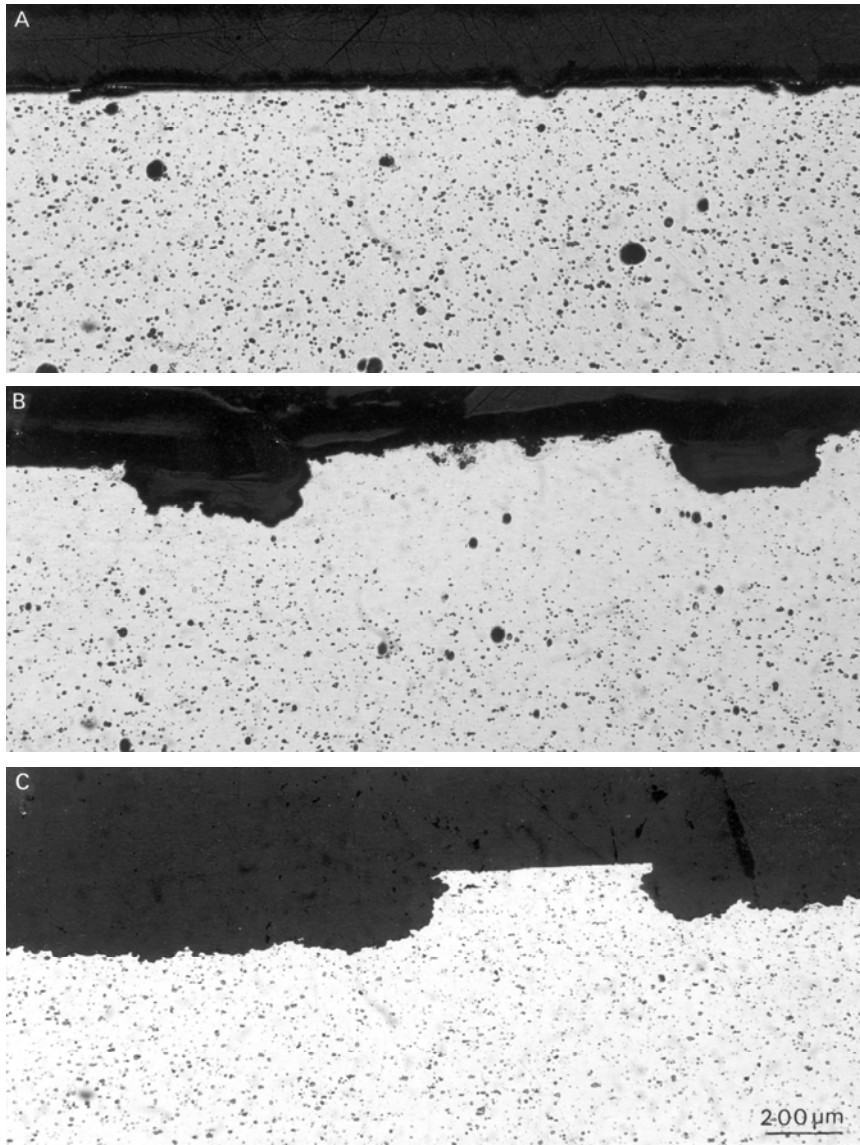
Figure 12. Optical Micrographs of Metallographic Cross Sections of Aluminum Alloy 2024-T3, Exposed to the CASS Environment, Showing Different Stages in Pitting

In the case of aluminum alloy 7075-T6, the initial pit morphology was in the form of small blisters, which are in fact layers of grains lifted off the surface. Following the initial attack, corrosion continued to occur preferentially along the grain boundaries, see Figure 13. Again, as in the case of alloy 2024-T3, the corrosion tended to spread over the surface, before it propagated into the sheet.
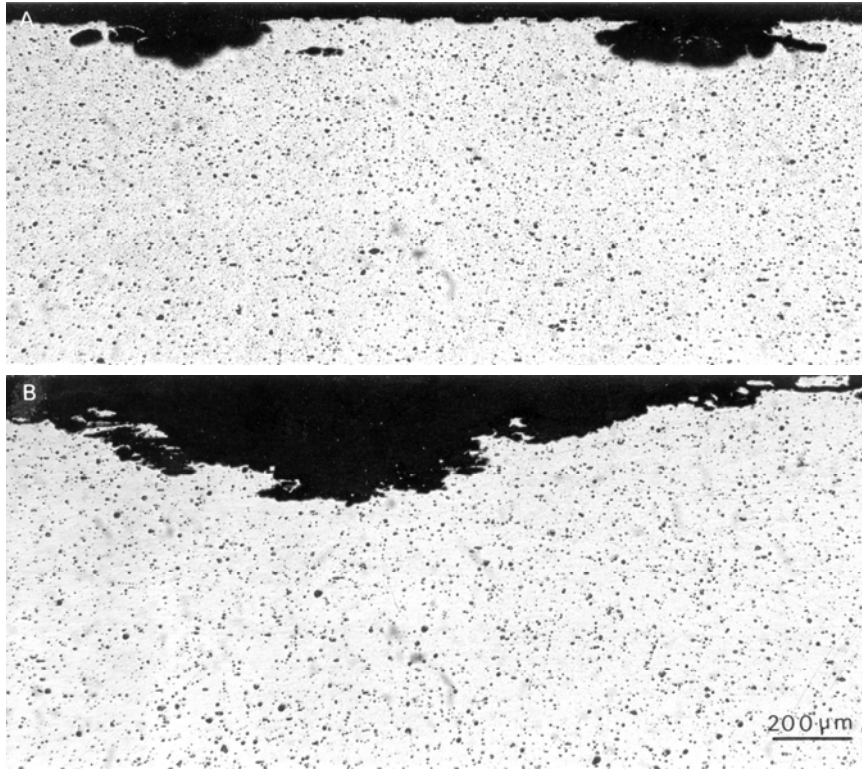
Figure 13. Optical Micrographs of Metallographic Cross Sections of Aluminum Alloy 7075-T6, Exposed to the CASS Environment, Showing Different Stages in Corrosion Attacks: a) 3 Days and b) 14 Days of Exposure

Because of the spreading of corrosion along the surface of both alloys, the width of localized attack was also measured. Again, the logarithm of the measured values were taken, and the mean and standard deviation were calculated. The probability distributions of the widths of corrosion attack of the two aluminum alloys, after exposures of 1, 4, 7, 14, and 21 days to the acidified salt spray are given in Figures 14 and 15, respectively.
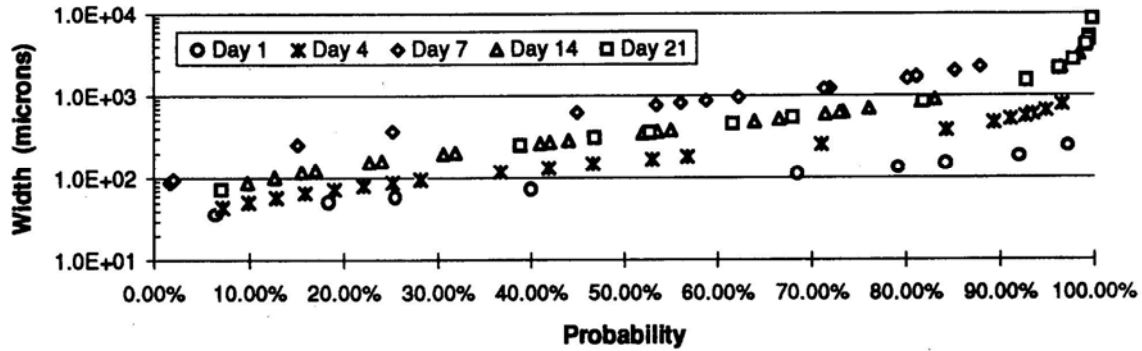
Figure 14. Pit Width Distributions for Aluminum Alloy 2024-T3 Exposed to the CASS Environment for 1, 4, 7, 14, and 21 Days
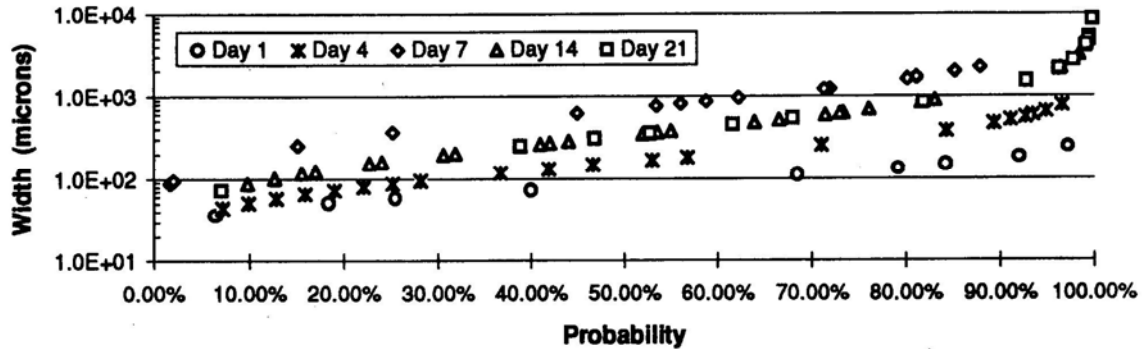
Figure 15. Pit Width Distributions for Aluminum Alloy 7075-T6 Exposed to the CASS Environment for 1, 4, 7, 14, and 21 Days

Finally, the cross-sectional area (pit depth x pit width) was calculated, and the probability distribution of these cross-sectional areas was also plotted for the various times of exposure to the salt fog environment. This area represents the total corroded area seen in the metallographic cross section. The probability distributions of the areas in alloys 2024-T3 and 7075-T6 are given in Figures 16 and 17, respectively.

18
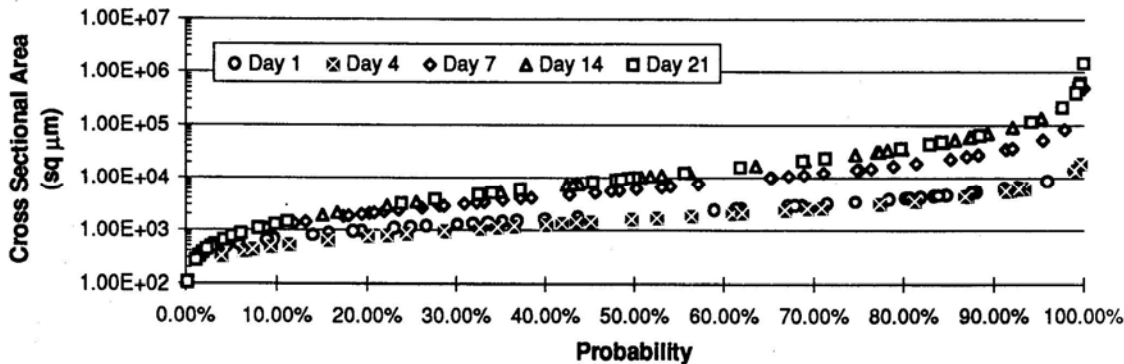
Figure 16. Pit Cross-Sectional Area Distributions for Aluminum Alloy 2024-T3 Exposed to the CASS Environment for 1, 4, 7, 14, and 21 Days
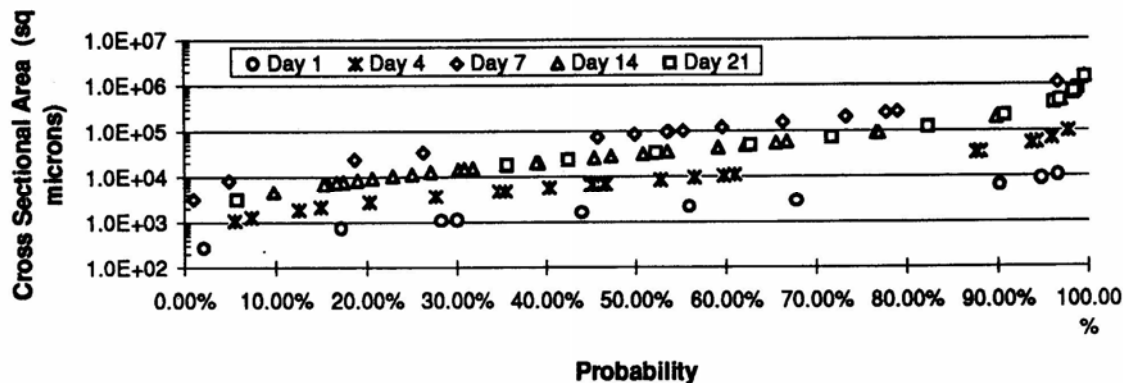
Figure 17. Pit Cross-Sectional Area Distributions for Aluminum Alloy 7075-T6 Exposed to the CASS Environment for 1, 4, 7, 14, and 21 Days

From the probability distribution diagrams shown above, the severity of localized corrosion can be predicted in a reproducible manner, as a function of exposure time to the copper accelerated acetic acid salt spray (CASS).

The CT specimens were exposed to an ASTM B-117 salt spray environment,[33] and the CASS environment for various lengths of time. The exposure times were based on the above described quantification experiments.

4.1.2.2 Exfoliation Corrosion

To simulate and quantify exfoliation corrosion, aluminum alloy test coupons were exposed to an EXCO (ASTM G-34)[34] solution for 1, 2, 4, and 6 days. The composition of the EXCO solution is given in Table 3. Metallographically cross-sectioned specimens of the test coupons were examined with an optical microscope and the extent of exfoliation in the cross sections was measured, see Figure 18.

19

Table 3. EXCO Solution Composition (ASTM G-34) to Induce Exfoliation Corrosion

Chemical Compound	Molarity	Weights and Volumes
NaCl	4.0	234 gm
KNO_3	0.5	50 gm
HNO_3	0.1	6.3 ml*

* pH = 0.4 (Initial), 4.0 (After 5 Days)
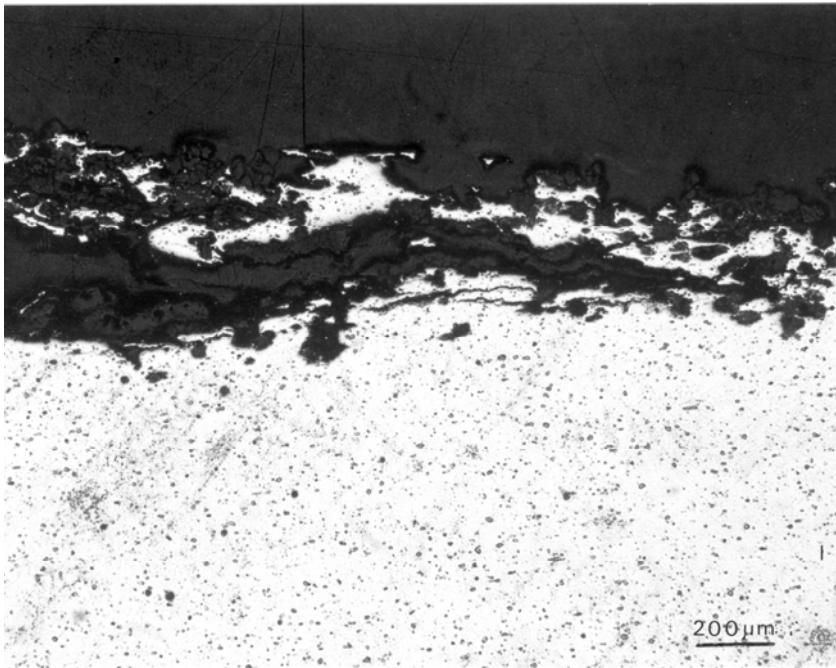
Figure 18. Optical Micrograph of Metallographic Cross Section of Aluminum Alloy 7075-T6, Exposed to the EXCO Solution, Showing Exfoliation Corrosion

For each test coupon, the average of the five deepest exfoliation penetrations was determined and plotted as a function of time, see Figures 19 and 20.
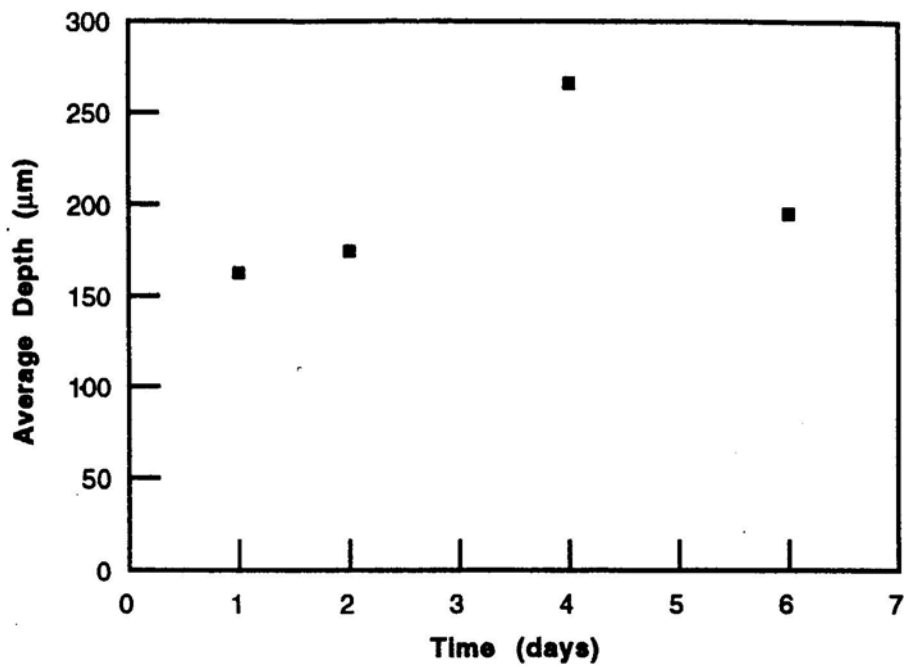
Figure 19. Exfoliation Depth of Aluminum Alloy 2024-T3 Exposed to the ASTM G34 EXCO Solution
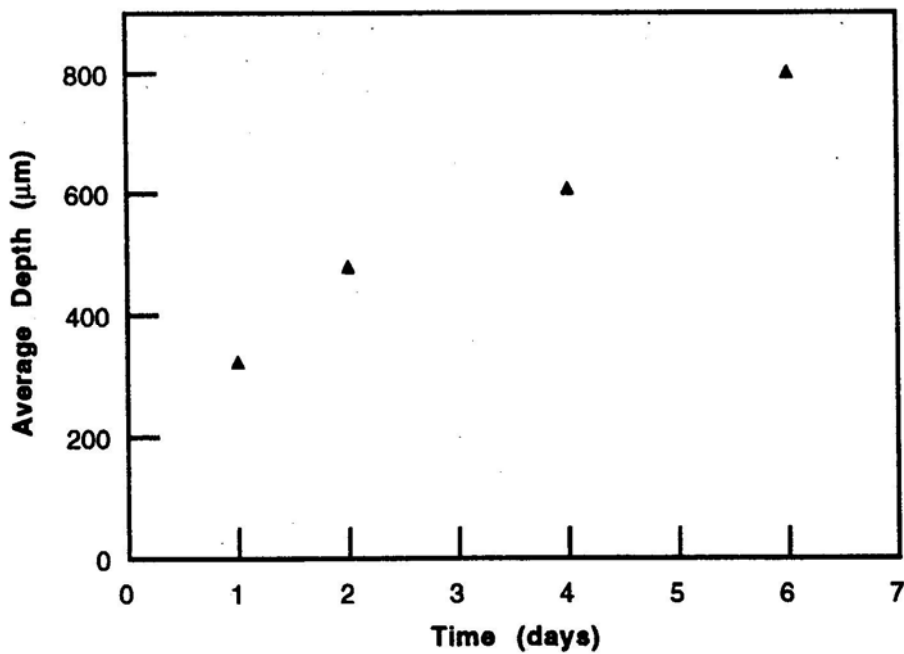
Figure 20. Exfoliation Depth of Aluminum Alloy 7075-T6 as a Function of Exposure Time in the ASTM G34 EXCO Solution

21

Based on the results of the quantification experiments, areas on the CT and modified CT specimens were corroded by exposure to the EXCO environment for various lengths of time up to 6 days, Table 4. Again, the specimens were masked off such that the regions exposed were similar to the machined areas shown in Figure 9.

Table 4. Exposure Conditions for Testing of Aluminum Alloys 2024-T3 and 7075-T6

Alloy	Specimen Type	Preexposure		
		EXCO (days)	CASS (days)	Salt Spray (hours)
2024-T3	Modified CT	2,6	6	8, 24
	Extended CT	2	2,6	---
	Slow strain rate	6	---	---
7075-T6	Modified CT	2, 6, 10	---	---
	Extended CT	2	2, 6	8, 24
	Slow strain rate	6	---	---
	CT	6	---	---

4.1.2.3 Hydrogen Charging

To evaluate the possible effect of hydrogen in the alloy lattice, hydrogen charging experiments were conducted. Hydrogen charging was achieved by cathodically charging in a 2N H_2SO_4 solution containing 1g/l $Na_2HAsO_47H_2O$ at room temperature, and at a current density of 1 mA/cm^2, using the procedure described by Ohnishi and Ito.[35] The time of charging was 12 hours.

4.1.3 Testing Procedures

Fatigue crack propagation tests were performed using a 22-kip servohydraulic machine. Clevis grips and pins were used to mount the specimens in the machine. A clip was used to measure COD. The crack length was computed from COD using a compliance equation. The increasing ΔK and constant ΔK testing procedures are discussed in the following sections.

4.1.3.1 Increasing ΔK Testing

Increasing ΔK tests were conducted on standard CT specimens. The ΔK values used for the CT specimens were computed from standard equations in ASTM Standard 647-91.[31]

$$\Delta K \;=\; \frac{\Delta P}{B\sqrt{W}}\frac{2+\alpha}{(1-\alpha)3/2}(0.886+4.64\alpha-13.32\,\alpha^2+14.72\,\alpha^3-5.6\,\alpha^4) \qquad (4)$$

where α = a/W; expression valid for a/W $\geq$ 0.2.

A precrack was formed by load shedding from 270 pounds (1220N) to 170 pounds (756N) in 58-pound (258N) decrements, until the crack reached a length of 0.1875 inch (4.76 mm). The test parameters were set to a sinewave with a maximum load of 150 pounds (667N). An R-ratio of 0.1 and a frequency of 1 Hz were used. Testing was performed in laboratory air, and data acquisition and analysis were performed. Cycle count averaged maximum/minimum load, and COD values were recorded at a rate of 10 points every 500 cycles. These data were then transferred to a spreadsheet and analyzed to obtain fatigue crack growth rates using the seven point incremental polynomial method described in ASTM E 647 (Recommended Data Reduction Techniques).[25] The fatigue crack growth rate was then plotted as a function of crack length and calculated ΔK. The ΔK was calculated using the actual thickness of the specimen. The actual specimen thickness was obtained by ultrasonic measurements and by measurements of metallographic cross sections, using an optical microscope equipped with a filar eye piece.

4.1.3.2 Constant ΔK Testing

To maintain a constant ΔK value, a fatigue crack growth program was utilized which automatically calculated crack length, da/dN and ΔK from COD readings. Required input for the program included pertinent specimen dimensions such as width, thickness and notch length. The program also required the material alloy and Young's Modulus. Finally, the desired constant ΔK values were entered, from which the program determined the initial testing load and the following load shedding sequence. The specimens were precracked in laboratory air using a 5 Hz sinewave with a 0.1 R ratio.

4.2 Task 2 - Effect of Preexisting Corrosion on Fatigue Crack Initiation

4.2.1 Specimen Configuration

To study the effect of preexisting corrosion on fatigue crack initiation in aircraft aluminum alloys 2024-T3 and 7075-T6, a blunt notch, extended compact tension (ECT) specimen, as shown in Figure 21, was selected. Prior to testing, the ECT specimens were precorroded in B-117 salt spray, CASS salt spray, and EXCO environments. The exposure times listed in Table 4.4 were selected such that corrosion of various degrees of severity could be accomplished. The specimens were masked off such that only the radius of the notch was exposed to the respective environments.
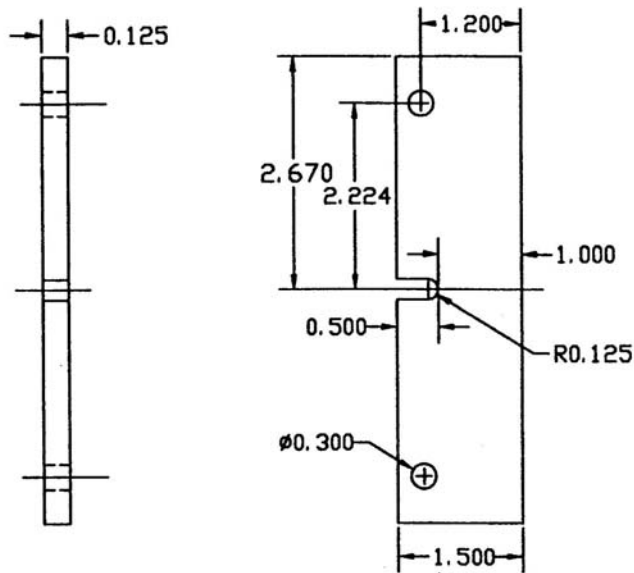
Figure 21. Schematic Drawing of a Blunt Notch, ECT Specimen, Used for Fatigue Crack Initiation and Short Crack Studies

4.2.2 Testing Procedures

For each pretreatment, a test matrix was established with maximum loads of 250, 350, 450, and 550 pounds (1112, 1557, 2002, 2446N), or 1.7, 2.3, 3, and 3.7 ksi, (11.72, 15.85, 20.69, and 25.51 MPa), respectively. The ECT specimens were tested in laboratory air using a sinewave loading with an R ratio of 0.1. The test frequency was 5 Hz. The dc electric potential drop method was used to measure the crack length. Current and voltage leads were attached to the specimen, as indicated in Figure 22, to measure the electrical potential drop. The measurements were recorded on an external data acquisition system which was synchronized with the servohydraulic machine data acquisition. At the conclusion of the test, the two data files were merged into one spreadsheet. These diagrams were used to define the cycles to fatigue crack initiation, where the curve deviates from the constant horizontal line. Representative plots of fatigue cycles versus potential drop are shown in Figures 23 and 24.
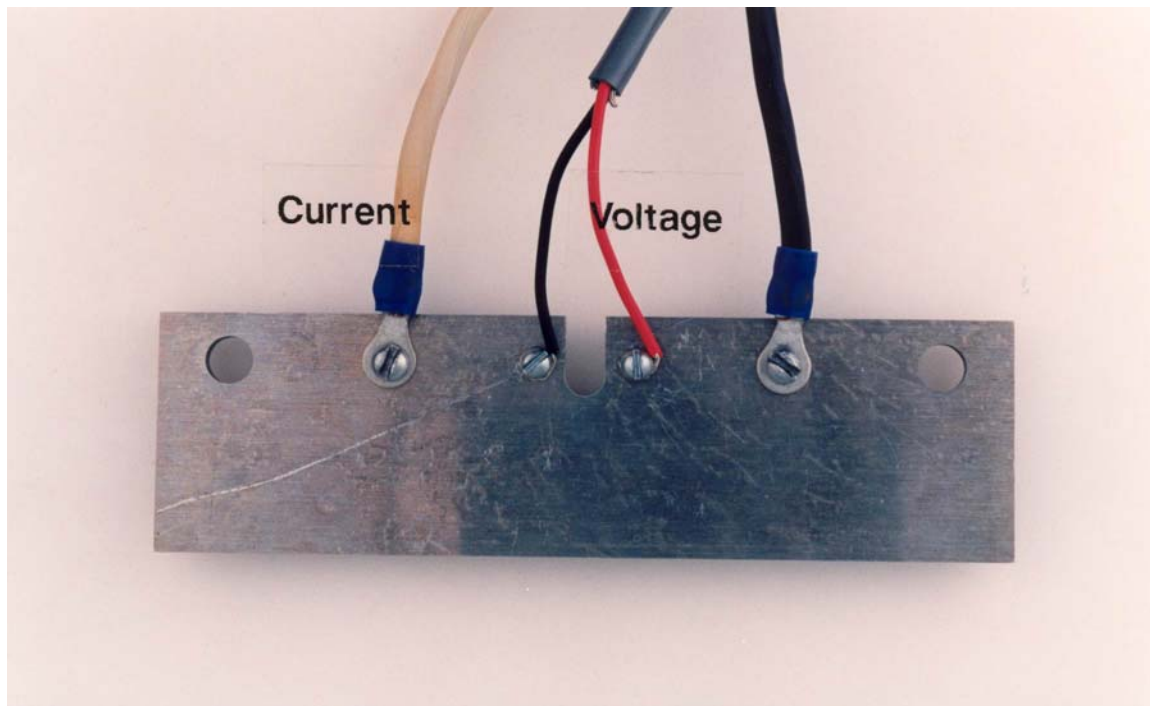
Figure 22. Photograph of ECT Specimen with Current and Voltage Leads Attached
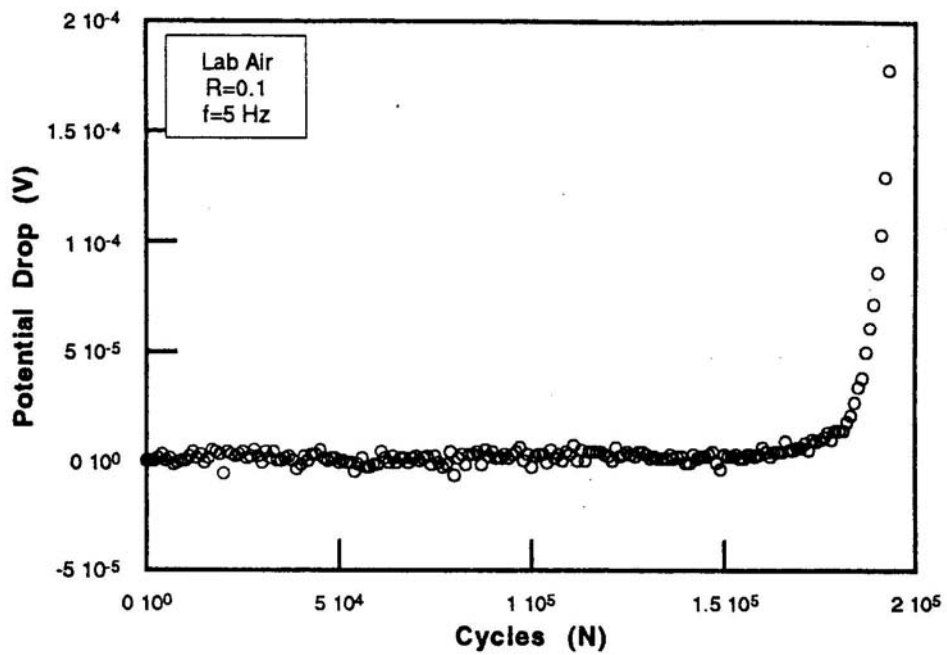
Figure 23. Diagram of dc Potential Drop as a Function of Fatigue Cycles in Aluminum Alloy 2024-T3
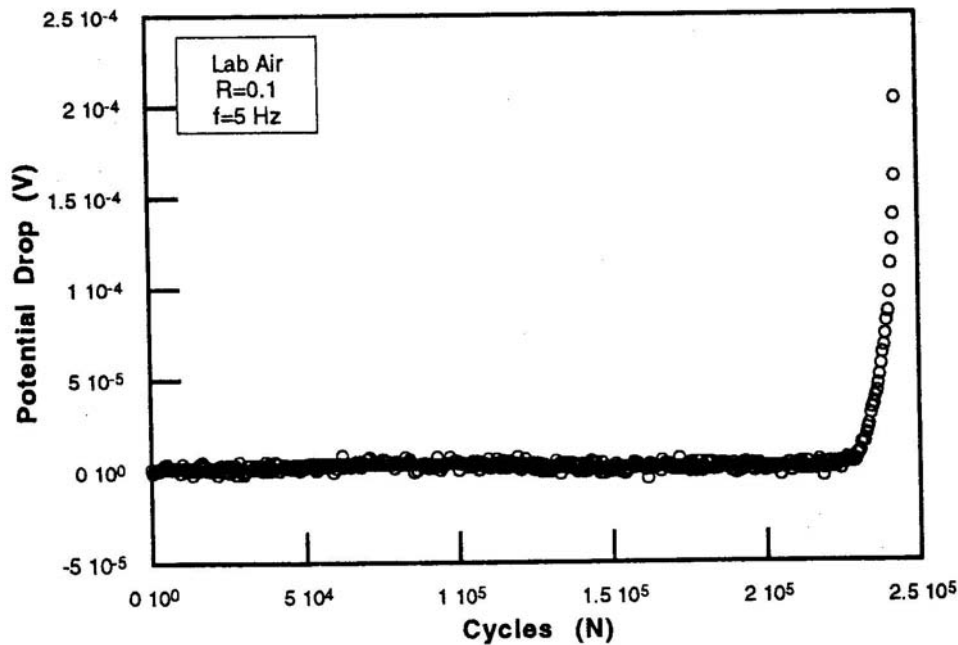
Figure 24. Diagram of dc Potential Drop as a Function of Fatigue Cycles in Aluminum Alloy 7075-T6

At the completion of the tests, S-N curves were plotted, and several specimens were metallographically cross sectioned to measure the extent of corrosion. Photomicrographs of the pits were taken at various depths to determine the pit size distribution along the blunt notch.

4.2.3 Slow Strain Rate Testing

To gain a better understanding of the effects of preexisting corrosion on the mechanical and physical properties of the two aluminum alloys, slow strain rate experiments were conducted.[37,38] One quarter inch-square bars of each alloy were cut from 0.25-inch (6.35 mm)-thick plates. Some of these bars were placed in EXCO solution for 6 days prior to machining of the slow strain rate specimens. The configuration and dimensions of the slow strain rate specimens are given in Figure 25. After machining, all specimens were visually inspected to ensure that no circumferential machining marks were present on the gage length. Using a center punch, marks were made on either end of the length. The distance between these two marks was measured before and after testing and from these measurements the percent elongation was calculated. Similarly, the percent reduction was calculated from initial and final section diameter measurements.
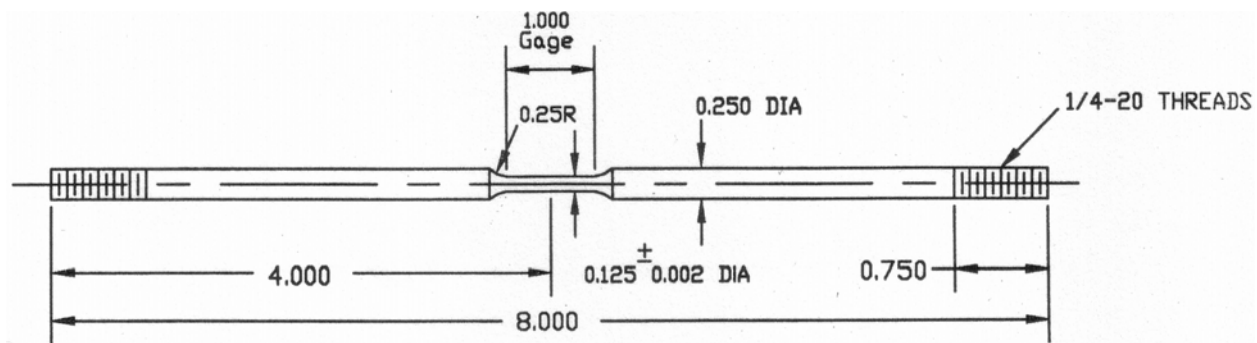
Figure 25. Configuration of Specimen for Slow Strain Rate Tensile Testing

The slow strain rate tests were conducted on a mechanical load frame at a strain rate of either 1×10^{-5} second^{-1} or 1×10^{-6} second^{-1}. Initial and final displacement readings, recorded with a calibrated dial gage mounted on the test frame, were used to verify the strain rate. The test environments included laboratory air, air with ≥ 95 percent relative humidity and dry nitrogen gas. In the latter two cases the environment was established within a test cell around the slow strain rate specimen for 1 hour prior to starting the test. A strip chart recorder was used to plot corresponding load and time values. Data from the strip chart were extracted and analyzed.

In addition to recording the mechanical properties, such as percent elongation, percent change in cross-sectional area, and tensile strength, detailed optical microscopy and fractography were performed to examine any significant changes on the fracture surface and on the gage length.

4.3 Task 3 - Modeling

Several modeling approaches were considered in an attempt to describe the effects of corrosion on fatigue cracking and other mechanical properties of aircraft aluminum alloys. Two different approaches were taken, namely a probabilistic approach and a deterministic finite element approach.

4.3.1 Probabilistic Modeling

Corrosion has traditionally been treated in aircraft structures as a durability issue. While the primary objective has been to prevent the initiation of corrosion through the proper choice of materials and coatings, corrosion does occur as evidenced by the high cost of corrosion related maintenance.[39] Although the scheduling of corrosion maintenance can be impacted by its frequency of occurrence for a particular fleet, no schedule adjustments are currently made for the structural safety inspections as determined by damage tolerance analyses.[40] However, as the aging fleets are used beyond their design lives, concern has developed because of the potential joint effects of corrosion and widespread fatigue damage on the structural integrity of critical details, i.e., on structural safety. As discussed in the Background Section, corrosion damage can, as a first approximation, be considered mechanical equivalent damage and be correlated using stress analysis and fracture mechanics concepts.

27

Initial sensitivity studies of corrosion effects on structural safety have been performed using deterministic analyses.[41] The analyses of this study were directed at a probabilistic analysis of corrosion effects. In particular, the effects of thickness loss were quantified in terms of the single flight fracture probability and the effects of pitting corrosion were evaluated by a comparison of equivalent crack size distributions. The risk analysis effects were calculated for a representative, critical structural detail from an observation class, ground support aircraft (OV-10). Since there are no current models for predicting thickness loss as a function of time (calendar months or flight hours), corrosion scenarios were defined by statically imposing 5 percent thickness reductions at two points in the life of an airframe. The fracture risks as a function of flight hours from the resulting corrosion scenarios were compared to the baseline fracture risks of no thickness loss throughout the usage intervals. The effects of pitting were evaluated by comparing the distributions of equivalent pitting crack sizes to those that resulted from the growth of the equivalent initial crack sizes.

The probabilistic analyses of the corrosion scenarios were performed using the PROF computer code.[29,30] PROF was specifically written to interface with the USAF Aircraft Structural Integrity Program (ASIP) and is based on the results of fracture mechanics data. Figure 26 schematic illustrates the types of data required to perform the PROF analysis and the probability of fracture (POF) output that is calculated as a function of flight hours. Under ASIP, crack life predictions (a versus T) are available for every known critical location. This implies the availability of 1) the flight stress spectrum (from which the distribution of maximum stress per flight can be obtained), 2) stress intensity factors as a function of crack size (a versus K/σ), and 3) fracture toughness, K_{cr}, (from which a distribution can be inferred). The initiating crack size distribution can be obtained from tear down inspections or, as in this study, from equivalent initial flaw sizes. Probability of detection (POD) as a function of crack size, POD(a), is a characterization of the capability of the nondestructive inspection system used during the safety inspections.
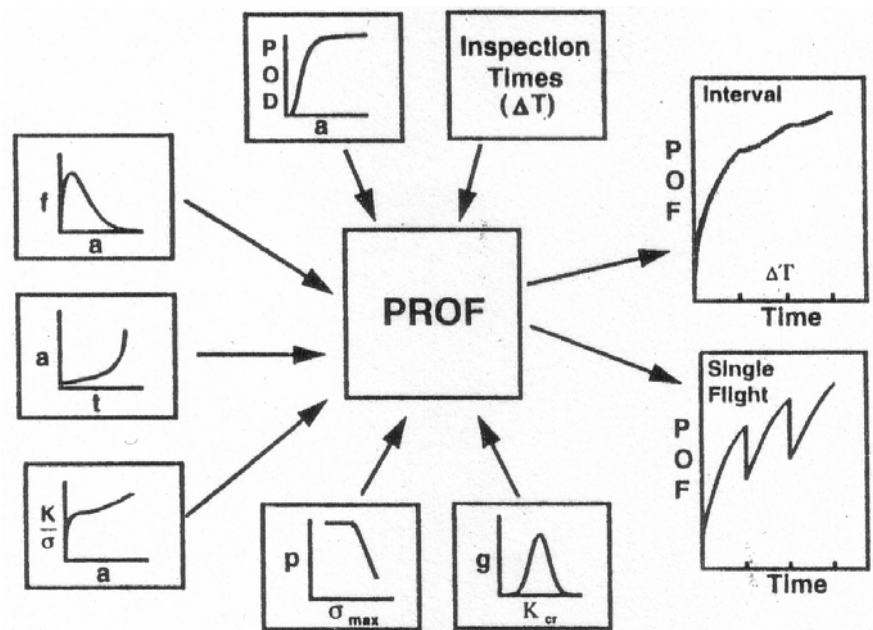
Figure 26. Probability of Fracture (PROF) Schematic

PROF uses the deterministic a-versus-T curve to project the percentiles of the crack size distribution as a function of flight hours, Figure 27. At a given number of flight hours, the single-flight POF is calculated from the distributions of crack size, maximum stress per flight, and fracture toughness. Specifically, single-flight POF is the probability that the maximum stress intensity factor (combination of the distributions of maximum stress per flight and crack sizes) during the flight exceeds the critical stress intensity factor. Single-flight POF as a function of flight (spectrum) hours provides a quantified basis for evaluating the risks associated with different cracking scenarios.
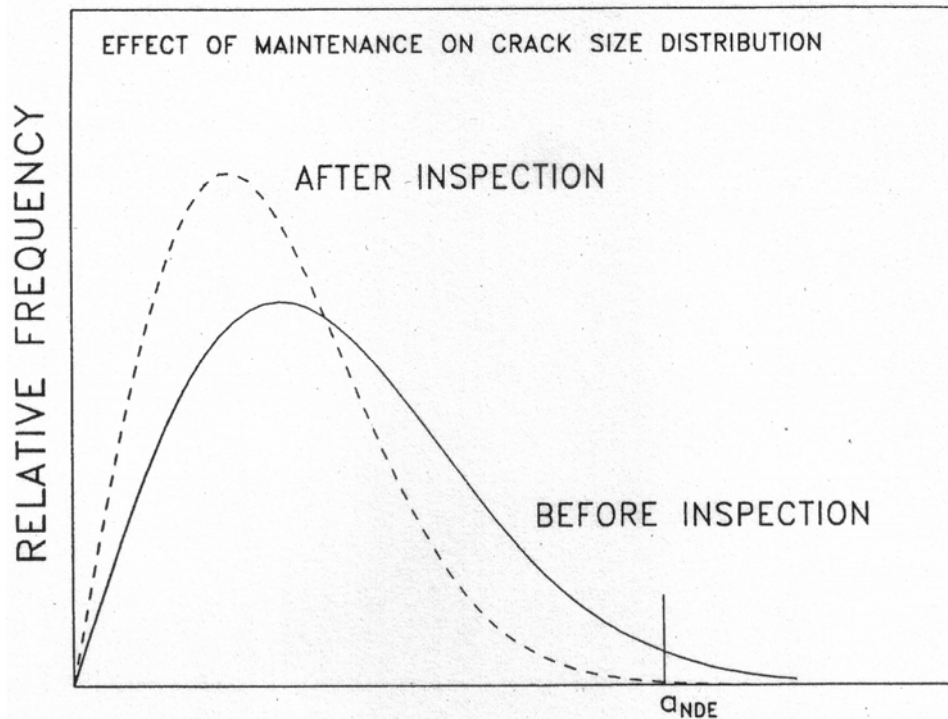
Figure 27. Crack Size Distribution as a Function of Flight Hours

At a maintenance cycle, the distribution of crack sizes changes in accordance with the POD(a) function and the equivalent repair crack size distribution, Figure 28. PROF outputs both the pre-inspection and post-inspection crack size distributions. The availability of these distributions allows changing the analysis conditions at the inspection times. This is accomplished by initiating a new analysis using intermediate outputs from the old analysis. For example, a new a-versus-T curve and a different distribution of maximum stress per flight could be introduced which would reflect the increased stresses that had resulted from corrosive material thinning. Further, the availability of the fatigue crack size distributions at the maintenance times allows at least a subjective evaluation of equivalent corrosion crack size distributions which qualify the effect of pitting.
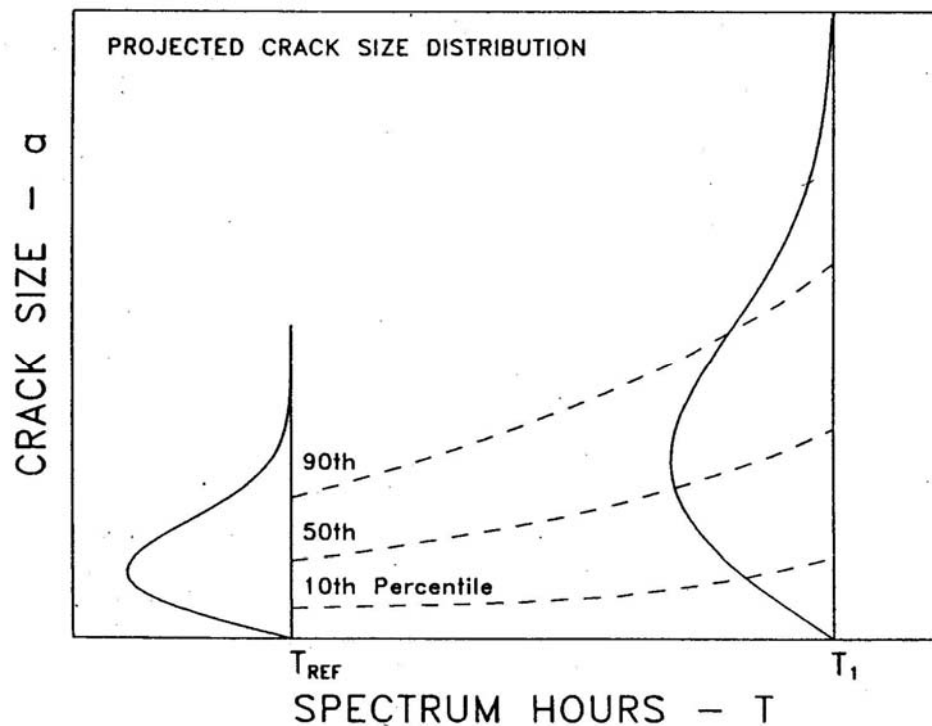
Figure 28. Change in Crack Size Distribution at an Inspection

The a-versus-T, a-versus-K/σ, and crack size distributions are input to PROF in tabular form. Fracture toughness is modeled by a normal distribution. Maximum stress per flight is modeled by the Gumbel extreme value distribution. The POD(a) function is modeled by a cumulative lognormal distribution with parameters μ and σ. Fifty percent of the cracks of size $\exp(\mu)$ would be detected. The parameter, σ, determines the flatness of the POD(a) function with smaller values of σ implying steeper POD(a) functions.

At present, there are no models for predicting the initiation and growth of corrosion damage as a function of time or for modeling the growth of fatigue cracks in the dynamic loads environment that would result from the continuous growth of corrosion damage. However, to obtain an indication of the potential risks associated with the threat of corrosion damage to aging aircraft, relatively static corrosion scenarios were defined in terms that are amendable to existing fracture mechanics analyses. Multiple runs of PROF were then made using relevant intermediate output as the initiating conditions for the corrosion scenarios. Multiple runs of PROF were then made using relevant intermediate output as the initiating conditions for the corrosion scenarios. These scenarios and the resulting analyses are described in Section 5.3.1.

Sensitivity studies have been performed on the application of PROF to representative problems.[29] These studies have indicated that, although the absolute magnitudes of the fracture probabilities are strongly dependent on the input, relative magnitudes tend to remain consistent when factors are varied one at a time. Because of the indefinite nature of some of the input data, particularly the crack size information, absolute magnitudes of the fracture probabilities are

31

highly suspect. However, it is believed that relative differences resulting from consistent variations in the better defined input factors are meaningful. In particular, the changes introduced through thickness reductions that will be associated with degrees of corrosion can be expected to produce meaningful relative differences. However, because of the uncertainty in specifying the equivalent initial and corrosion crack size distributions for the example problem, the evaluation of the effects of pitting were made on a different, somewhat subjective basis. In particular, an equivalent corrosion crack size distribution was inferred from information in reference 30, and compared with crack size distributions from PROF runs related to the corrosion scenarios.

PROF was originally written in Fortran to run on a DEC VAX 11-780, VMS operating system with VT220 emulation. As part of the probabilistic modeling of this study, PROF was converted to run on a personal computer (PC) under the Windows operating system. The execution of the example problem identified modification to PROF output that would facilitate the multiple runs required by corrosion scenarios. These modifications were also incorporated in PROF.

4.3.2 Finite Element Modeling

A finite element model (FEM) was built for the ECT specimens to gain a better understanding of the stress distribution in these specimens during the fatigue crack initiation and growth process. COSMOS/M was the program used to create the FEM models.[42] COSMOS/M is a modular finite element system with various applications, including stress analysis, heat transfer, fluid mechanics, and electromagnetics. For the present application, a linear elastic static stress analysis was conducted to produce results in terms of von Mises stress distribution along the centerline of the specimen.

5. RESULTS

5.1 Task 1 - Effect of Preexisting Corrosion on Fatigue Crack Propagation

In this task, the effect of precorrosion on fatigue crack growth was studied with different types of specimens and loading procedures. Initially, crack propagation tests were conducted on CT specimens at increasing ΔK. In an attempt to better distinguish between the crack growth rates in CT specimens with different pretreatment conditions, some constant ΔK tests were conducted as well.

5.1.1 Increasing ΔK Testing

5.1.1.1 Alloy 2024-T3 - Continuous Corrosion Path

When comparing the fractographic features of the precorroded alloy 2024-T3 with the as-received material, some differences were noted. Figures 29 and 30 show fractographic features which are typical for aluminum alloy 2024-T3 fatigued in air. On the low-magnification fractograph in Figure 29, relatively flat areas can be seen, interrupted by small crater-like features, which likely have resulted from fracture through or around the constituent particles in the alloy. The higher magnification fractograph of one of these flat areas shows the distinct crack-arrest markings or striations, which are characteristic features for fatigue cracking in this alloy. Again, the presence of constituent particles on the fracture surface is evident.

Specimens precorroded in the CASS or the EXCO environments for 6 days to form pitting or exfoliation corrosion, exhibited a somewhat different fracture surface. Figures 31 to 34 show fractographs of the fracture surface of an aluminum alloy 2024-T3 modified CT specimen precorroded in the CASS solution for 6 days. Areas near the pitted surface, Figures 31 and 32 show the presence of smooth surfaces on which the fatigue striations can barely be distinguished. Also, apparent debris was found on the fracture surfaces near the corroded surface. Further from the pitted surface, the fracture features become sharper and resemble the well-defined features found on the fracture surfaces of as-received material. Specifically, Figures 33 and 34 show fracture surfaces that are very similar to those of the noncorroded specimens, shown in Figures 29 and 30. Again, flat areas on which the fatigue striations are clearly defined can be seen, as well as the crater-like areas which indicate the presence of constituent particles.
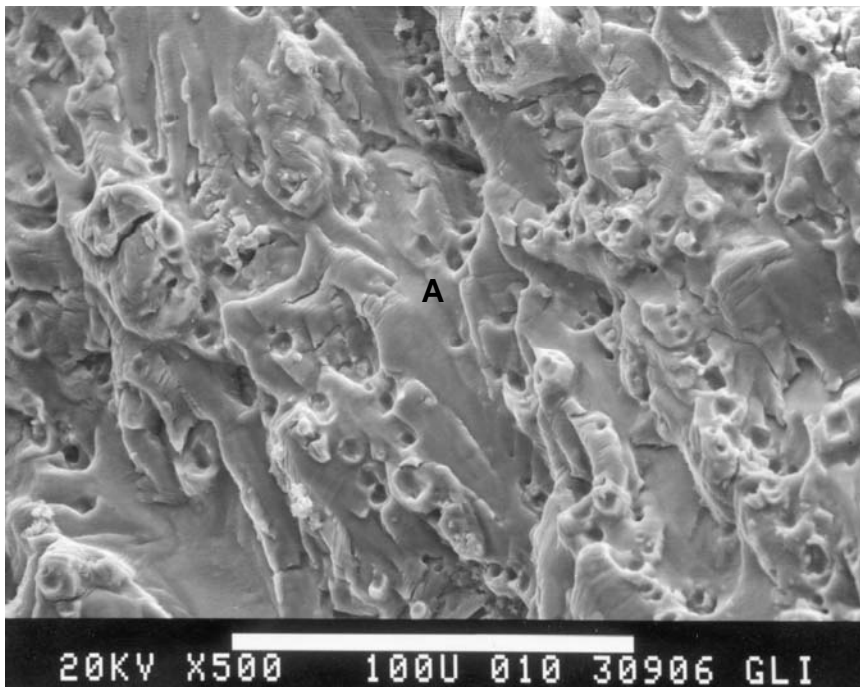
Figure 29. SEM of Fracture Surface of Aluminum Alloy 2024-T3 Fatigued in Laboratory Air (1 Hz, R=0.1)
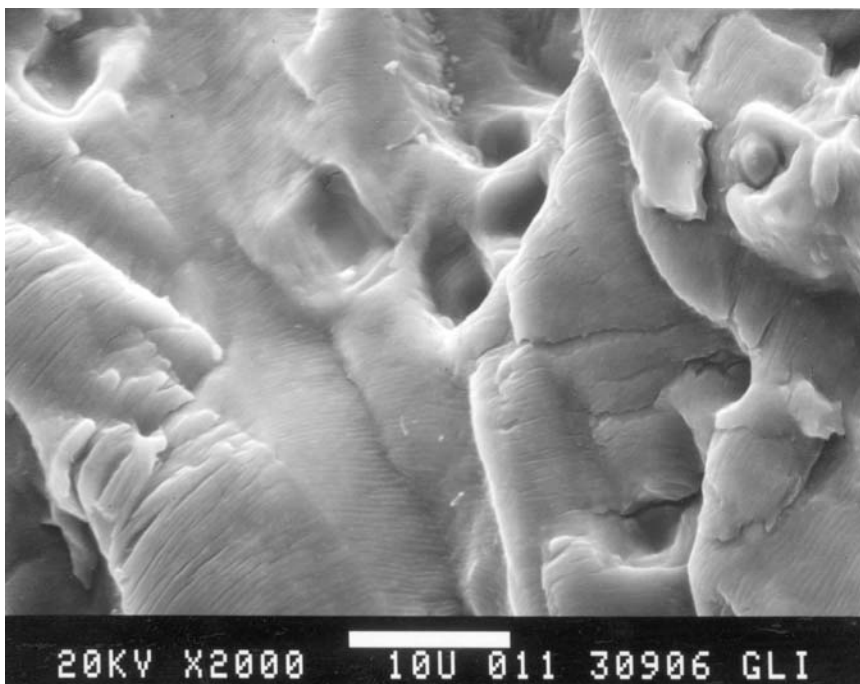
Figure 30. Detail of Area A in Figure 29
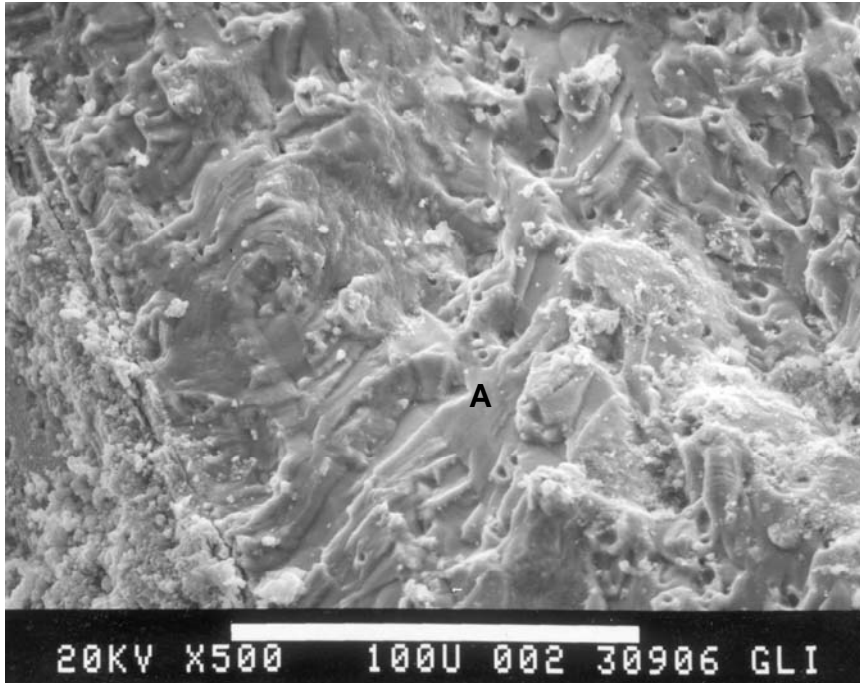
Figure 31. SEM of Fracture Surface of Aluminum Alloy 2024-T3 Precorroded in the CASS Environment and Fatigued in Laboratory Air (1 Hz, R=0.1)
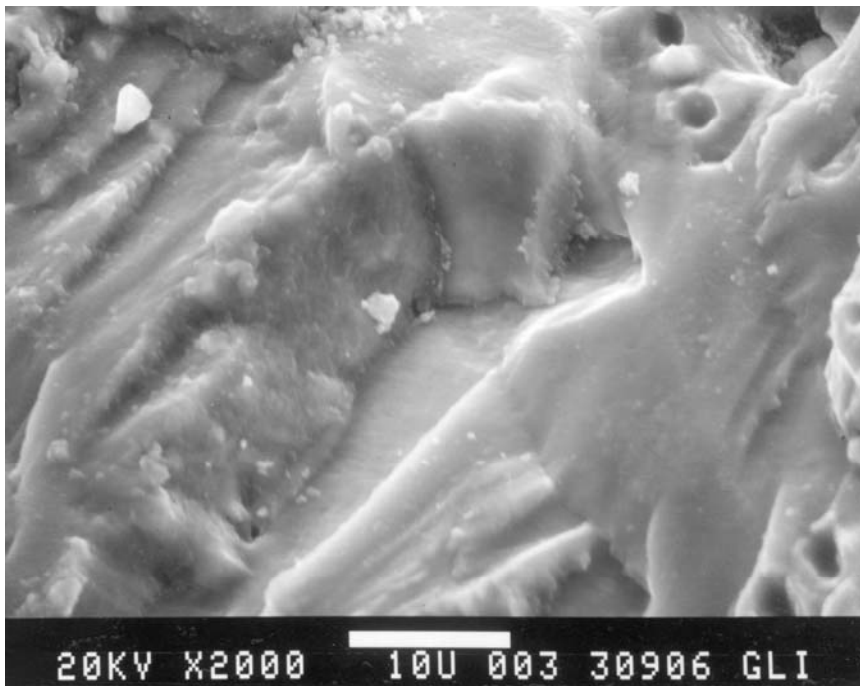
Figure 32. Detail Of Area A In Figure 31
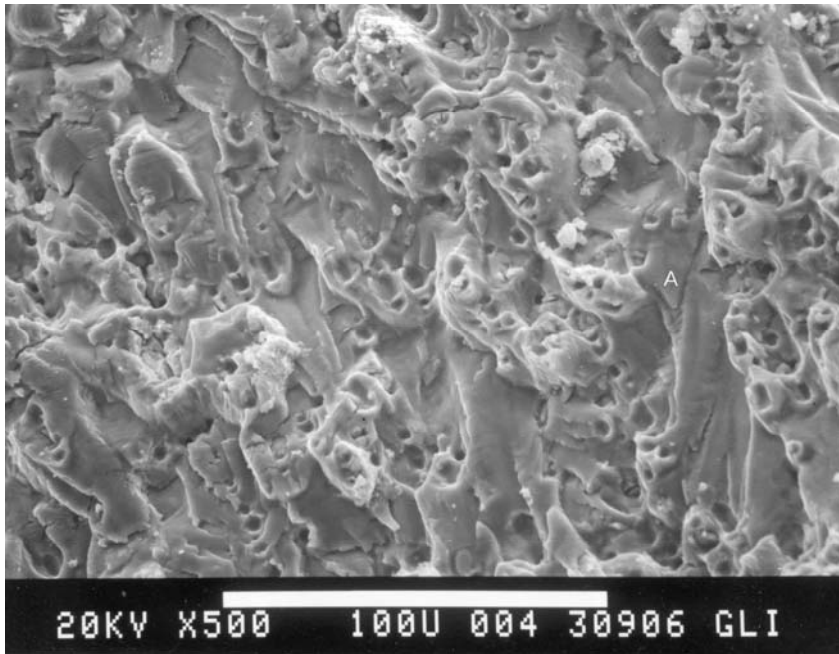
Figure 33. SEM of Fracture Surface of Aluminum Alloy 2024-T3 Precorroded in the CASS Environment and Fatigued in Laboratory Air (1 Hz, R=0.1)
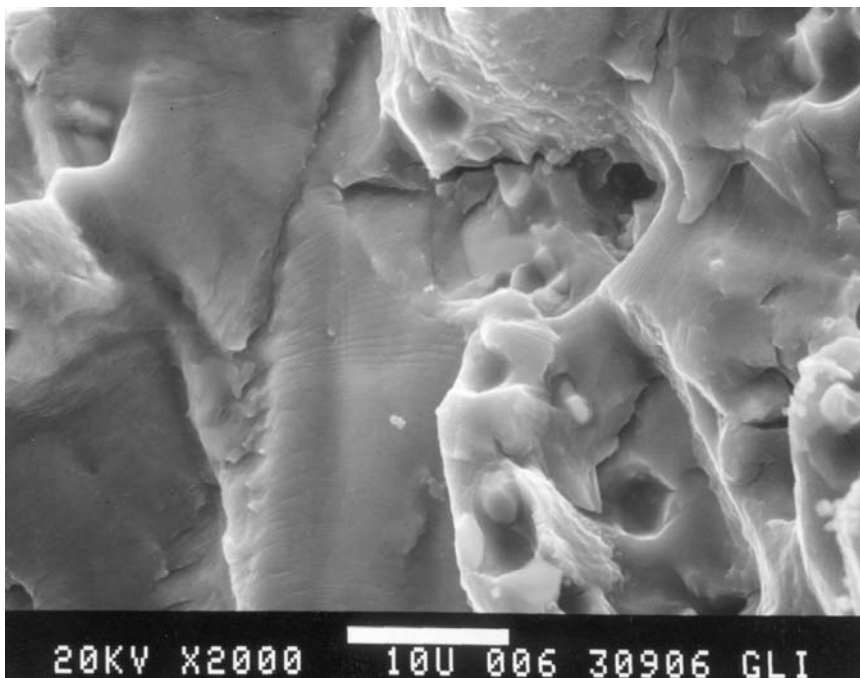
Figure 34. Detail of Area A in Figure 33

Figures 35 to 43 show fractographs of aluminum alloy 2024-T3 precorroded in the EXCO solution to induce exfoliation corrosion. The fracture surfaces both near and away from the exfoliated surface are quite different from the fracture surfaces of the noncorroded material. Specifically, at various locations on the fracture surfaces, mud-cracking features can be seen. These are characteristic of environmentally induced cracking such as corrosion-fatigue and stress-corrosion cracking. Higher magnification fractographs, as in Figures 37, 39, 41, and 43, show details of the mud cracking as well as the lack of distinct fatigue-arrest markings.

In addition to machining and precorrosion treatments, and prior to fatigue crack growth testing, alloy 2024-T3 test coupons were charged with hydrogen, using the method described in Section 4.1.2.3.[35] The resulting fracture surfaces presented in Figures 44 to 47 show features that were observed on different locations on the fracture surface that were similar to those observed on the fracture surfaces of both uncorroded and corroded specimens. The fracture surfaces shown in Figures 44 and 46 show more surface relief than the fracture surface of the noncorroded coupon, with a mixture of ductile and brittle fracture. Figures 46 and 47 show particularly brittle crack arrest markings. Deposits similar to those found on the fracture surface of corroded specimens were found on the fracture surface of the hydrogen-charged coupon.
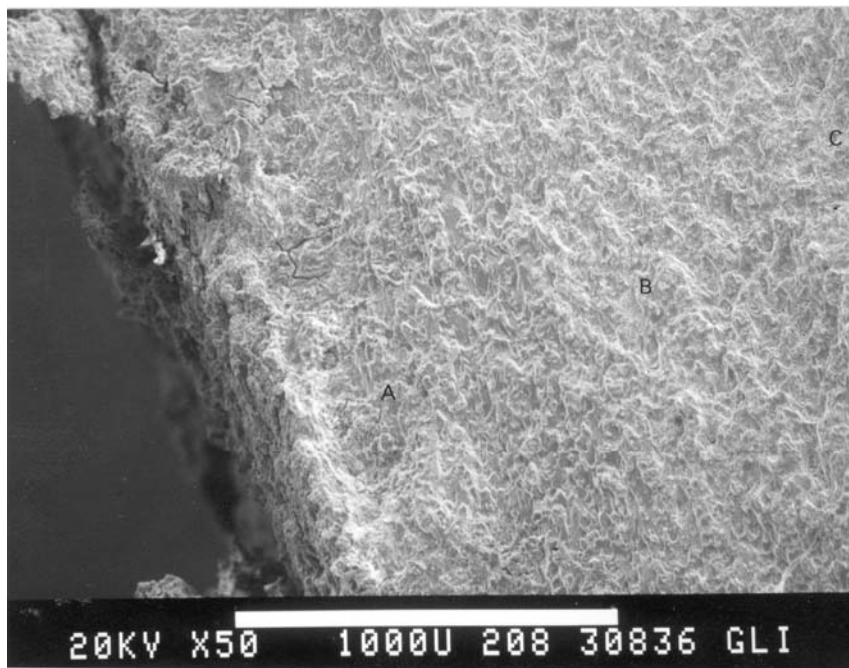
Figure 35. SEM of Fracture Surface of Aluminum Alloy 2024-T3 Precorroded in the EXCO Solution and Fatigued in Laboratory Air (1 Hz, R=0.1) with Exfoliation Corrosion Shown on Left Side of Micrograph
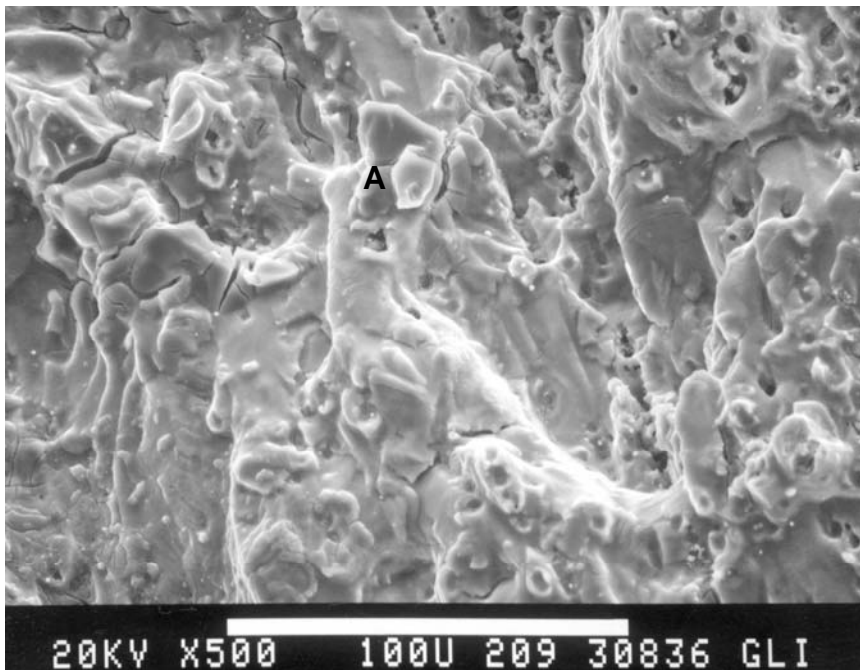
Figure 36. SEM of Area A in Figure 35; Adjacent to the Exfoliated Surface
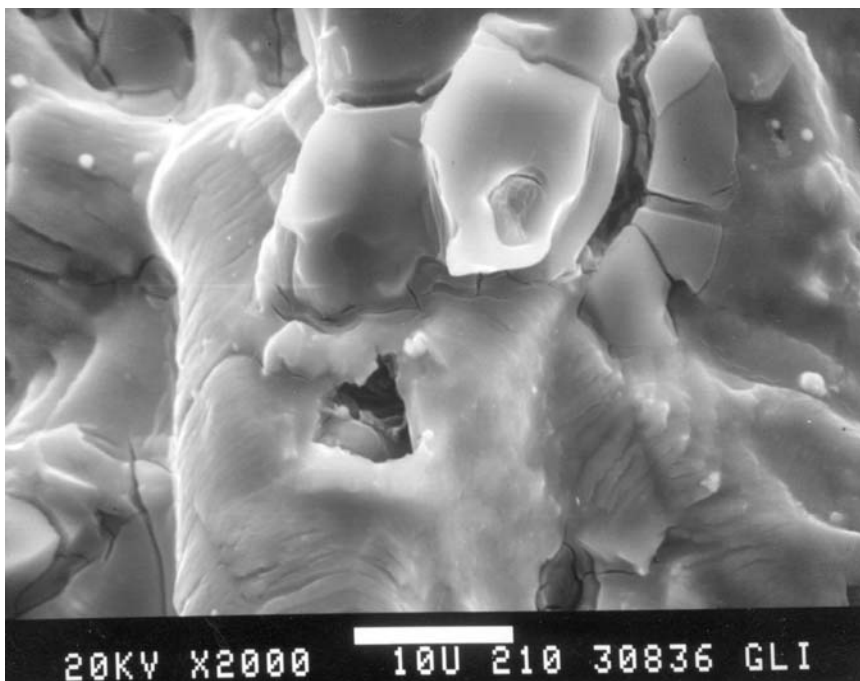
Figure 37. Detail of Area A in Figure 36 Showing Characteristic Mud Cracking
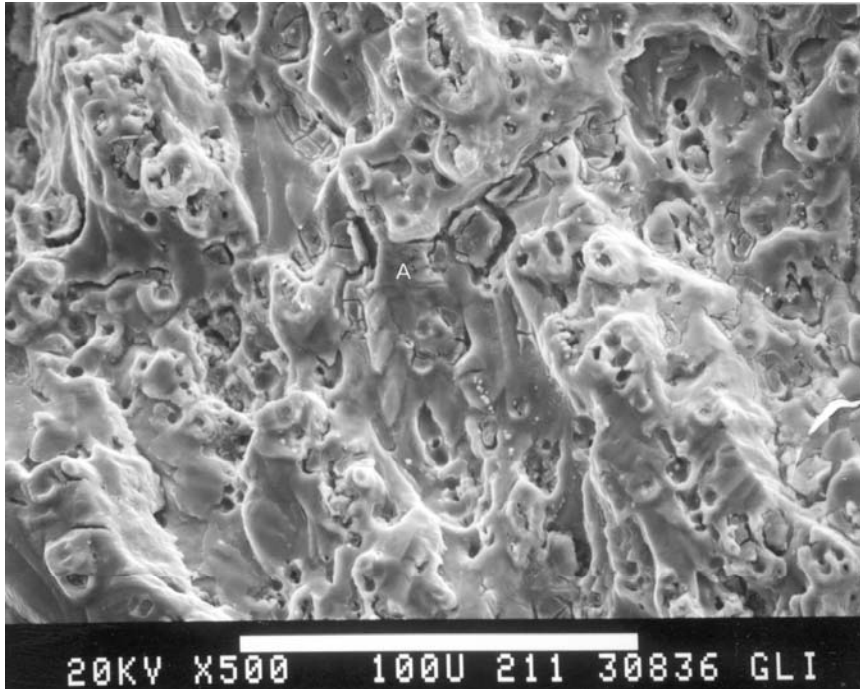
Figure 38. SEM of Area B in Figure 35; Middle of Fracture Surface Away from the Corroded Surface
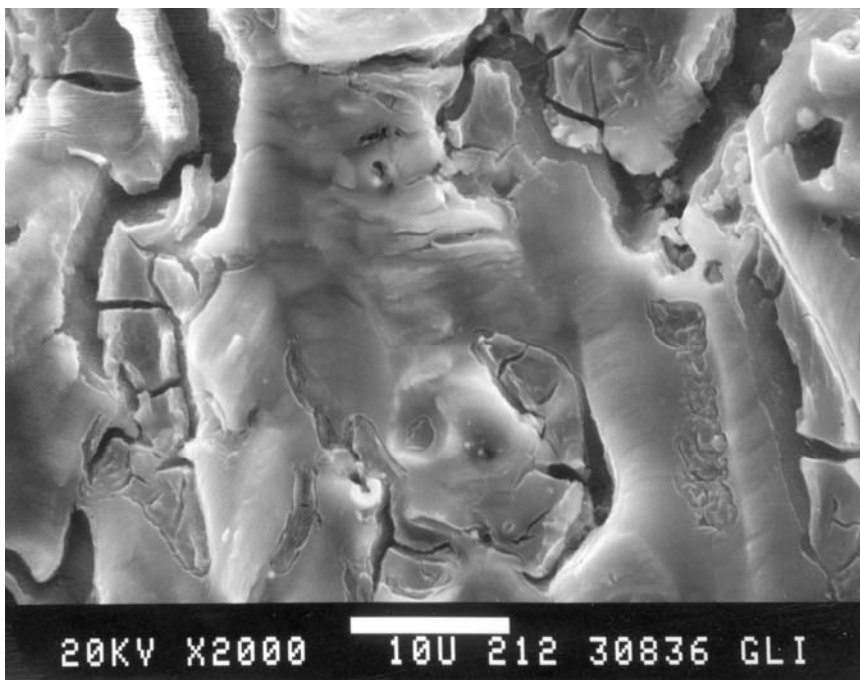
Figure 39. Detail of Area A in Figure 38 Showing Characteristic Mud Cracking
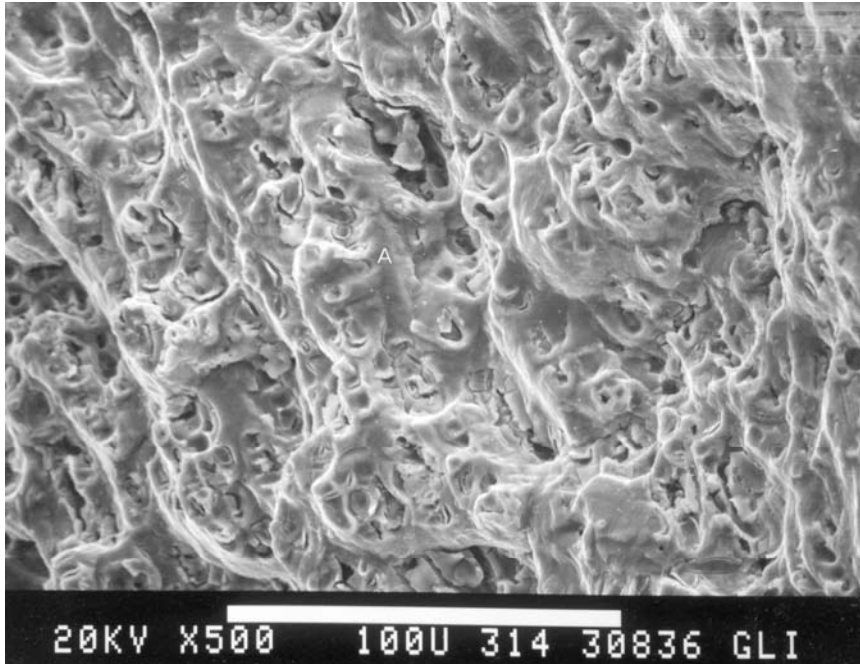
Figure 40. SEM of Area C in Figure 35; Near the Corrosion-free Surface Away from the Corroded Surface
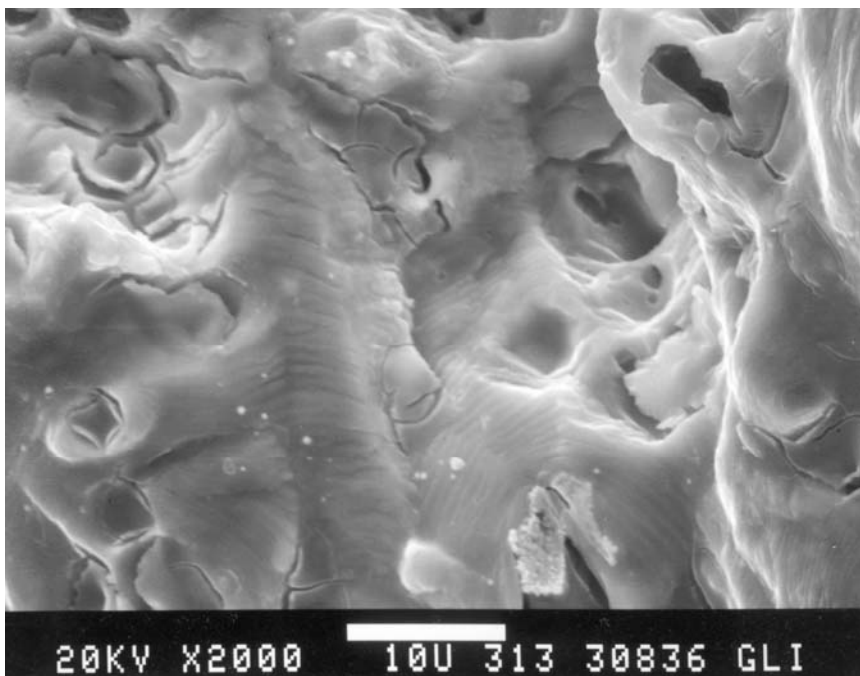
Figure 41. Detail of Area A in Figure 40 Showing Characteristic Mud Cracking and Vague Fatigue Striations
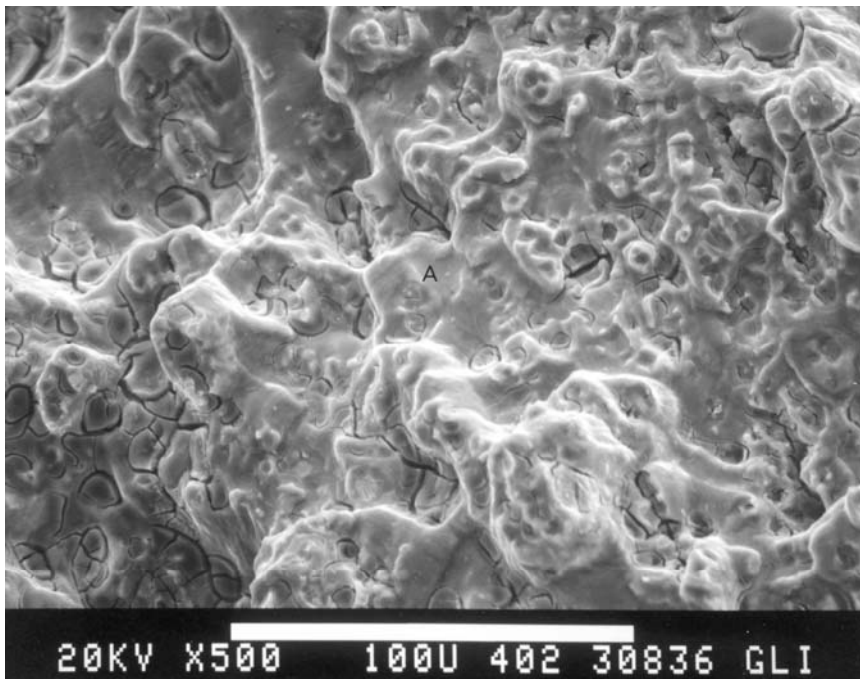
Figure 42. SEM of Area D in Figure 35; Near the Corrosion-free Surface Away from the Corroded Surface
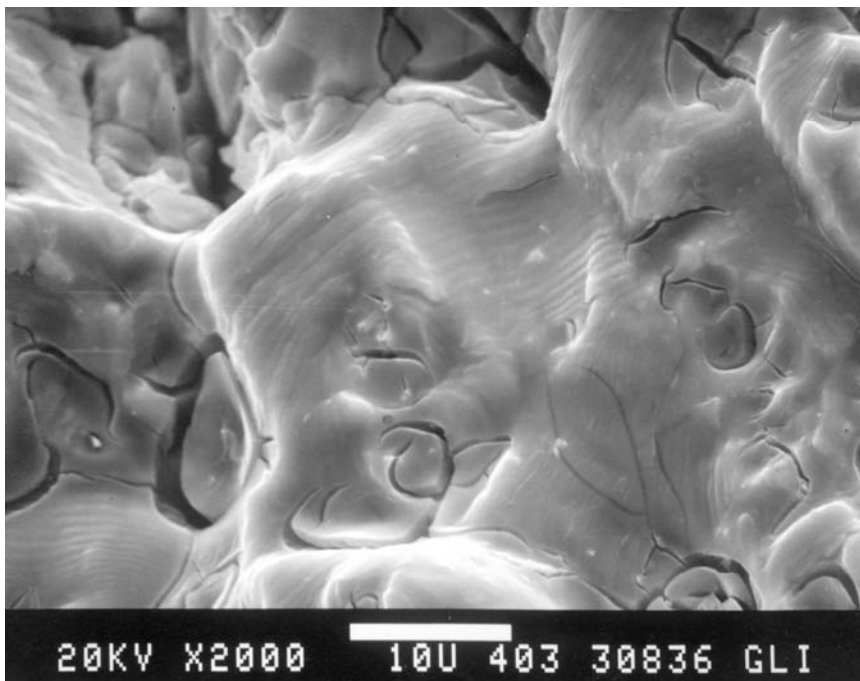
Figure 43. Detail of Area A in Figure 42 Showing Characteristic Mud Cracking and Vague Fatigue Striations
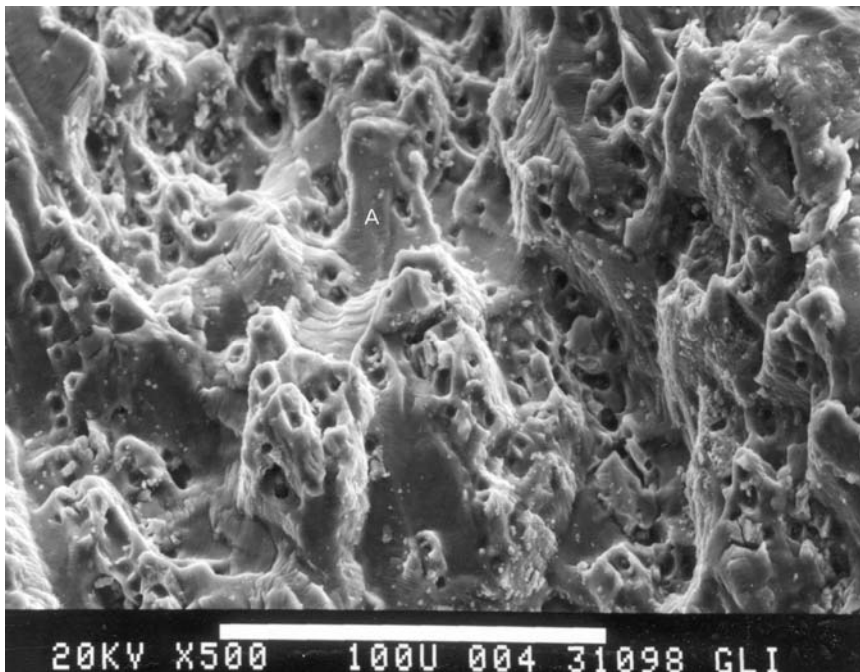
Figure 44. SEM of Aluminum Alloy 2024-T3 Precharged with Hydrogen and Fatigue Laboratory Air (1 Hz, R=0.1); Near the Specimen Surface
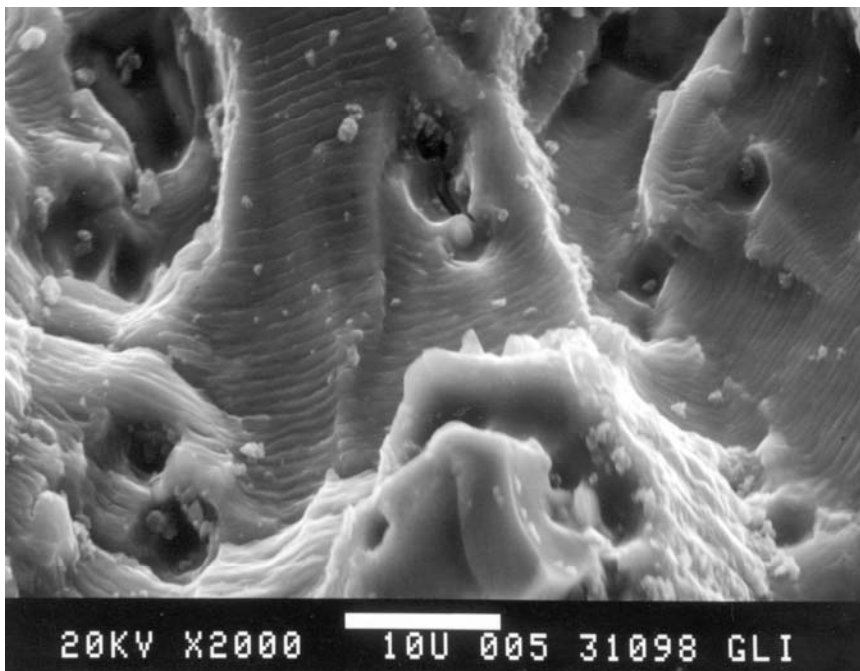
Figure 45. Detail of Area A in Figure 44 Showing a Mixture of Areas with Fatigue Striations and Ductile Rupture
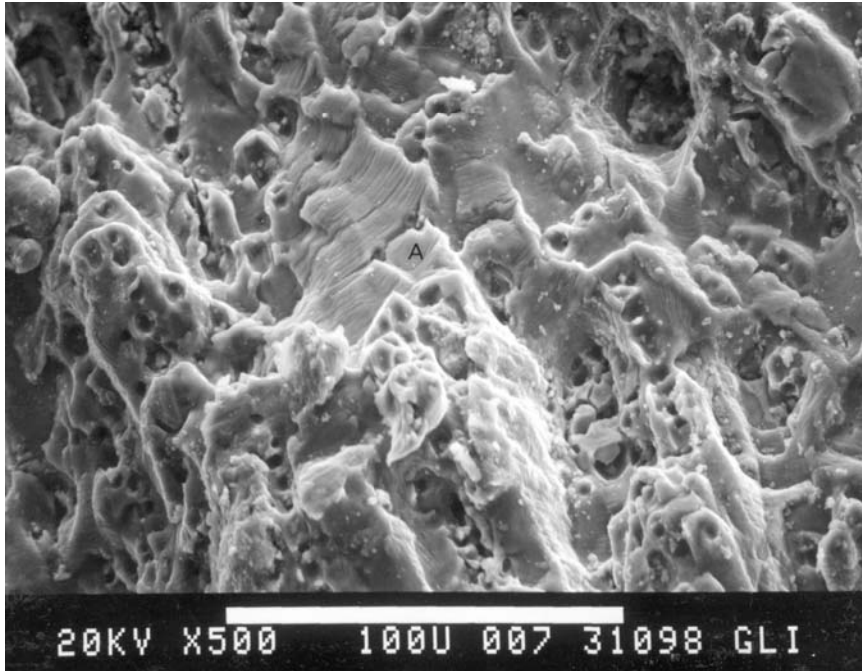
Figure 46. SEM of Aluminum Alloy 2024-T3 Precharged with Hydrogen and Fatigue in Laboratory Air (1 Hz, R=0.1); Away from Specimen Surface
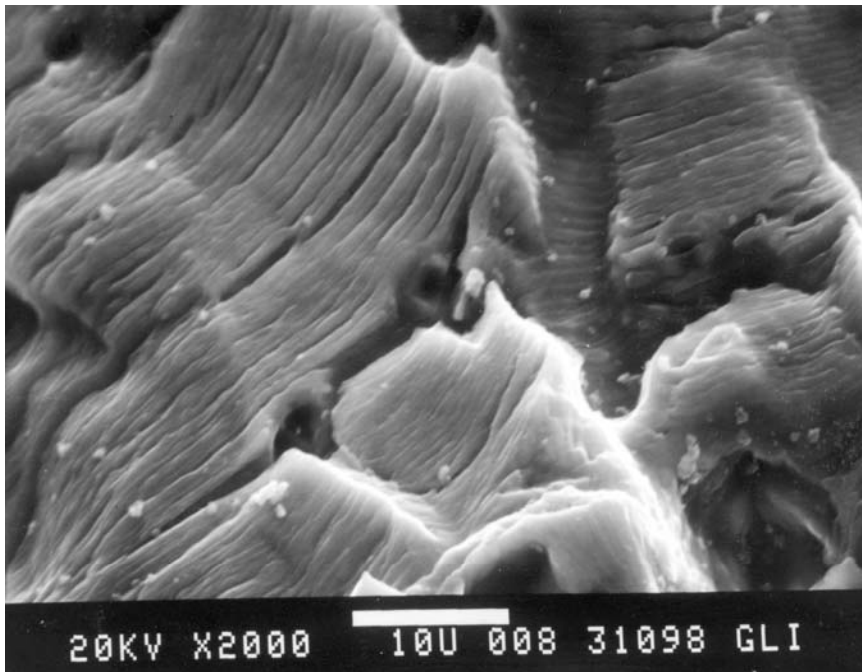
Figure 47. Detail of Area A in Figure 46 Showing Brittle Fatigue Arrest Markings

5.1.1.2 Alloy 2024-T3 - Discontinuous Corrosion Path

To study the fatigue crack propagation behavior for cracks moving in and out of corroded areas, specific areas along the crack path were corroded or machined, see Figure 48.
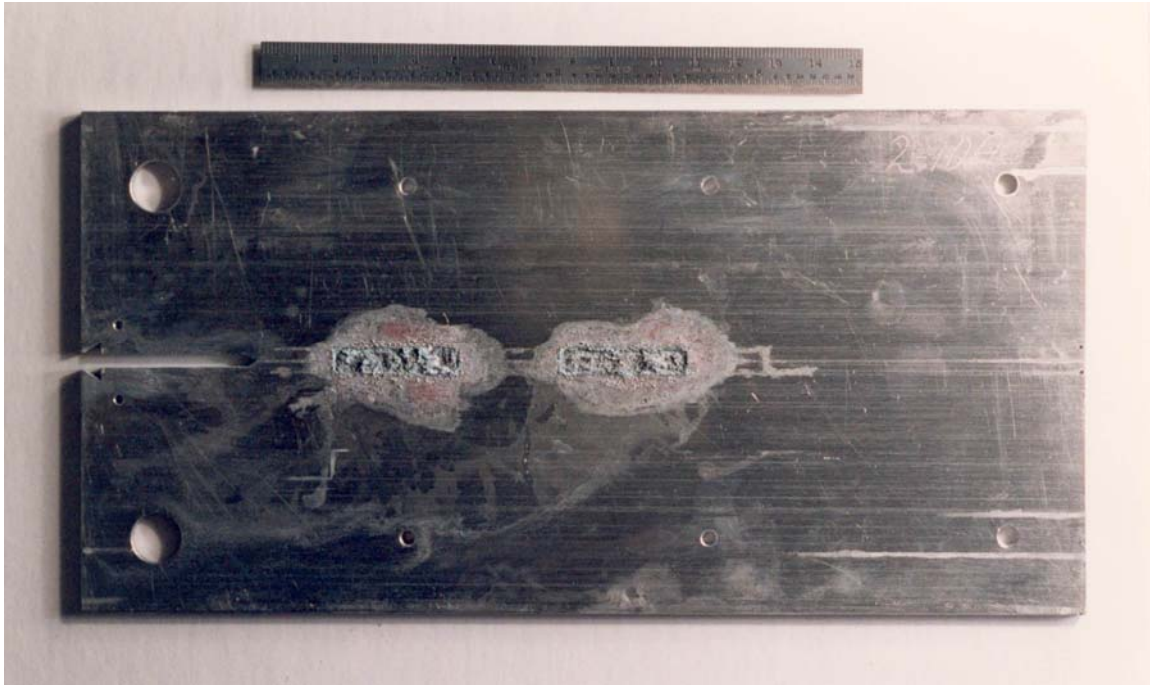
Figure 48. Modified CT Specimen with Corroded Areas in Crack Path; Corroded Areas Created via Two-day Exposure to EXCO Solution

5.1.1.3 Alloy 7075-T6 - Continuous Corrosion Path

Fractography of precorroded (2 and 6 days exposure to the EXCO solution, respectively) and fatigued alloy 7075-T6 coupons is shown in Figures 49 to 52. The fractographs show very little difference in fracture surface appearance for the two exposure times, and indicate, in both cases, a relatively rough surface with a mixture of well-defined striations and apparent ductile fracture. Also, the presence of crater-like features indicates the location of constituent particles. The higher magnification fractographs in Figures 50 and 52 show areas of particularly well defined fatigue striations alongside ductile areas.
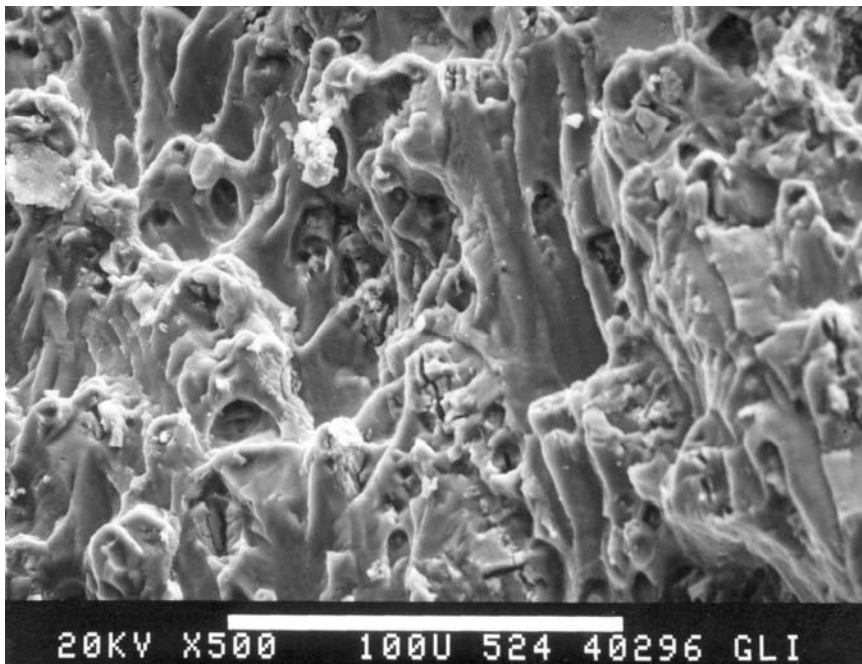
Figure 49. SEM of Aluminum Alloy 7075-T6 Precorroded in the EXCO Solution for 2 Days and Fatigued in Laboratory Air (1 Hz, R=0.1)
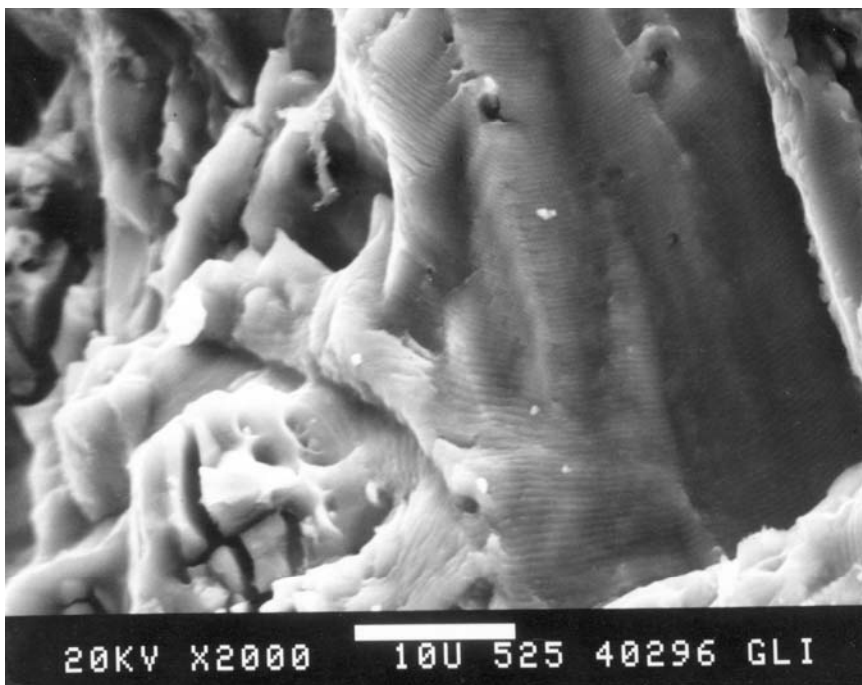
Figure 50. Detail of Area A in Figure 49
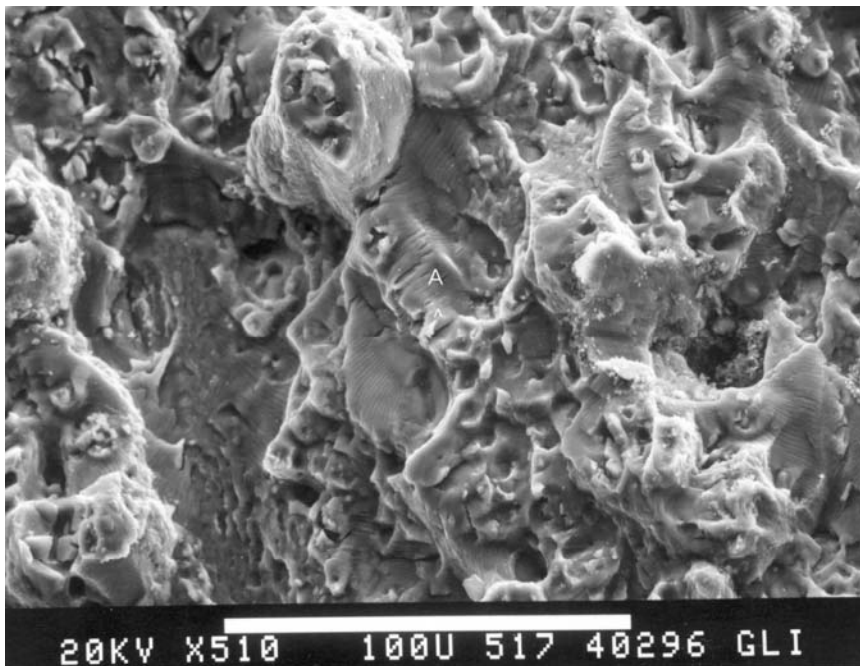
Figure 51. SEM of Aluminum Alloy 7075-T6 Precorroded in the EXCO Solution for 6 Days and Fatigued in Laboratory Air (1 Hz, R=0.1)
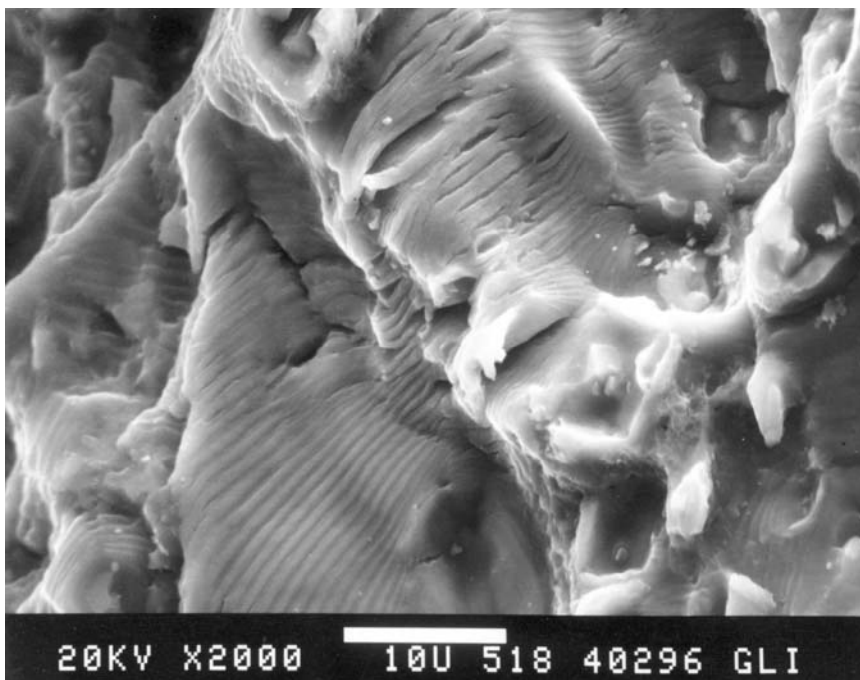
Figure 52. Detail of Area A in Figure 51

To further investigate the possible effect of hydrogen in the alloy lattice on the fatigue crack behavior of alloy 7075-T6, specimens were changed with hydrogen prior to fatigue testing. The method used is described in Section 4.1.2.3.[35] The scanning electron microscope (SEM) micrographs in Figures 53 to 55 show a much rougher fracture surface than those observed on the noncorroded 7075-T6 specimens. Figure 54 show a typical fracture surface with a mixture of relatively flat areas with well-defined fatigue-arrest markings and ductile rupture. Also, particles were found on the fracture surface, similar to those found on the fracture surfaces of the precorroded specimens.

Figure 53. SEM of Aluminum Alloy 7075-T6 Precharged with Hydrogen and Fatigued in Laboratory Air (1 Hz, R=0.1)
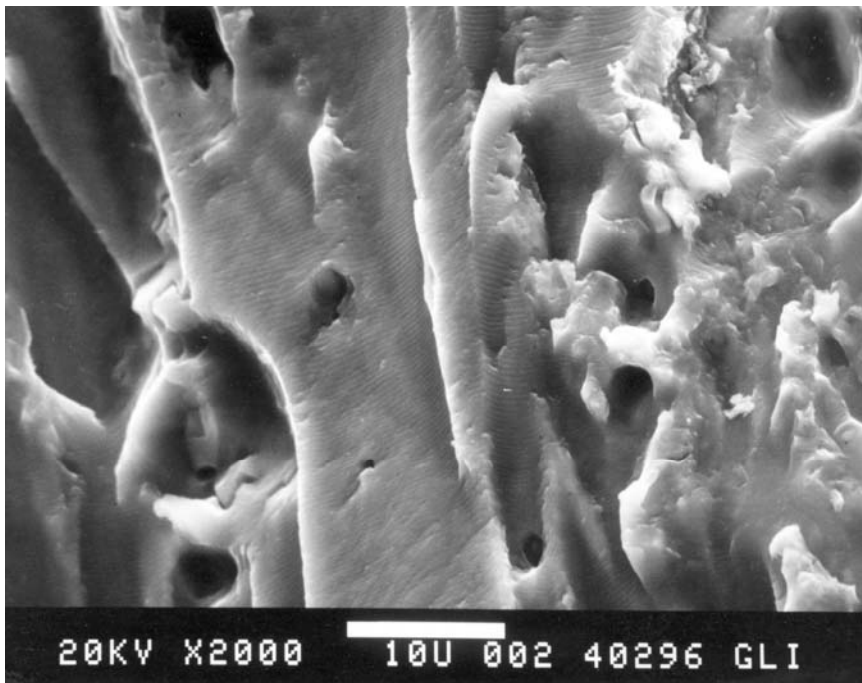
Figure 54. Detail of Area A in Figure 53
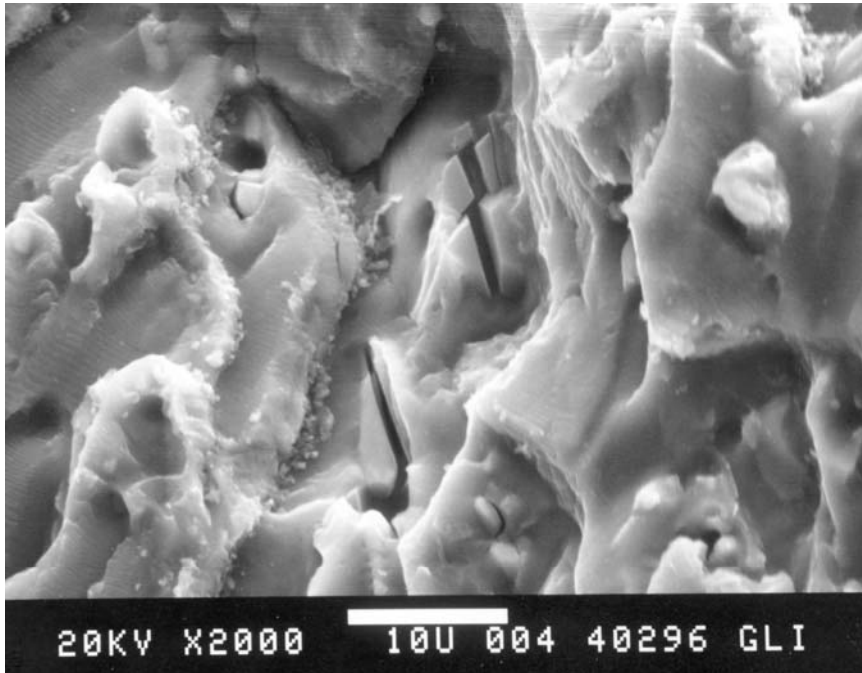
**Figure 55. Detail of Area B in Figure 53 Showing Brittle Secondary Cracking**

5.1.1.4 Alloy 7075-T6 - Discontinuous Corrosion Path

Similar to the tests described above for alloy 2024-T3, fatigue crack propagation experiments were conducted on partially machined and corroded modified CT coupons.

5.1.2 Constant ΔK Testing

The results of the constant ΔK tests on standard CT 7075-T6 specimens are presented in Figure 56. Figure 56 indicates that crack growth rates generated from the reference specimen are higher than those from the corroded specimen. This behavior may be explained by the fact that, when calculating the ΔK for these specimens, the actual thickness in the crack path rather than the nominal thickness was used. Therefore, in the case of specimens with reduced thickness, a lower load was applied, resulting in lower crack velocities.
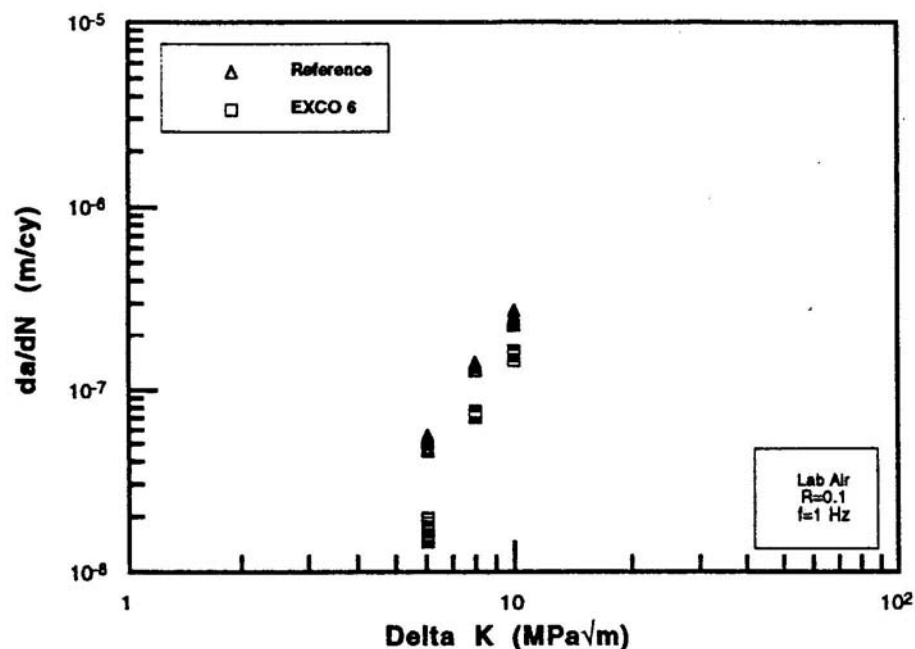
Figure 56. Fatigue Crack Growth Data for Aluminum Alloy 7075-T6 CT Specimens in As Received Condition and Precorroded in the EXCO Solution for 2 Days; Fatigue cracked at Three(3) Constant ΔK Levels

Figure 57 compares crack growth curves derived from increasing ΔK testing of standard CT specimens with different amounts of corrosion. No effects of the preexisting corrosion on fatigue crack growth were observed for this type of specimen.
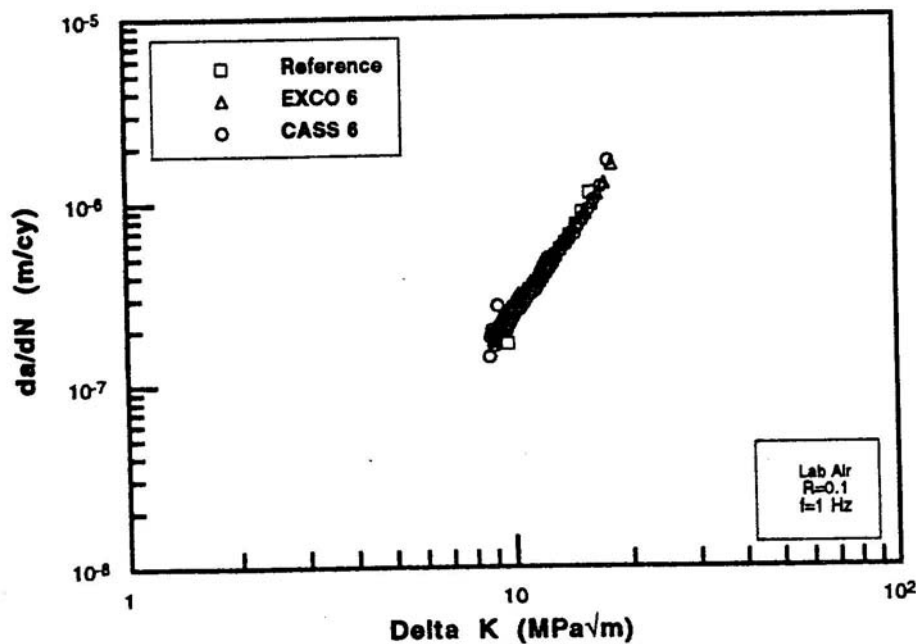
Figure 57. Fatigue Crack Growth Data for Aluminum Alloy 7075-T6 CT Specimens with Different Degrees of Corrosion

5.2 Task 2 - Effect of Preexisting Corrosion on Fatigue Crack Initiation

The results of the initiation experiments as well as the results of additional fractographic and optical examinations are presented for aluminum alloys 2024-T3 and 7075-T6 in the following sections. In the first part, the results for fatigue crack initiation and crack growth in extended blunt notch specimens are presented. In the second part, the results of crack initiation in tensile type specimens under slow-strain-rate conditions are presented.

5.2.1 Fatigue Crack Initiation and Crack Growth

5.2.1.1 Aluminum Alloy 2024-T3

To gain insight into the effects of different types and degrees of corrosion on fatigue crack initiation of aluminum alloy 2024-T3, the net stress was plotted as a function of number of cycles-to-initiation (N_i), as measured with the dc electrical potential drop method. Net stresses were also plotted as a function of number of cycles-to-failure (N_f). Figures 58 and 59 show the S-N_i and S-N_f for various types and degrees of corrosion. The cycles-to-crack initiation were defined with the potential drop method, as was discussed in more detail in Section 4.2.2.

50
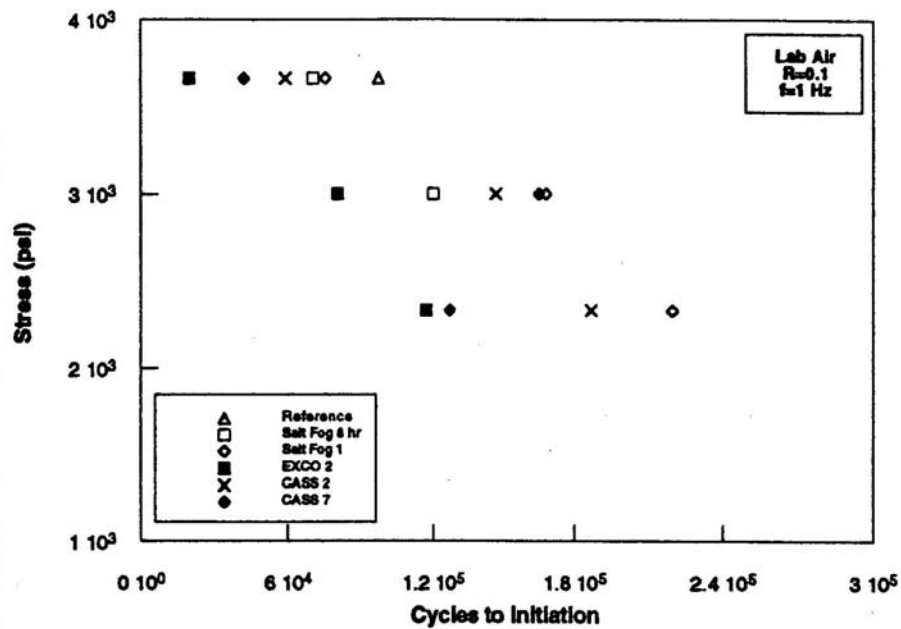
Figure 58. S-N Curves Showing Cycles to Fatigue Crack Initiation in Aluminum Alloy 2024-T3 as a Function of Stress for ECT Specimens with Different Degrees of Corrosion
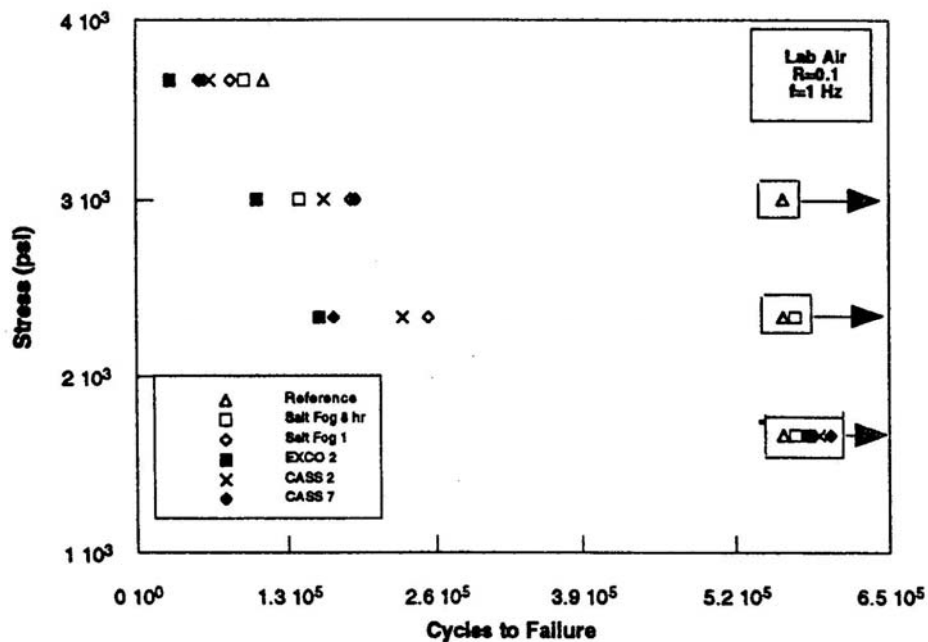
Figure 59. S-N Curves Showing Cycles to Failure of Aluminum Alloy 2024-T3 as a Function of Stress for ECT Specimens with Different Degrees of Corrosion

51

The degrees of corrosion in Figures 58 and 59 are ranked in a qualitative manner, ranging from 8 and 24 hours exposure to a 5-percent NaCl salt spray environment (light pitting), to 2 and 7 days exposure to a CASS environment (severe pitting), and 2 days exposure to an EXCO environment (exfoliation corrosion). The corrosion depths were measured optically from metallographic cross sections at locations along the thickness of the specimens (see Figures 60 and 61). Based on these measurements, the maximum pit depth in the notch was determined. The depth of exfoliation corrosion was fairly uniform along the thickness of the specimen (see Figure 62).

Fractographic examination of the pitted and fatigued specimens show a peculiar pit morphology. As shown in Figures 63 and 64, the pits are disc shaped and oriented along or parallel to the grain boundaries. Fractography and optical microscopy demonstrate that the deepest pit is not necessarily the nucleation site for fatigue cracks. Specifically, fractography, shown in Figures 64 and 65, indicates that crack nucleation sites are often along the side of a pit at a constituent particle or other discontinuity, rather than at the tip or bottom of the pit. The fatigue crack nucleation site indicated in Figure 65 further indicate that the initial crack growth appears to be quasi-cleavage cracking. Figures 66 and 67 show scanning electron fractographs of alloy 2024-T3, precorroded in an EXCO solution for 2 days. The fractographs indicate multiple initiation sites along the corroded region near the notch of the specimen. Also, Figure 67 shows extensive quasi-cleavage near the corroded area.
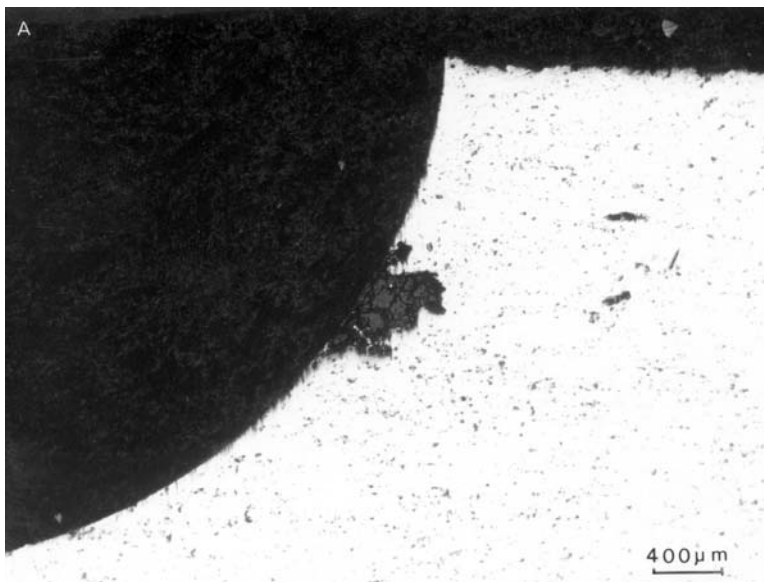
Figure 60. Optical Micrographs of Metallographic Cross Sections of Aluminum Alloy 2024-T3 ECT Specimens Precorroded in the CASS Environment for 7 Days: (a) Cross Section at 0.045 Inch (1.14 mm) from Surface
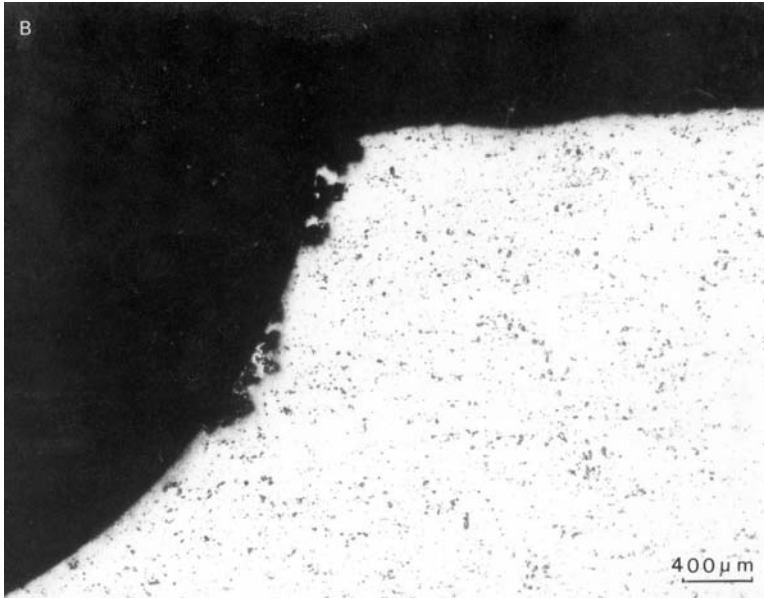
Figure 61. Optical Micrographs of Metallographic Cross Sections of Aluminum Alloy 2024-T3 ECT Specimens Precorroded in the CASS Environment for 7 Days; Cross Section at 0.061 Inch (1.55 mm) from Surface
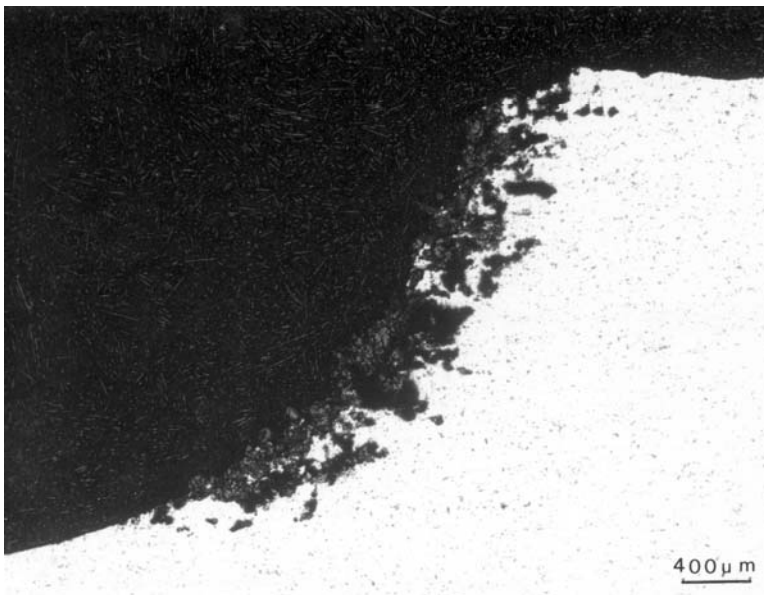
Figure 62. Optical Micrograph of Metallographic Cross Section through an Aluminum Alloy 2024-T3 ECT Specimen Precorroded in the EXCO Solution for 2 Days and Fatigued in Laboratory Air (5 Hz, R=0.1)
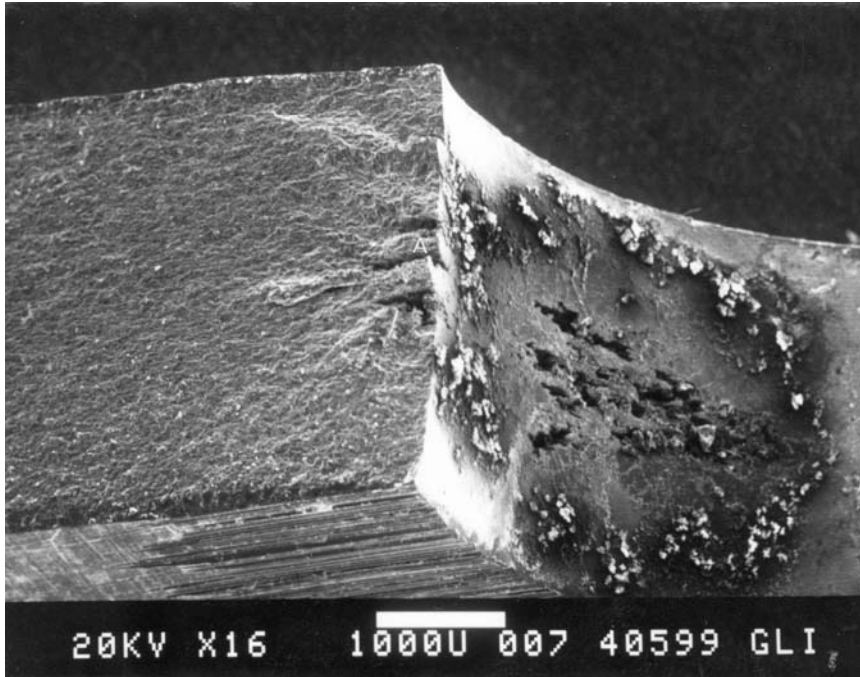
Figure 63. SEM of Aluminum Alloy 2024-T3 ECT Specimen Precorroded in the CASS Environment for 7 Days and Fatigued in Laboratory Air (5 Hz, R=0.1)
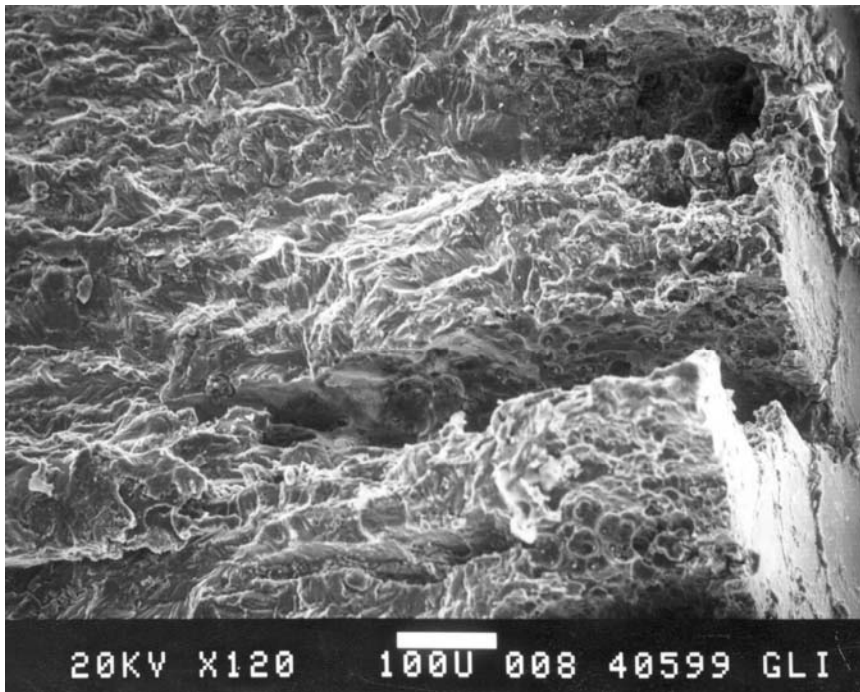
Figure 64. Detail of Area A in Figure 63 Showing the Deep Pits from Which Fatigue Cracking Originated
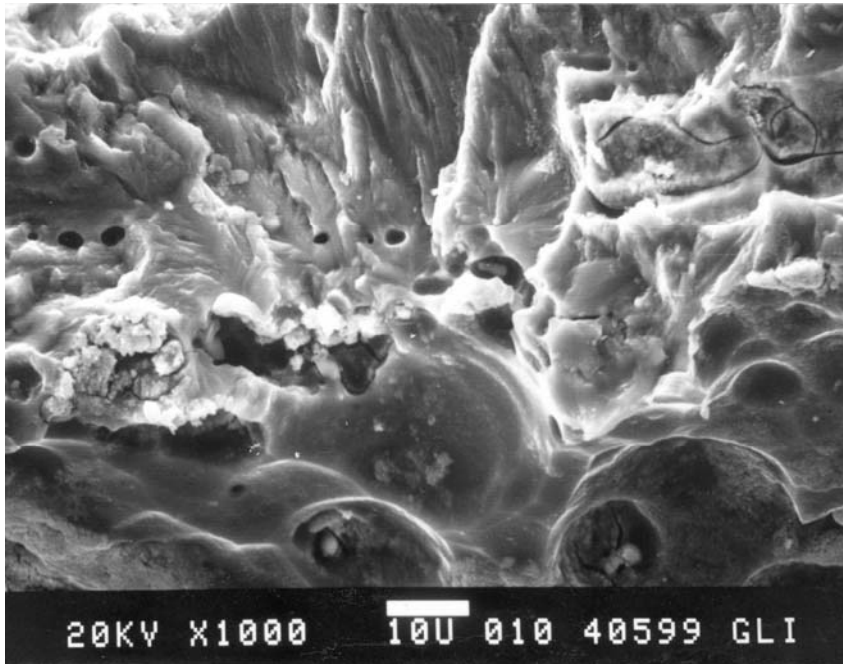
Figure 65. Detail of Area A in Figure 64 Showing a Nucleation Site for Fatigue Cracking on the Side of an Elongated Pit
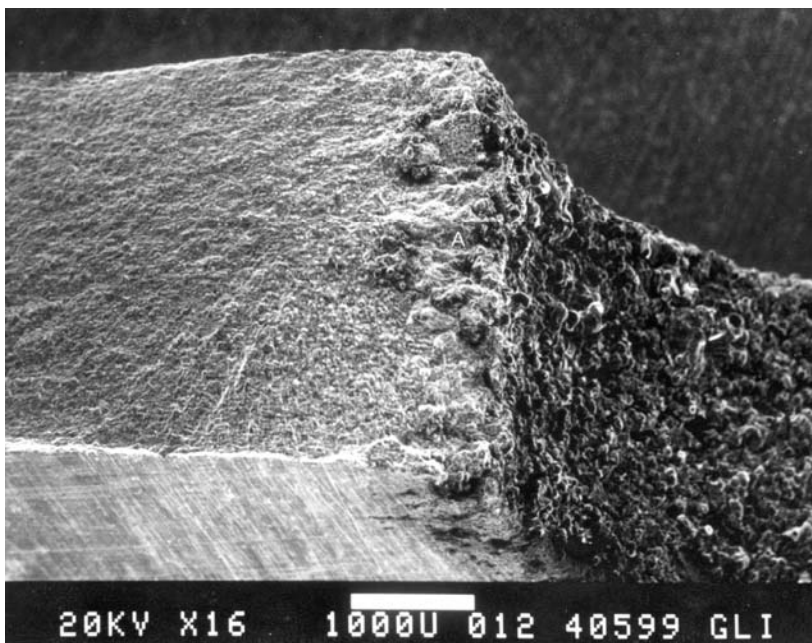
Figure 66. SEM of Fracture Surface of an Aluminum Alloy 2024-T3 ECT Specimen Precorroded in the EXCO Solution for 2 Days and Fatigued in Laboratory Air (5 Hz, R=0.1)
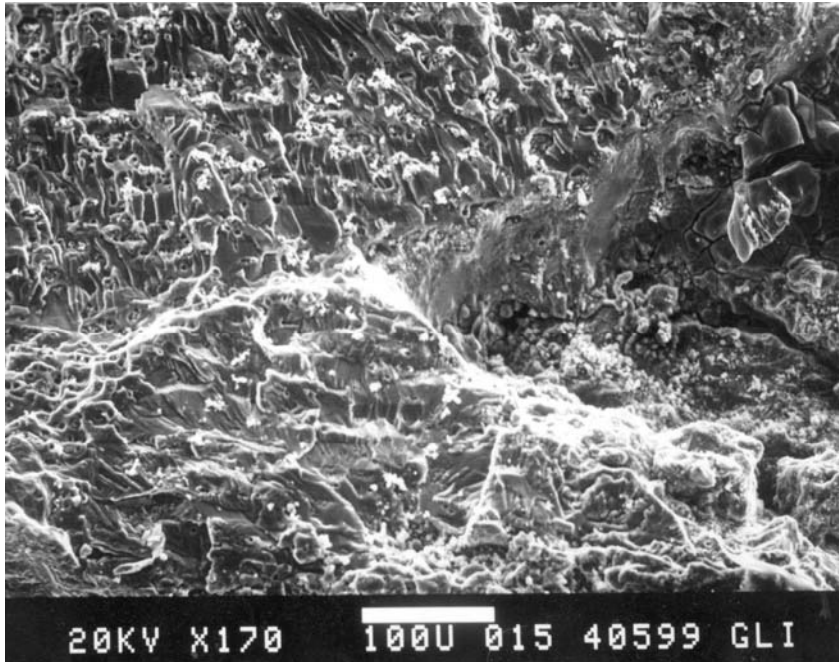
Figure 67. Detail A in Figure 66 Showing Quasi-Cleavage Origination from Various Nucleation Sites
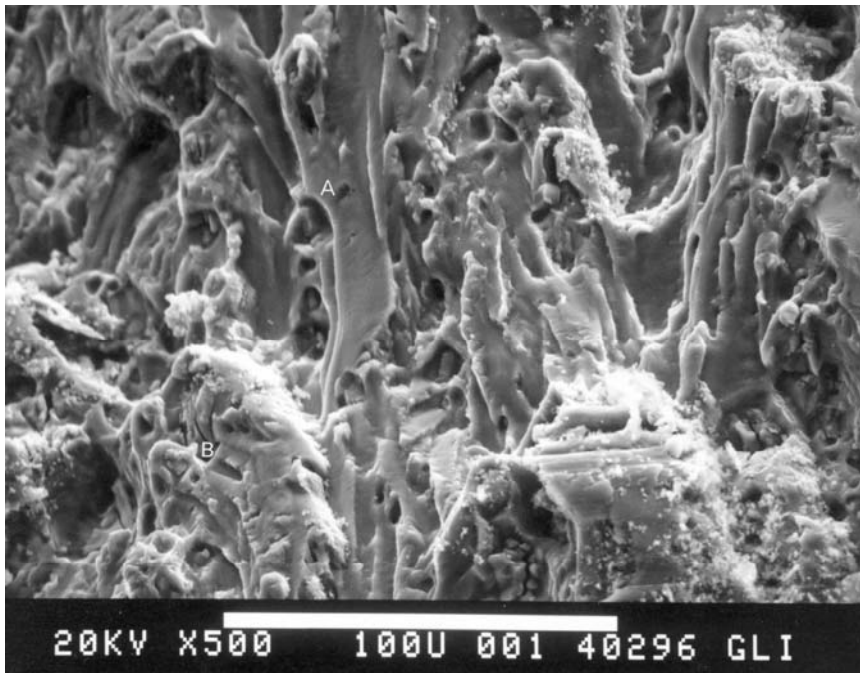
5.2.1.2 Aluminum Alloy 7075-T6

As in the case of alloy 2024-T3, the maximum net stress was plotted as a function of the cycles-to-fatigue-crack-initiation and cycles-to-failure, see Figures 68 and 69. Comparison of Figures 58 and 68 indicates that corrosion has a far greater effect on fatigue crack initiation in alloy 7075-T6 than on fatigue crack initiation in alloy 2024-T3. Although the S-N_i and S-N_f curves for uncorroded 2024-T3 and 7075-T6 appear similar, the cycles-to-crack initiation and cycles-to-failure are much lower for the 7075-T6 alloy. Further examination of the curves indicate that most of the differences in failure time of the two alloys are the result of crack nucleation and early crack propagation.
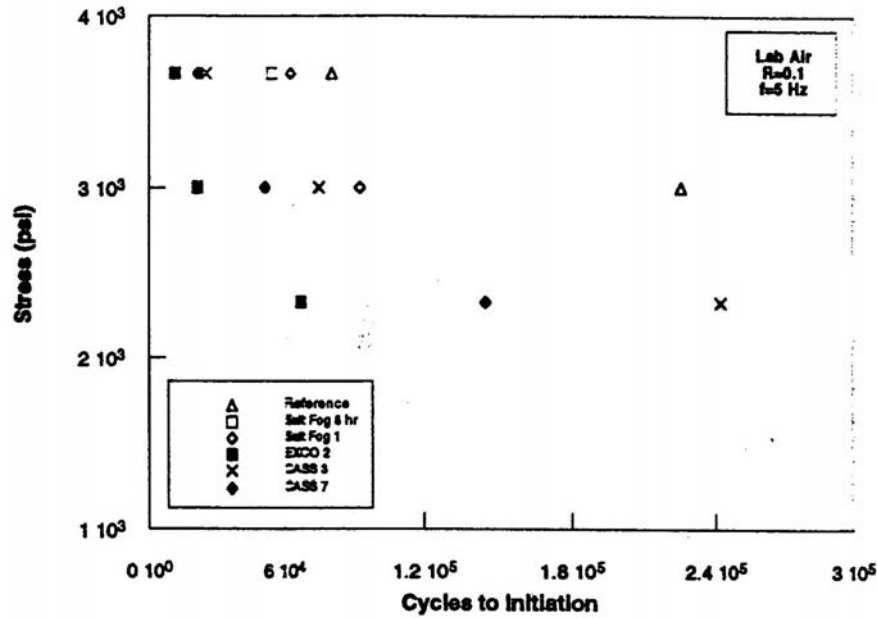
Figure 68. S-N Curves Showing Cycles-to-Fatigue Crack Initiation of Aluminum Alloy 7075-T6 as a Function of Stress for ECT Specimens with Different Degrees of Corrosion
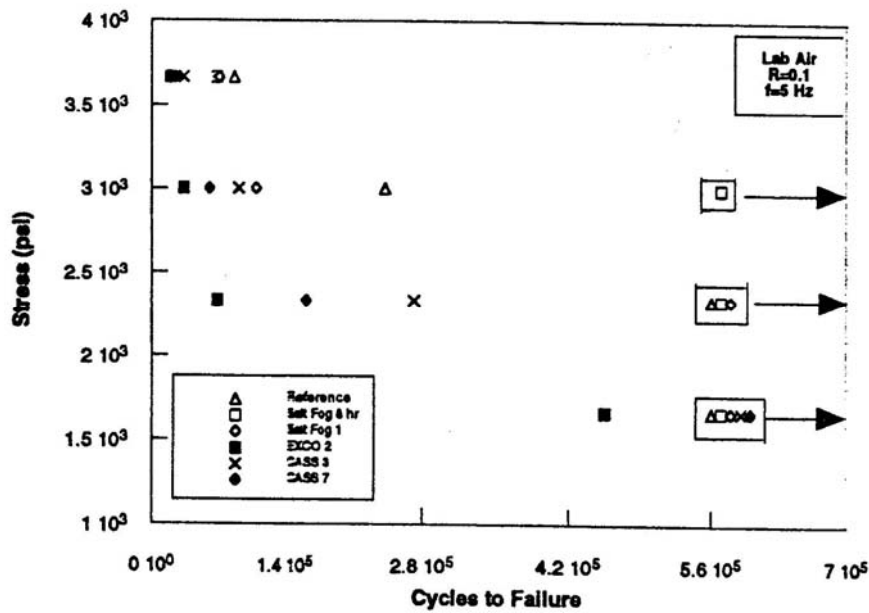
Figure 69. S-N Curves Showing Cycles-to-Failure in Aluminum Alloy 7075-T6 as a Function of Stress for ECT Specimens with Different Degrees of Corrosion

Following the fatigue tests, detailed fractography and metallography were conducted. Figure 70 shows a low power fractograph of an extended blunt-notched specimen exposed to the EXCO solution for 2 days prior to fatigue loading, and fatigued at a maximum stress of 3.8 ksi (26.2 MPa). The fractograph shows exfoliation corrosion in the lower right corner with various crack nucleation sites. A higher magnification SEM in Figure 71 shows a detail of the root of the notch and various crack nucleation areas with quasi-cleavage fracture. Detailed micrographs such as in Figure 72 show better evidence of quasi-cleavage features, as well as secondary cracks which are perpendicular to the main fracture surface and appear to have originated from the corroded regions. Optical micrographs of metallographic cross sections perpendicular to these secondary cracks, show that corrosion had propagated along the grain boundaries. Moreover, the micrograph shows extensive intergranular attack, particularly in the middle of the specimen. The intergranular cracking is similar to intergranular stress corrosion cracking observed in susceptible 7000-series aluminum alloys.
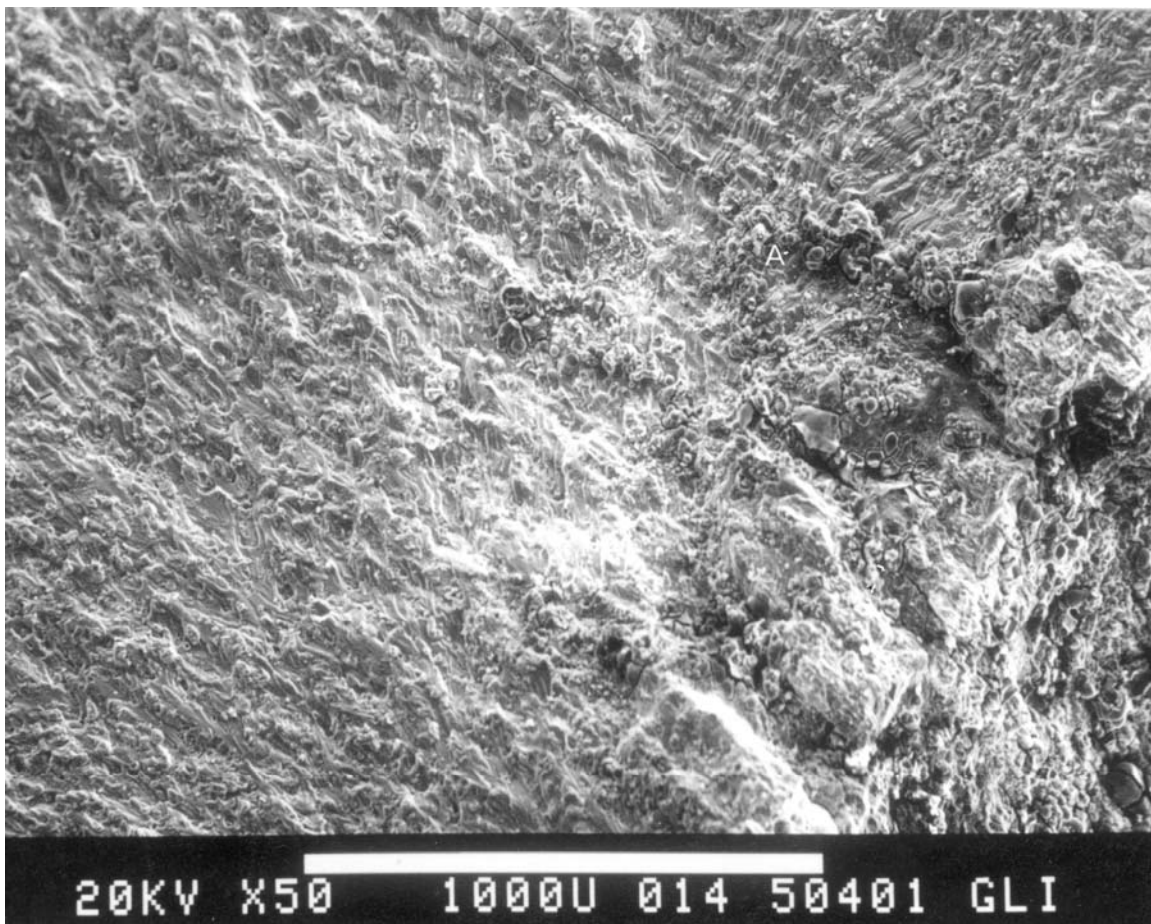
Figure 70. SEM of Fracture Surface of Alloy 7075-T6 ECT Specimen Precorroded in the EXCO Solution for 2 Days and Fatigued in Laboratory Air (5 Hz, R=0.1); Exfoliation Corrosion is Seen on the Right Side of the Micrograph
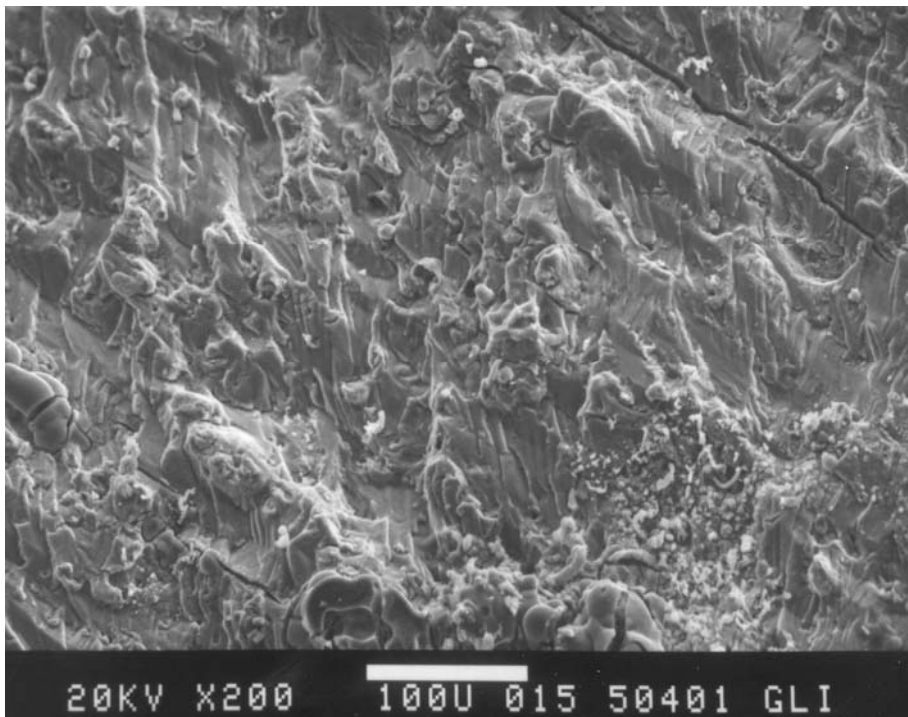
Figure 71. Detail A in Figure 70 Showing Secondary Crack
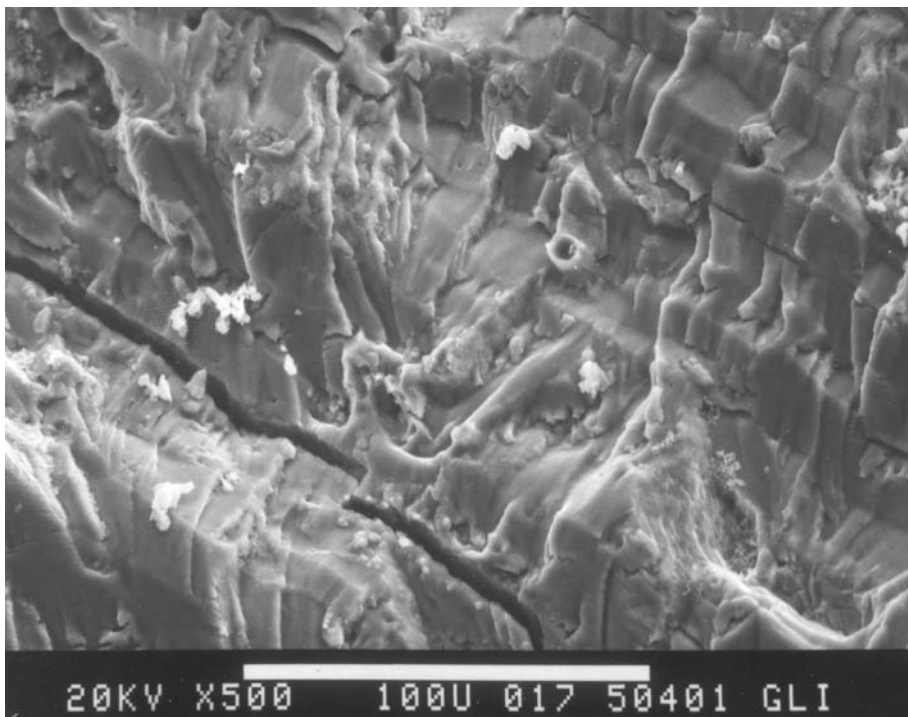
Figure 72. Detail of Secondary Crack Shown in Figure 71

59

Figure 73. Optical Micrograph of Metallographic Cross Section Across the Secondary Crack Shown in Figures 71 and 72
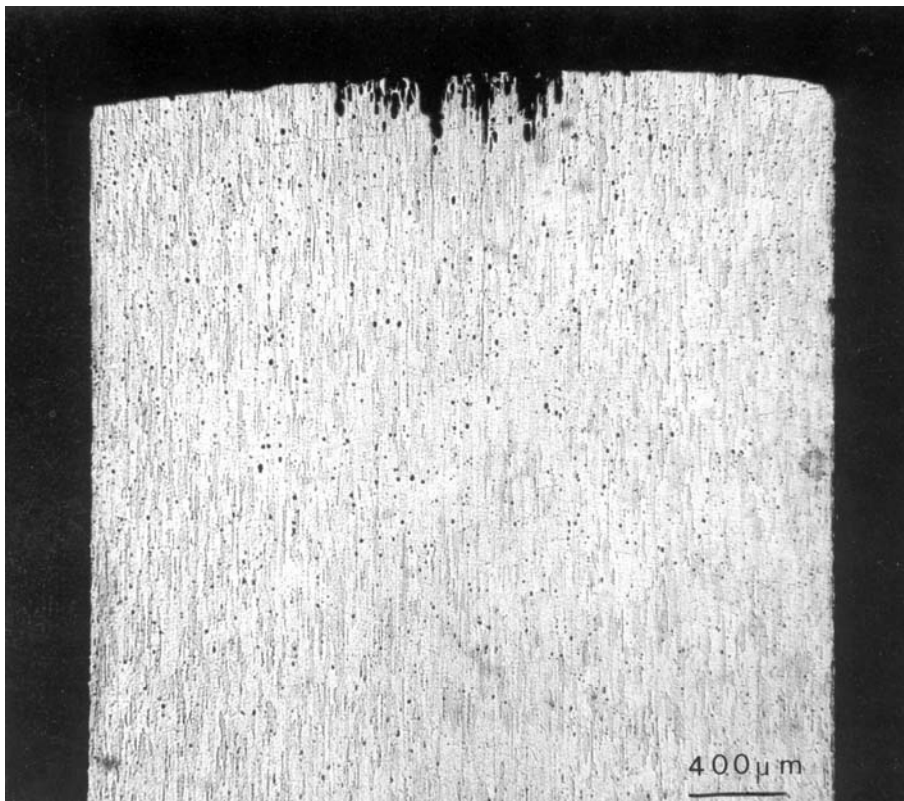
Figure 74. Optical Micrograph of Metallographic Cross Section through the Thickness of an Aluminum Alloy 7075-T6 ECT Specimen Exposed to the EXCO Solution for 2 Days

To examine whether the intergranular cracking observed in Figures 72 and 73 is not just the result of intergranular corrosion from the EXCO exposure, a metallographic cross section was made of a specimen exposed to the EXCO solution for 2 days, but not fatigue cracked. The optical micrograph, shown in Figure 74, was made of a metallographic cross section through the thickness of the specimen, and showed extensive intergranular corrosion. However, no intergranular cracking in the center of the specimen, as shown in Figure 73, was observed.

The observation of extensive intergranular cracking in the direction of the applied load away from the corroded notch suggests that the secondary crack load propagated by a stress-corrosion cracking mechanism. To demonstrate that a stress-corrosion crack could have sufficient driving force to propagate, a FEM was developed. The model shown in Figure 75 demonstrated that the triaxial stress at the tip of the propagating fatigue crack (X-axis) increases as the fatigue crack propagates. The figure also shows that in the triaxial stress away from the main fatigue crack, which decays as function of distance from the main crack. However, these stresses never fall below 10 ksi (68.95 MPa), which is above the threshold stress for stress-corrosion cracking in this alloy, loaded in the short transverse (ST) direction (8 ksi - 55.16 MPa).[43] It is of significance that the stress-corrosion crack could propagate at a considerable distance from the

61

corroded material well into the uncorroded alloy without the presence of an external corrosive environment.
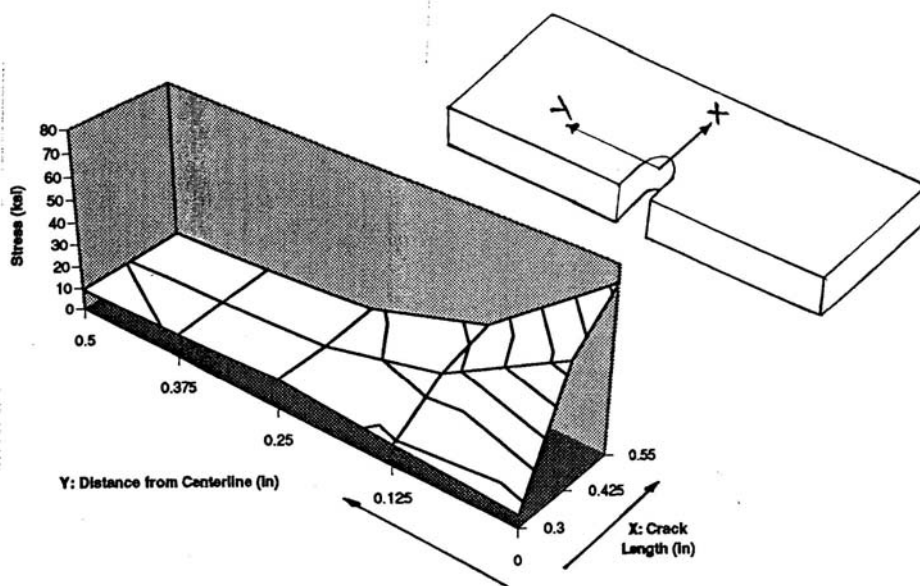
Figure 75. Finite Element Modeling Data Showing the Stress Along the Center Line in an Extended Blunt-Notch Specimen as a Function of Crack Length and Distance from the Centerline

5.2.2 Slow Strain Rate Testing

In an attempt to shed further light onto the possible susceptibility of the aluminum alloys to hydrogen embrittlement and to find a possible link between hydrogen related effects and fatigue cracking in precorroded material, slow strain rate experiments were performed.

Since there is a strong indication that hydrogen plays a role in the interaction between preexisting corrosion and fatigue cracking of aluminum alloy 7075-T6, slow strain rate experiments were conducted for this alloy only. To gain an insight into possible hydrogen contribution to cracking, the test specimens were pulled at two different strain rates, i.e., 1×10^{-5} and 1×10^{-6} sec^{-1}, and in three different environments – laboratory air at a typical relative humidity (RH) of 35 percent, humid air at $\geq$ 95 percent RH, and dry N_2 gas.

However, despite the scatter in the measured data, definite trends can be detected. In Table 5, the results for slow strain rate tests at 10^{-5} sec^{-1} shows little effect of testing environment (laboratory air, air at $\geq$ 95 percent RH, and dry N_2 gas) on the mechanical parameters. This indicates that the strain rate was too high for environmental parameters to have a significant effect on the fracture parameters. However, precorrosion in the EXCO solution did appear to

have an effect on the three mechanical parameters, suggesting a change in material properties as a result of the precorrosion treatment.

Table 5. Slow Strain Rate Results for Alloy 7075-T6 at Strain Rate of 10^{-5} sec^{-1}

Preexposure Environment and Time (days)	Test Environment	Actual Strain Rate (sec^{-1})	Time to Failure (hours)	Max Stress (MPa)	% Elong
None	Lab air	1.07E-5	3:42	525.41	10.5
		1.00E-5	3:00	482.65	8.5
		1.00E-5	4:52	518.50	15.5
EXCO 6	Lab air	1.00E-5	2:45	510.90	7.4
		1.53E-5	2:48	511.00	8.3
		1.34E-5	3:38	539.27	13.2
None	N$_2$	1.00E-5	3:00	502	8.7
		1.09E-5	4:12	529	12.3
None	100% RH	1.08E-5	3:12	503	7.7
		6.25E-6	4:12	535	12.6

Slow strain rate tests at 10^{-6} sec^{-1} showed a definite effect of testing environment on the mechanical parameters of alloy 7075-T6. For example, Table 6 shows a significant increase in time to failure when testing occurs in dry N$_2$ gas. However, unlike in the case of the high strain rate, the effect of precorrosion in the EXCO solution is relatively small.

Table 6. Slow Strain Rate Results for Alloy 7075-T6 at Strain Rate of 10^{-6} sec^{-1}

Preexposure Environment and Time (days)	Test Environment	Actual Strain Rate (sec^{-1})	Time to Failure (hours)	Max Stress (MPa)	% Elong
None	Lab air	1.12E-6	32:36	511.56	9.7
		1.15E-6	31:30	511	11.4
EXCO 6	Lab air	1.14E-6	34:48	520.5	11.4
		1.16E-6	24:30	480	5.8
		1.15E-6	31:36	519.61	13.5
None	N$_2$	1.84E-6	40:06	537.81	13.9
		1.19E-6	43:00	541.12	13.9
None	100% RH	1.17E-6	>30	524	14.6
		1.13E-6	36:24	519	10.5
EXCO 6	N$_2$	1.20E-6	39:44	532.29	11.7
		1.13E-6	42:00	524	14.1

The appearance of the fracture surface and the presence of secondary cracks in the section are qualitative indications of environmentally induced cracking. For example, some specimens were tested in an environment (RH >95 percent), which is known to cause SCC in alloy 7075-T6. Figures 76 and 77 show the fracture surface of a slow strain rate specimen pulled in humid air at a rate of 10^{-6} sec^{-1}. Typically, the fracture surface was very uneven with a mixture of intergranular and ductile transgranular fracture. Moreover, Figure 78 shows extensive secondary cracking on the specimen section. Metallographic cross sections of the specimen gage length clearly showed this secondary transgranular cracking as well as some intergranular attack, see Figures 79 and 80.
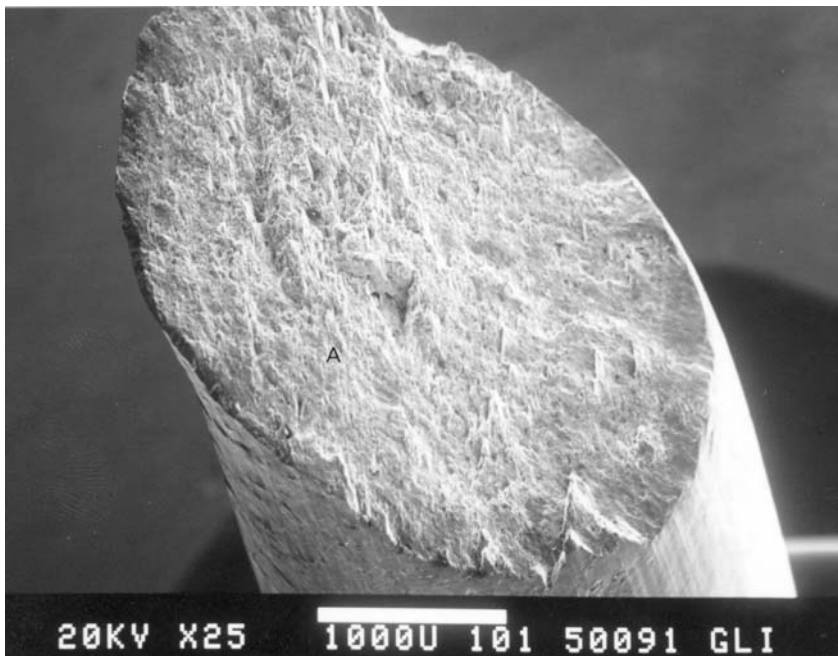
Figure 76. SEM of Fracture Surface of Slow Strain Rate Specimen Pulled at 10^{-6} sec^{-1} in Air with >95 Percent RH
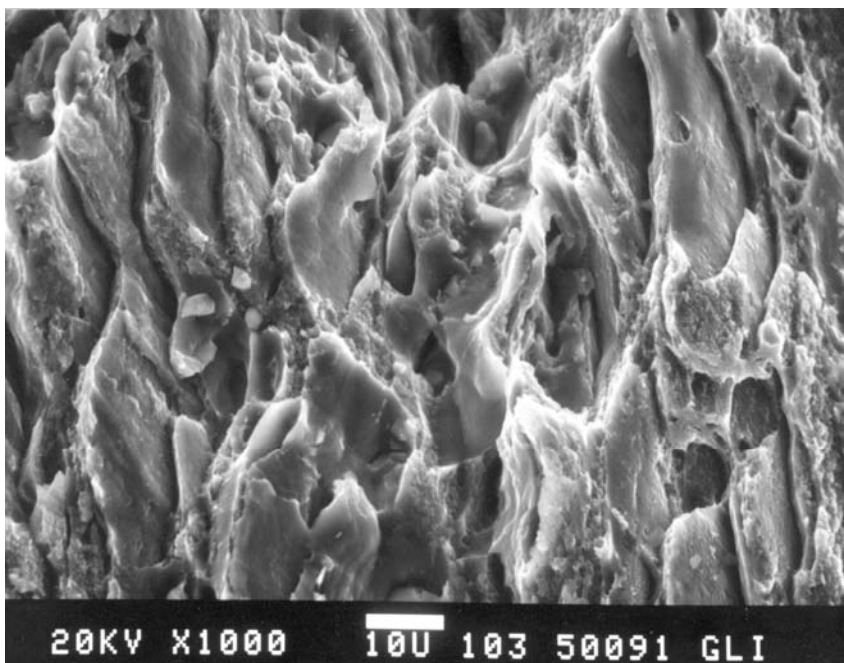
Figure 77. Detail of Area A in Figure 76 Showing Extensive Intergranular Attack
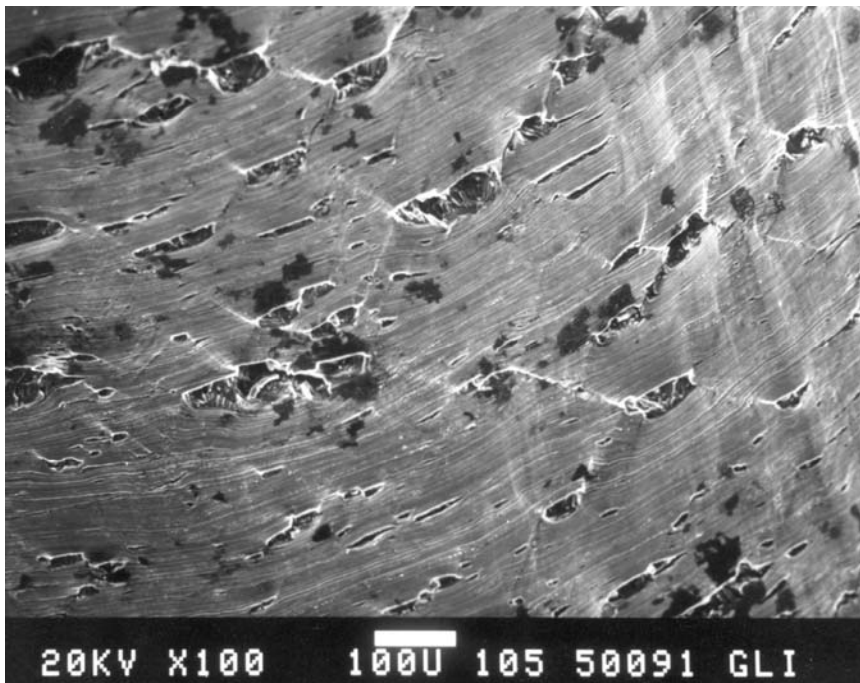
Figure 78. SEM of Length of Specimen Shown in Figure 76
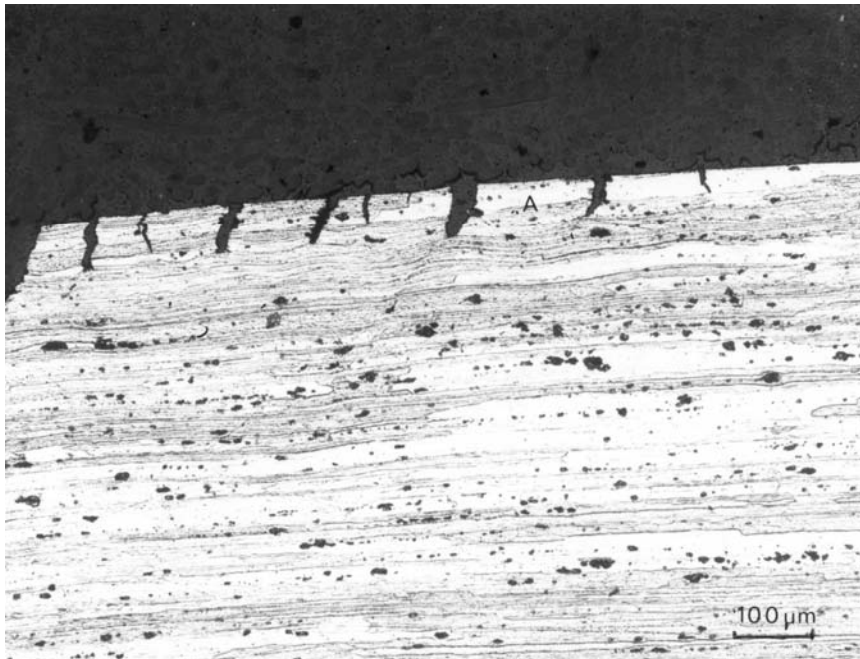
Figure 79. Optical Micrograph of Metallographic Cross Section through Gage Length of Specimen Shown in Figure 76, Showing Extensive Secondary Cracking
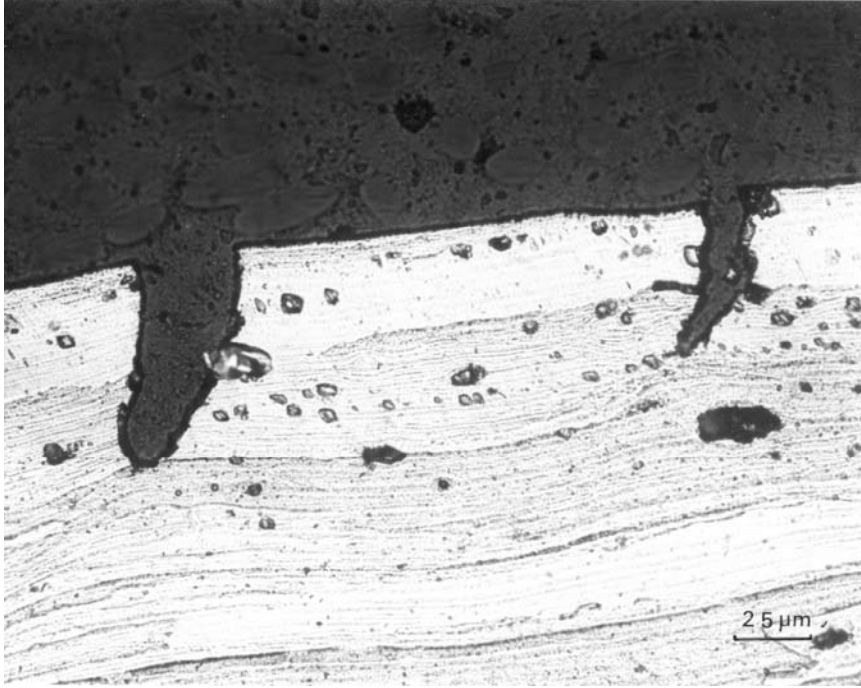
Figure 80. Detail of Area A in Figure 79 Showing Transgranular Secondary Cracking, as Well as Intergranular Attack

When comparing the fracture features of specimens fractured in high humidity air with those of specimens fractured in laboratory air, differences could be observed. The fracture surface in Figure 81 and 82 show primarily ductile failure with little intergranular attack. Specimens precorroded in the EXCO solution for 6 days and pulled in air at 10^{-5} sec^{-1} show fracture features more similar to those obtained in humid air. The so-called precorroded specimens were prepared by exposing bars to the corrosive solution and then machining slow strain rate specimens, such that there was no evidence of corrosion left on the surface of the section. Figures 84 and 85 show extensive intergranular attack perpendicular to the fracture surface. Also, secondary cracks could be detected on the gage length of the slow strain rate specimen.
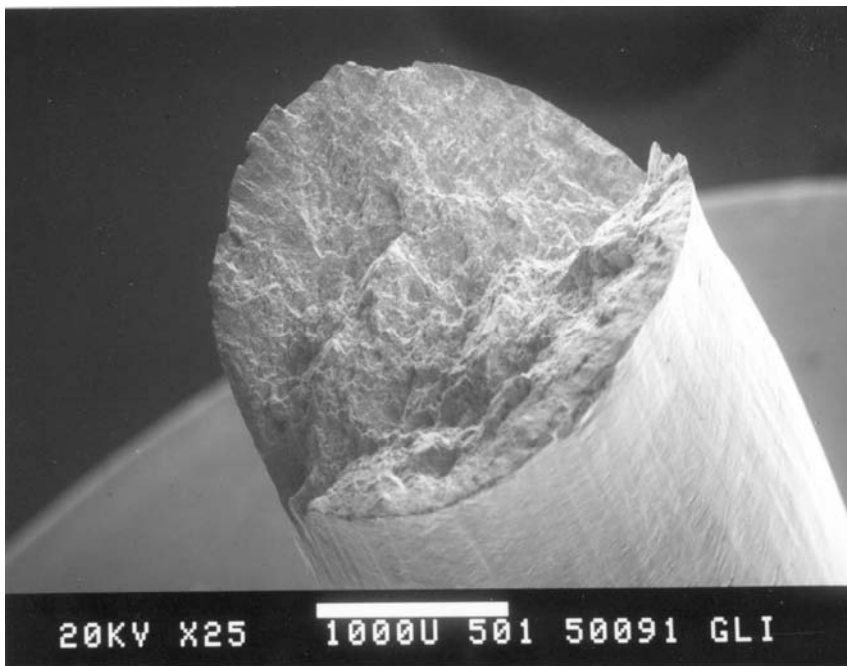
Figure 81. SEM of Fracture Surface of Slow Strain Rate Specimen Pulled at 10^{-6} Sec^{-1} in Laboratory Air
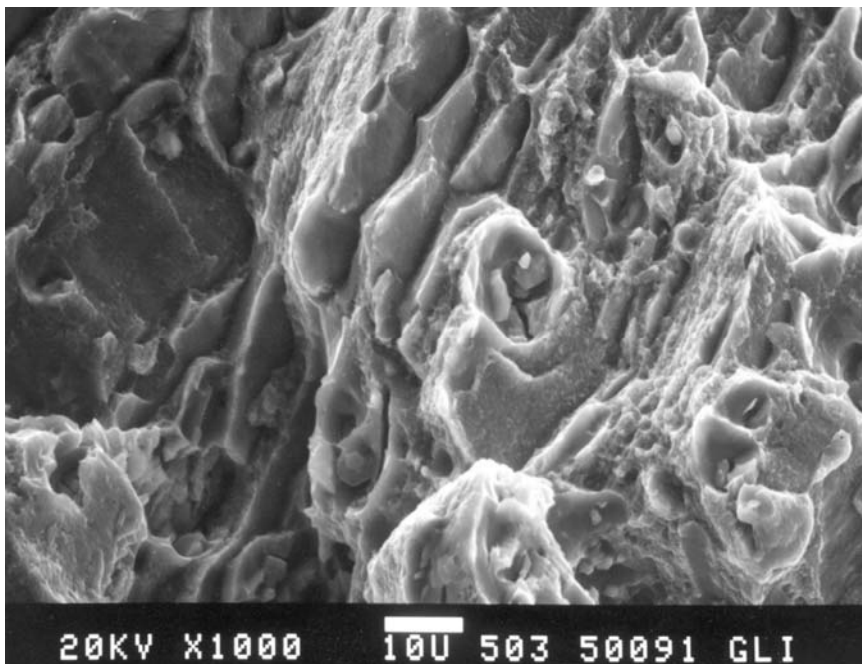
Figure 82. Detail of Figure 81
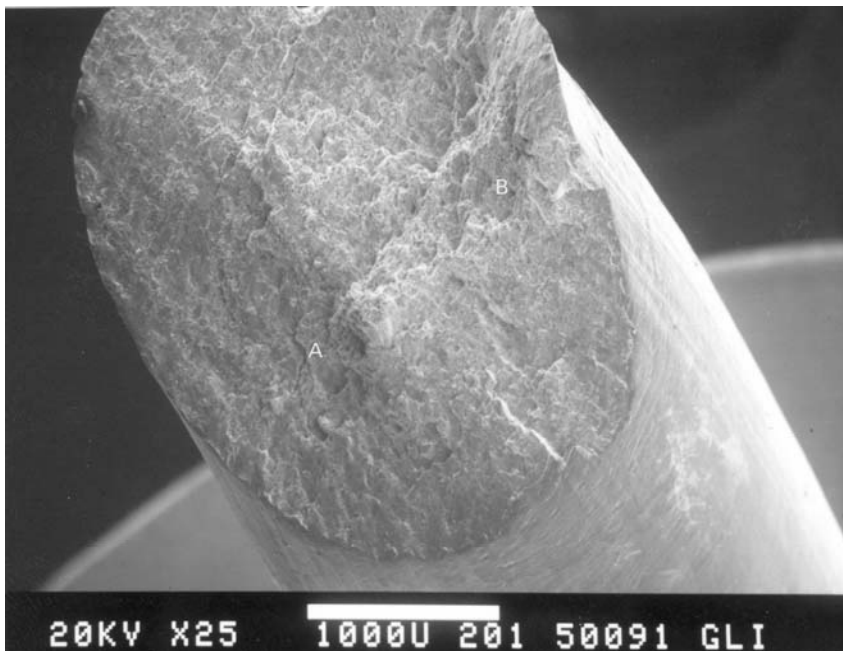
Figure 83. SEM of Fracture Surface of Alloy 7075-T6 Slow Strain Rate Specimen Exposed to the EXCO Solution for 6 Days Prior to Machining and Pulled at 10^{-6} Sec^{-1} in Laboratory Air
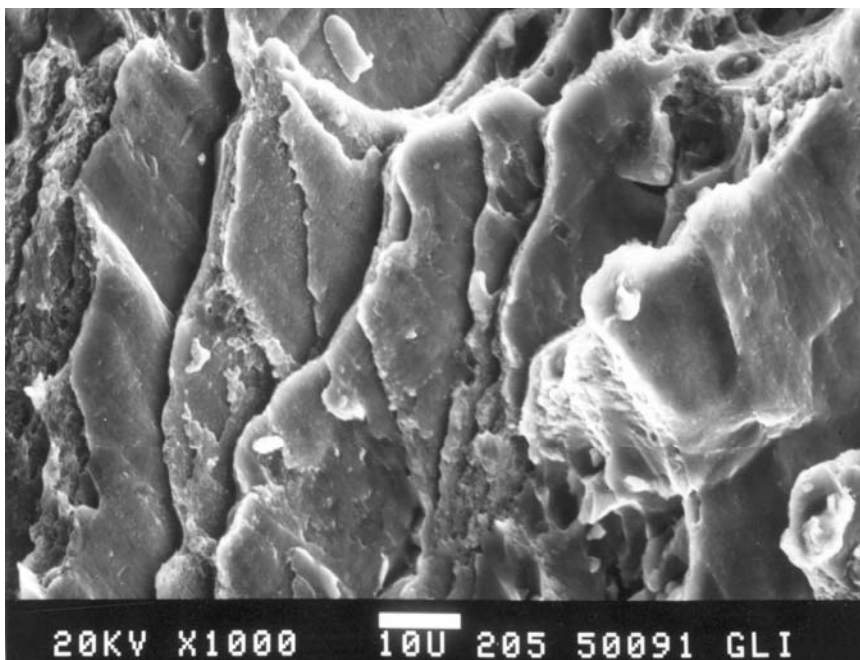
Figure 84. Detail of A in Figure 83 Showing Extensive Intergranular Fracture

69
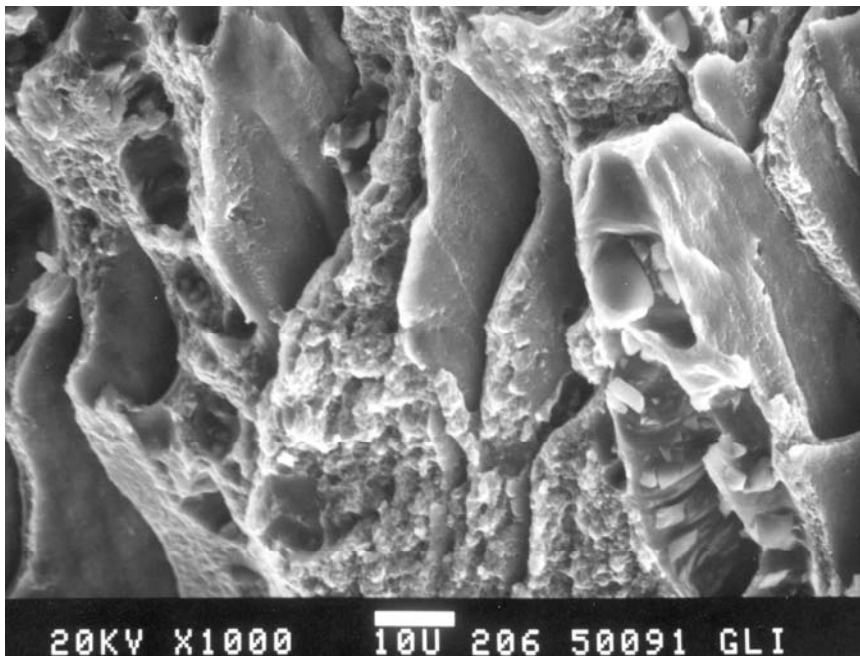
Figure 85. Detail of Area B in Figure 83 Showing Extensive Intergranular Fracture
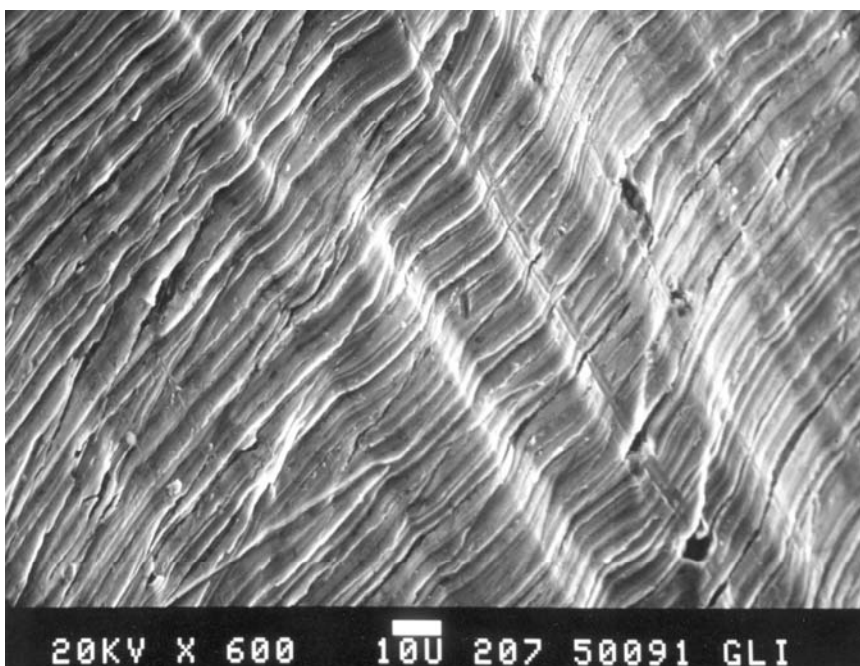
Figure 86. SEM of Gage Section of Specimen in Figure 83

The similarity in fracture behavior between the precorroded and machined specimen fractured in laboratory air, and the specimen fractured in humid air, suggested that failure may have occurred

70

by a similar mechanism. Since it is widely accepted, as discussed in Section 3, that SCC in 7075-T6 occurs by some hydrogen embrittlement mechanism, it may be assumed that preexposure to the EXCO solution resulted in hydrogen enhanced fracture. Since during specimen preparation, all mechanical effects from corrosion were machined away, any possible mechanical effects did not play a role in the fracture process.

5.3 Task 3 – Modeling

5.3.1 Probabilistic Modeling

Data from the damage tolerance analysis of the OV-10A[44] were used as representative input for a risk analysis of a critical, corrosion-prone structural detail. The following paragraphs present a description of the structural detail, the definition of the corrosion scenarios and the results of the risk analysis. It should be noted that for the purpose of this analysis, corrosion is considered to be equivalent to mechanical damage.

5.3.1.1 Details of the Representative Structure

The structural detail selected for this sensitivity analysis was a critical location on the wing lower front spar vertical flange of an observation class, ground-support aircraft, Figure 87. The detail was manufactured from 2024-T3511 aluminum. All of the data from the damage tolerance analyses of 20 locations were available for the aircraft. This particular location was selected because it was in a region of concern with respect to corrosion and it ranked fourth in severity among the 20.
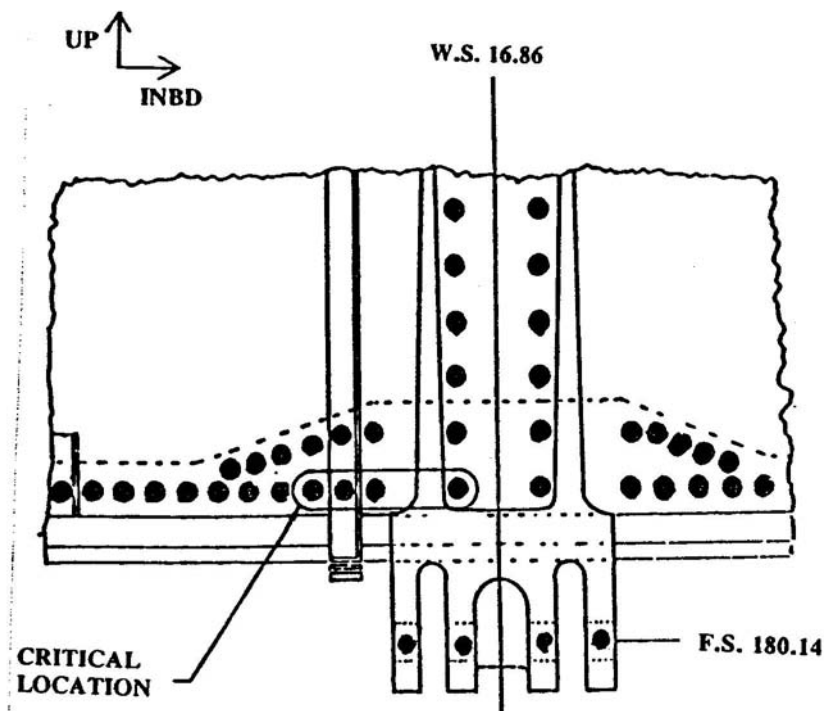
Figure 87. Critical Location at Wing Lower Front Spar Vertical Flange

Figure 88 presents the crack growth life curves (a-versus-T) for the baseline condition (labeled 100 percent) as well as for the detail when the thickness was reduced to 95 and 90 percent. The USAF method for determining inspection intervals for this location is also indicated in Figure 88. The first inspection at this location would be performed at 850 flight hours, i.e., half the flight time required for a 0.05 inch (1.27 mm)-crack to grow to failure under the expected usage spectrum. Because the reliably detected crack size was stated as (0.1 inch - 2.54 mm) for this location, the second and subsequent inspections would be performed at 600 hours (half the flight time required for a 2.54-mm crack to grow to failure. For later reference, note that the 95 percent and 90 percent crack growth life curves would require inspection intervals of 485 and 400 hours, respectively, for the second and subsequent inspections.
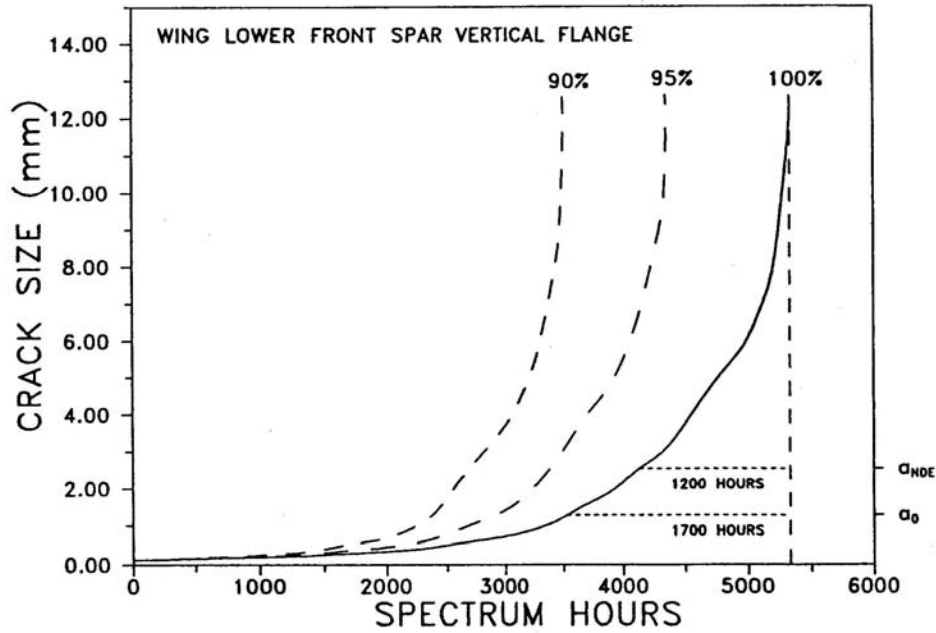
Figure 88. Crack Growth Life Curves for Critical Location at Wing Lower Front Spar Vertical Flange

The flight-by-flight spectrum used to generate the crack growth life curves was obtained from exceedance curves representative of aircraft usage. The Gumbel fit of the maximum stress per flight distribution was obtained using the method outlined in Reference 30. This distribution was applied only to the analyses using the baseline data. When analyses were performed using decreased thickness, the parameters of the Gumbel distribution were scaled as follows. If X has a Gumbel distribution and Y=cX,

$$P\{X \leq x\} = \exp\{-\exp-[x-A]/B\} \tag{5}$$

and

$$P\{Y \leq y\} = P\{cX \leq y\} = P\{X \leq y/c\} \tag{6}$$

$$= \exp\{-\exp-[y-cA]/cB\} \tag{7}$$

The distribution of maximum stress per flight from the scaled stress was also Gumbel with the original parameters multiplied by the scaling factor.

73

The reset crack length after an inspection for the critical location was set at $a_{NDE} = 0.1$ inch (2.54 mm). This quality of inspection could be achieved by using an eddy current system. A common characterization of a_{NDE} is that, given a population of cracks of size a_{NDE}, 90 percent of the cracks will be detected using the inspection system. Experience in the characterization of semi-automated or automated eddy current systems has indicated that a value of σ of about 0.5 is reasonable. Therefore, assuming that POD(1.27) = 0.5 and POD(2.54) = 0.9 lead to $\mu = \ln(1.27)$ and $\sigma = 0.54$. These are the values that were used in all of the PROF runs.

Since there were no available data from which to infer a crack size distribution to initiate the stochastic analyses, it was assumed that the structure had an initial quality equivalent to that which was determined for the A-7D aircraft.[45] This initial quality can be characterized in terms of a Weibull distribution of equivalent crack sizes with a scale parameter of 0.0012 inch (0.03 mm) and a shape parameter of 0.77. Crack growth for very small crack sizes was modeled by back exponential extrapolation from fracture mechanics based crack growth which began at 0.0051 inch (0.13 mm). Very small cracks have no influence on the POF.

There also were no data to characterize the quality of the sites in which cracks have been detected and repaired. Therefore, based on engineering judgment, it was assumed that the quality of repaired cracks can be characterized by an exponential distribution of equivalent crack sizes with the parameter, β, determined such that the probability of an equivalent repair crack exceeding 1.27 mm was 0.001, $\beta = 0.007$ inch (0.18 mm).

Using the baseline conditions, as defined above, the PC version of PROF was used to calculate the single flight probabilities of fracture, as shown in Figure 89. PROF does not output POF values less than 10^{-12}. The sharp drops in POF at 600-hour increments are caused by the reduction in the crack size distributions at the maintenance cycles. After about 3,850 hours, the cycles of fracture risks tend to stabilize. The absolute magnitudes of these baseline fracture probabilities should not be precisely interpreted.
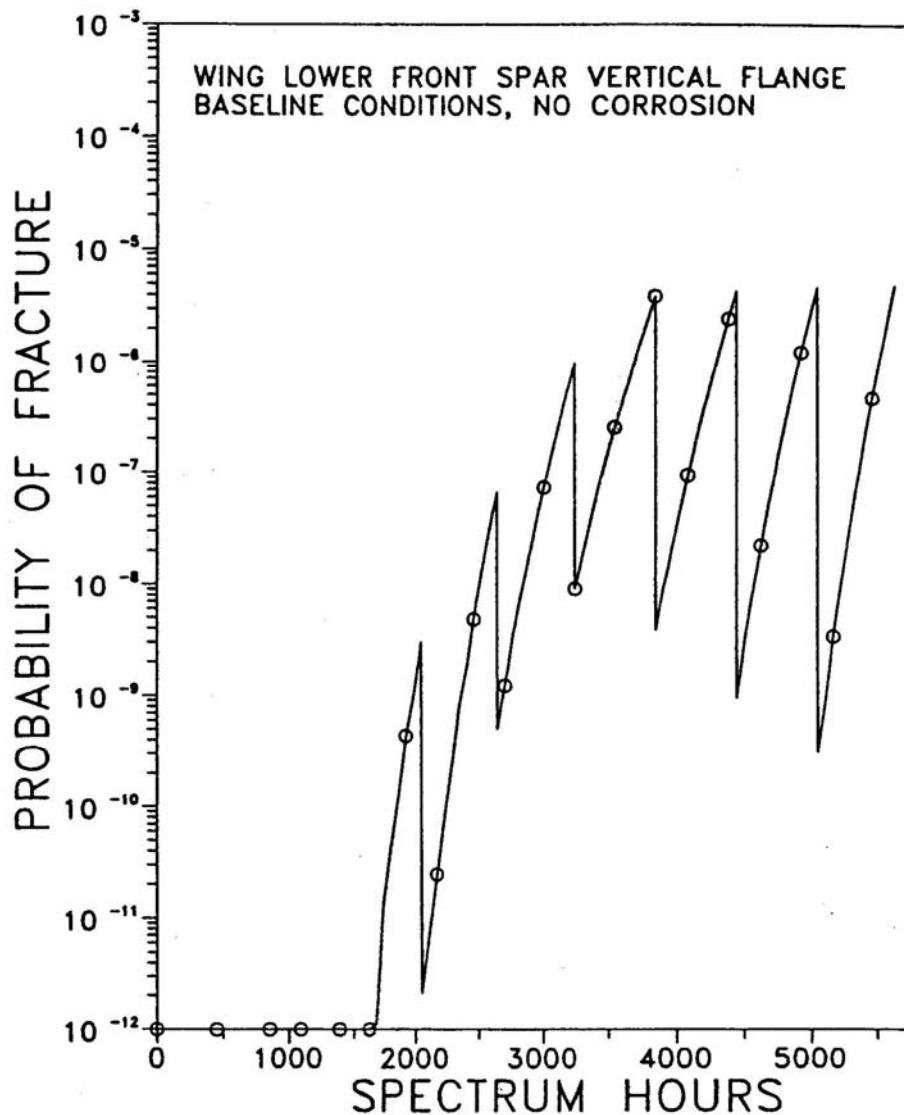
Figure 89. Fracture Risks for Baseline Conditions

5.3.1.2 Corrosion Scenarios

For the purposes of this first order analysis of the effects of corrosion on the POF, corrosion scenarios were defined for both thickness reduction (by the introduction of thickness reductions at two fixed numbers of flight hours) and for pitting. Since this aircraft was being operated an average of 27 hours per month in a corrosive environment, an effective 5-percent thickness reduction at the 2,050 hour inspection (76 months) would not be unreasonable. A second 5-percent reduction (for a total of 10 percent) would not be unreasonable after another 1,800 hours (67 months). Six scenarios were defined from these two corrosion events for comparison with

the baseline single flight fracture probabilities of Figure 89. (Note: 5-percent corrosion should be interpreted as corrosion damage that produces an effective thickness reduction of 5 percent.)

The six thickness reduction scenarios are as follows:

Case 1) 5 percent corrosion at 2,050 hours - undetected.

Case 2) 5 percent corrosion at 2,050 hours - detected.

Case 3) Case 1 plus 5 percent more corrosion at 3,850 hours undetected.

Case 4) Case 1 plus 5 percent more corrosion at 3,850 hours detected.

Case 5) Case 2 plus 5 percent more corrosion at 3,850 hours undetected.

Case 6) Case 2 plus 5 percent more corrosion at 3,850 hours detected.

The scenarios are also presented in the schematic of Figure 90, which more clearly displays the combinations.
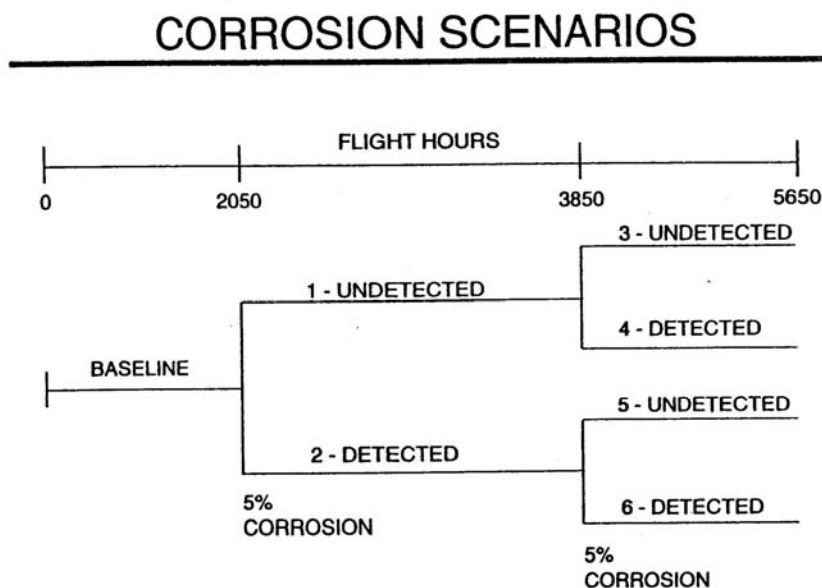
Figure 90. Schematic of Corrosion Thinning Scenarios

When the corrosion is detected, it is repaired by returning the detail to the as manufactured quality but reduced in thickness to the corrosion level. Thus, the structure with repaired corrosion damage is essentially a new structure but with increased operating stresses.

Although not included in this study, an upper bound could be calculated for the continuously increasing corrosion damage by also running the analysis for the reduced thickness conditions

76

for previous usage intervals. For example, using the 5-percent reduced thickness stress spectrum for the initial conditions would be an upper bound for the corrosion damage that could be evolving between 0 and 2,050 hours. Such bounds can almost be inferred from the fracture probabilities presented for the above six cases.

The pitting scenario was defined in terms of corrosion equivalent crack sizes. Because of the sensitivity of the fracture probabilities to the crack size distribution and the indefinite nature of this distribution for the application of this study, it is not sensible to directly compare the fracture probabilities from the assumed initial crack size distribution and the assumed distribution properties of the corrosion equivalent crack sizes. Therefore, the pitting scenario was evaluated by a subjective comparison of projected crack size distributions to a reasonable crack size distribution inferred from a documented range of equivalent corrosion crack sizes.

5.3.1.3 PROF Results for Thinning

<u>Case 1</u> Figure 91 compares the fracture probabilities for the scenario in which 5 percent corrosion is introduced and not detected at 2,050 hours. As the large equivalent initial cracks mature into real cracks, the ratio of the fracture probabilities range between one and two orders of magnitude and the gap between the two is increasing. The reduced thickness structure has not reached the equilibrium that is typical of PROF risk analyses. This case may not be realistic as corrosion damage was assumed to be present but not increased over the period of 13 years represented in the 3,600 flight hours.
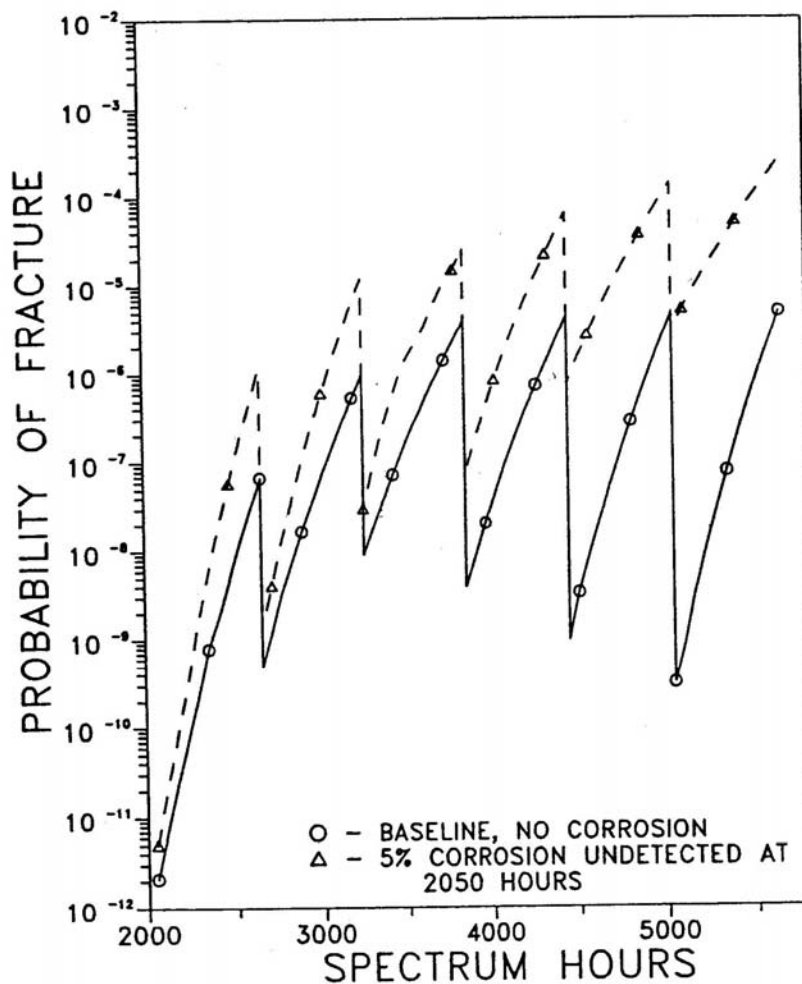
Figure 91. Fracture Risks for Baseline Conditions and 5 Percent Corrosion Undetected at 2,050 Hours

Because the crack growth life curve for the 5-percent reduced thickness structure led to inspection intervals of 485 hours (Figure 88), the risk analysis was performed with this reduced inspection interval. These results are shown in Figure 92 for the complete time history of probability of fracture. To reduce the clutter of Figure 92, only the maximum POF in each usage interval is plotted in Figure 93. With the reduced inspection intervals, the fracture probabilities are essentially equivalent to those of the baseline (uncorroded) structure. That is, the analysis indicates that shortening the intervals between inspections would provide equivalent safety. However, since corrosion was not detected at this location, some other criterion would be needed to trigger the reduced inspection intervals.

78
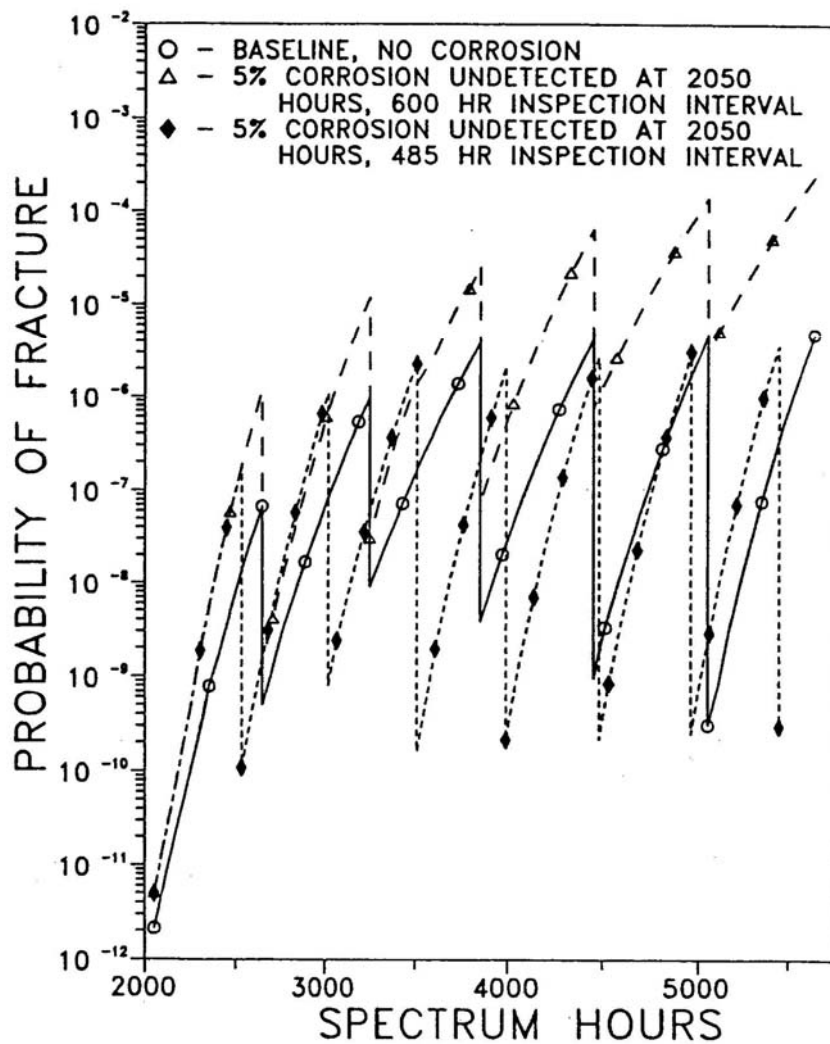
Figure 92. Fracture Risks for Baseline Conditions and 5 Percent Corrosion Undetected at 2,050 Hours - Two Inspection Intervals
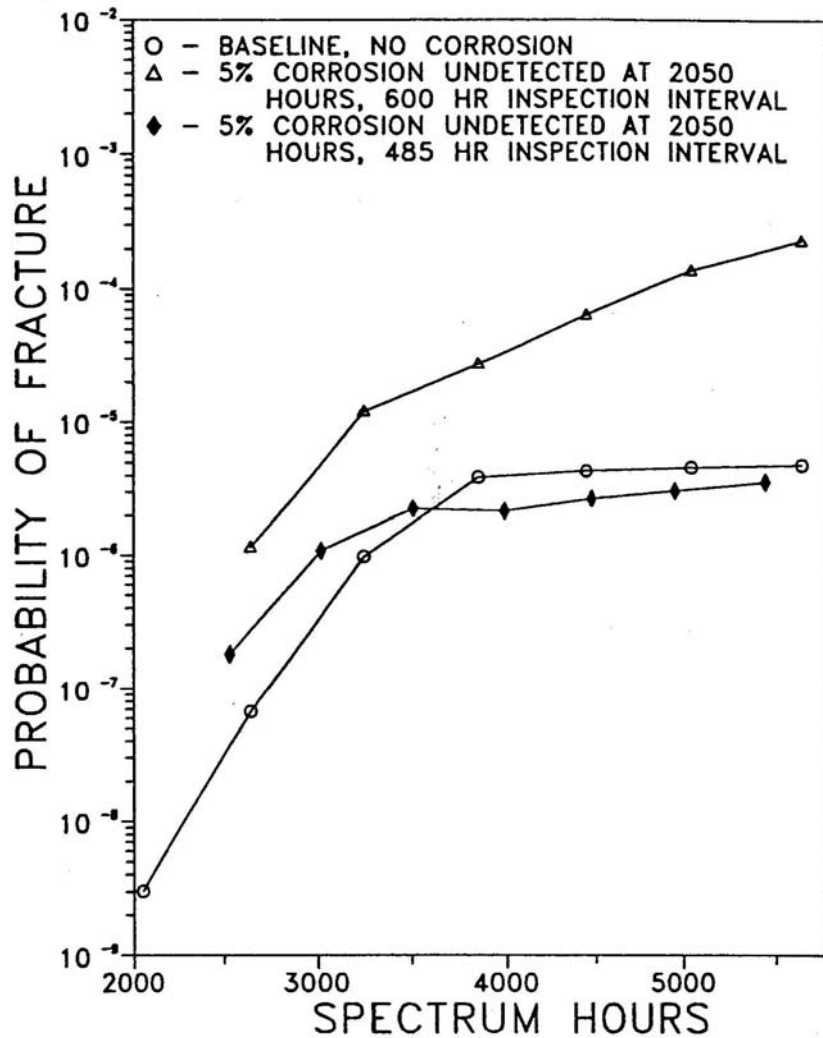
Figure 93. Maximum Fracture Risks per Interval, Baseline Conditions and 5 Percent Corrosion Undetected at 2,050 Hours - Two Inspection Intervals

Case 2 In Case 2, Figure 94, it is assumed that the corrosion is detected and repaired, returning the structure to an essentially pristine, albeit thinner, condition. Initially, the fracture probabilities are orders of magnitude smaller for the repaired structure, but, because of the higher stress levels in the repaired structure, the failure risks eventually exceed those of the baseline, uncorroded structure.
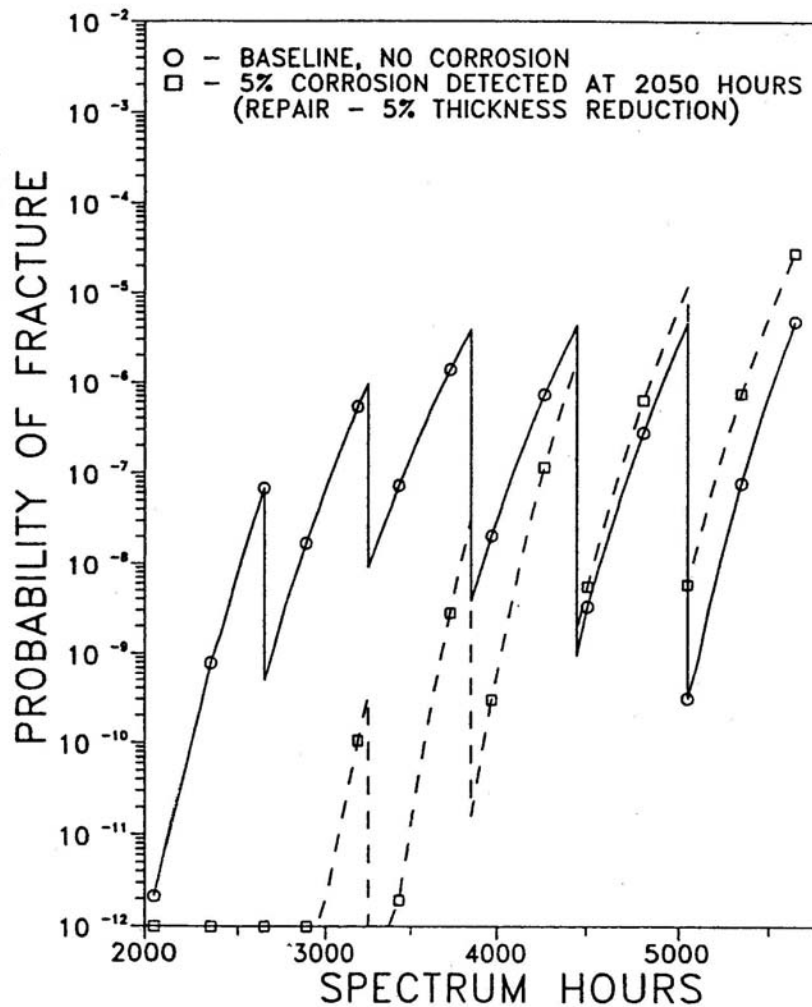
Figure 94. Fracture Risks for Baseline Conditions and 5 Percent Corrosion Detected at 2,050 Hours

Case 3 When the second round of corrosion thinning is introduced at 3,850 hours (1,800 hours after the first) and is not detected, the POF increases by at least another factor of 5 in the next 1,800 hours (Figure 95). Under this severe scenario, the risk to the corroded structure at the end of the analysis is about 500 times greater than that of the uncorroded, baseline structure. Using the 400-hour inspection intervals, as calculated from the crack growth life curve for the 90 percent structure, again greatly reduces the risks of fracture but not to the same extent as was apparent in the analysis of the 5-percent corrosion (Figures 96 and 97).

81
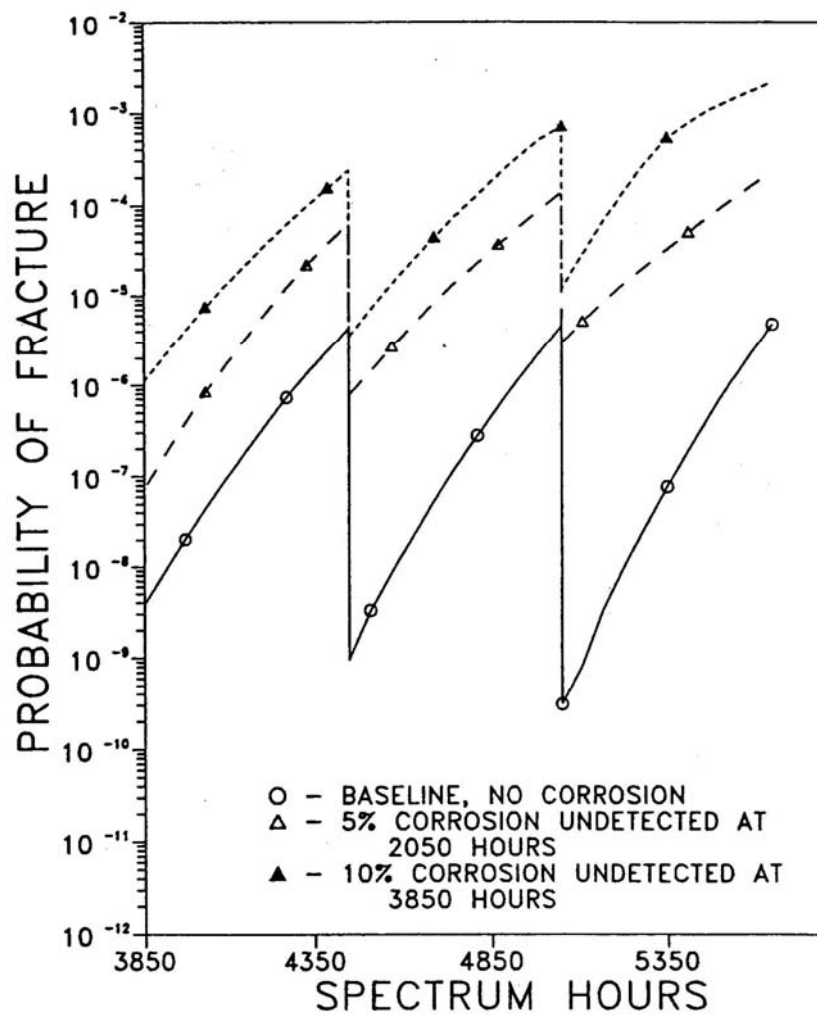
Figure 95. Fracture Risks for Baseline Conditions, 5 Percent Corrosion Undetected at 2,050 Hours, and 5 Percent More Corrosion Undetected at 3,850 Hours

82
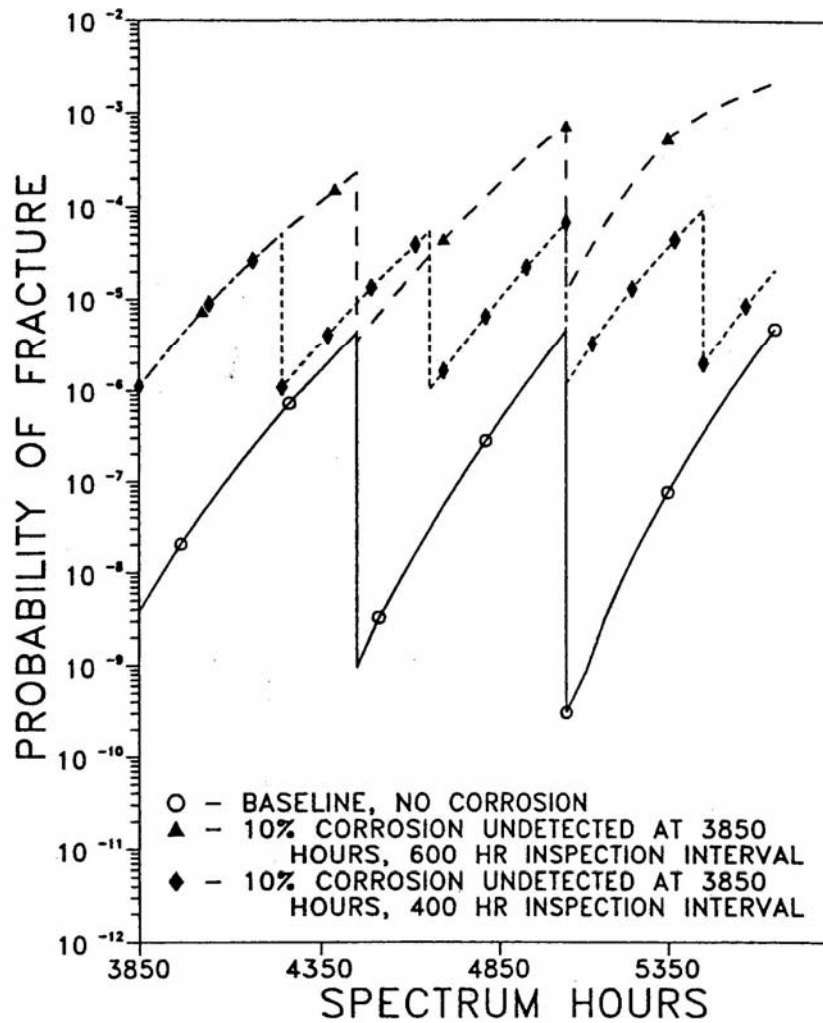
Figure 96. Fracture Risks for Baseline Conditions, 5 Percent Corrosion Undetected at 2,050 Hours, and 5 Percent More Corrosion Undetected at 3,850 Hours - Two Inspection Intervals
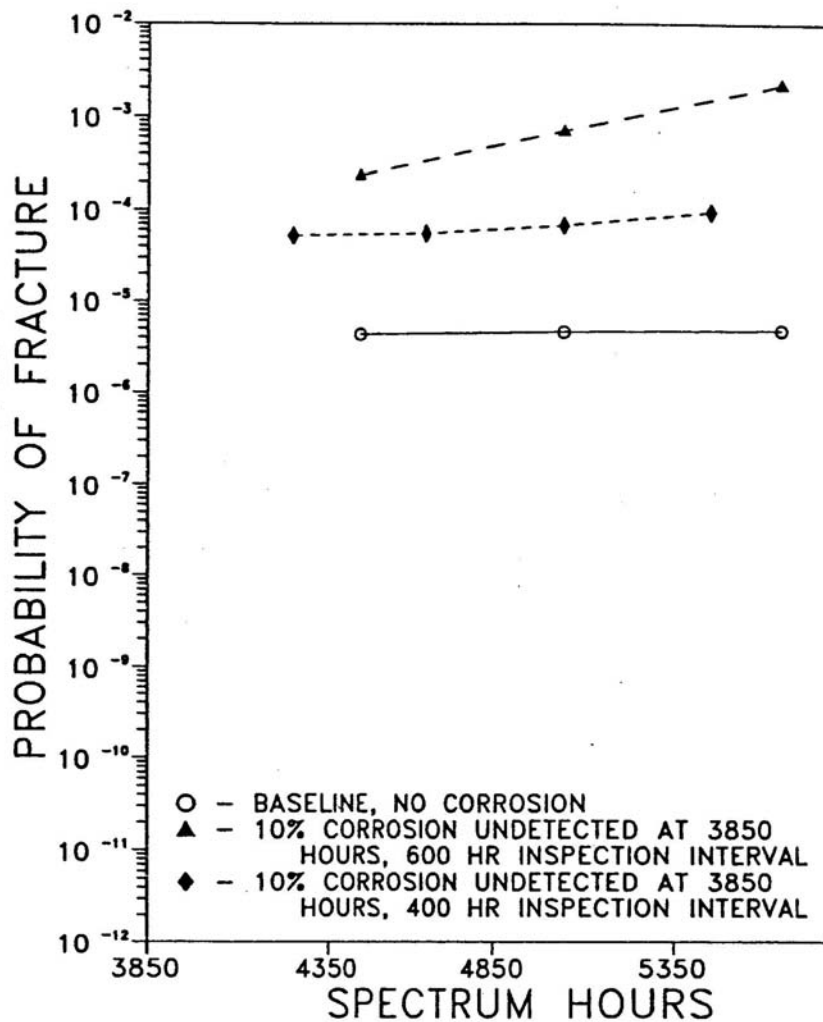
Figure 97. Maximum Fracture Risks Per Interval, 5 Percent Corrosion Undetected at 2,050 Hours, and 5 Percent More Corrosion Undetected at 3,850 Hours - Two Inspection Intervals

Case 4 If the 10-percent corrosion damage is detected for the first time at 3,850 hours, the structure was again assumed to be returned to its pristine state. Now, however, the stress level are 10 percent greater, the equivalent initial cracks grow faster, and the corresponding fracture probabilities become equivalent to those of the baseline structure (Figure 98). Had the analysis continued beyond 5,650 hours, the risks associated with the ten percent thinned structure would have exceeded those of the baseline. It might be noted that a 10-percent thickness reduction is typically permitted in the repair of corrosion and at this level the differences in fracture probabilities might become unacceptable in aging aircraft fleets.
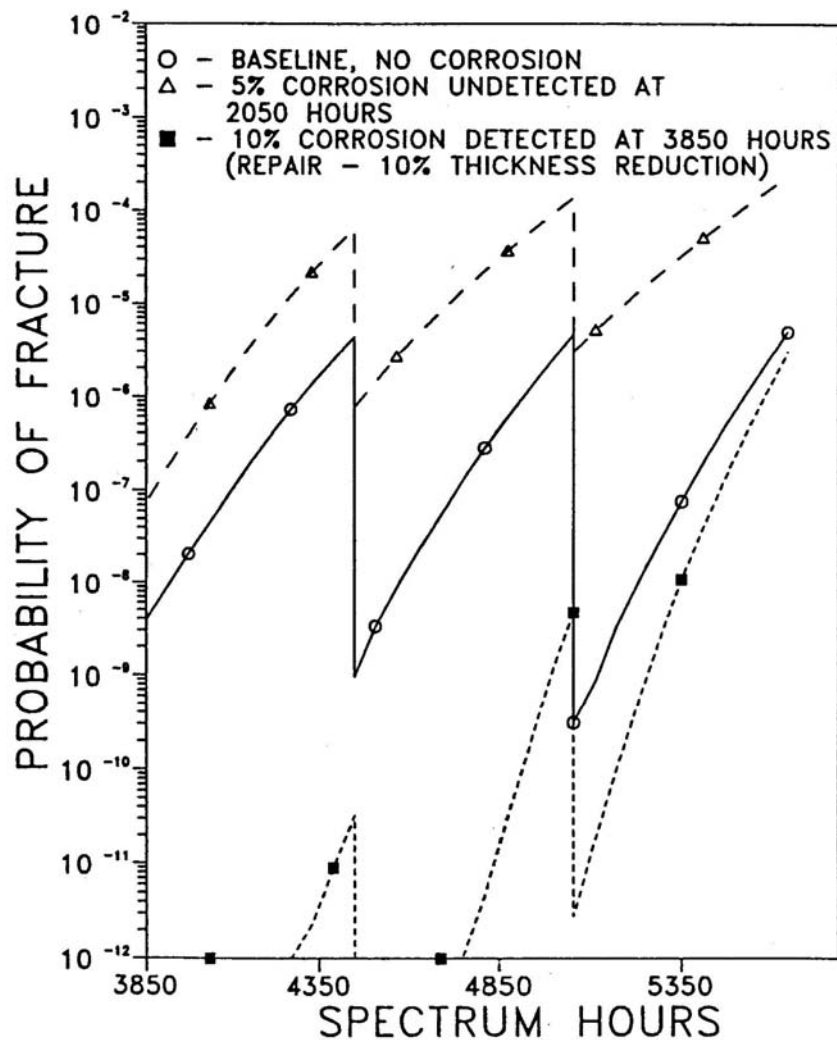
Figure 98. Fracture Risks for Baseline Conditions, 5 Percent Corrosion Undetected at 2,050 Hours, and 10 Percent Corrosion Detected at 3,850 Hours

Case 5 Figure 99 presents the fracture probabilities for the scenario in which the 5-percent corrosion at 2,050 hours is detected and repaired, but the 5-percent additional corrosion reduction at 3,850 hours is not detected. These results are entirely consistent with those that have been observed earlier. The structure was renewed at 2,050 hours and the fracture probability at 3,850 hours is still less than that of the baseline. However, because of the increased stress levels, the risks associated with the thinned material rapidly surpass those of the baseline structure.
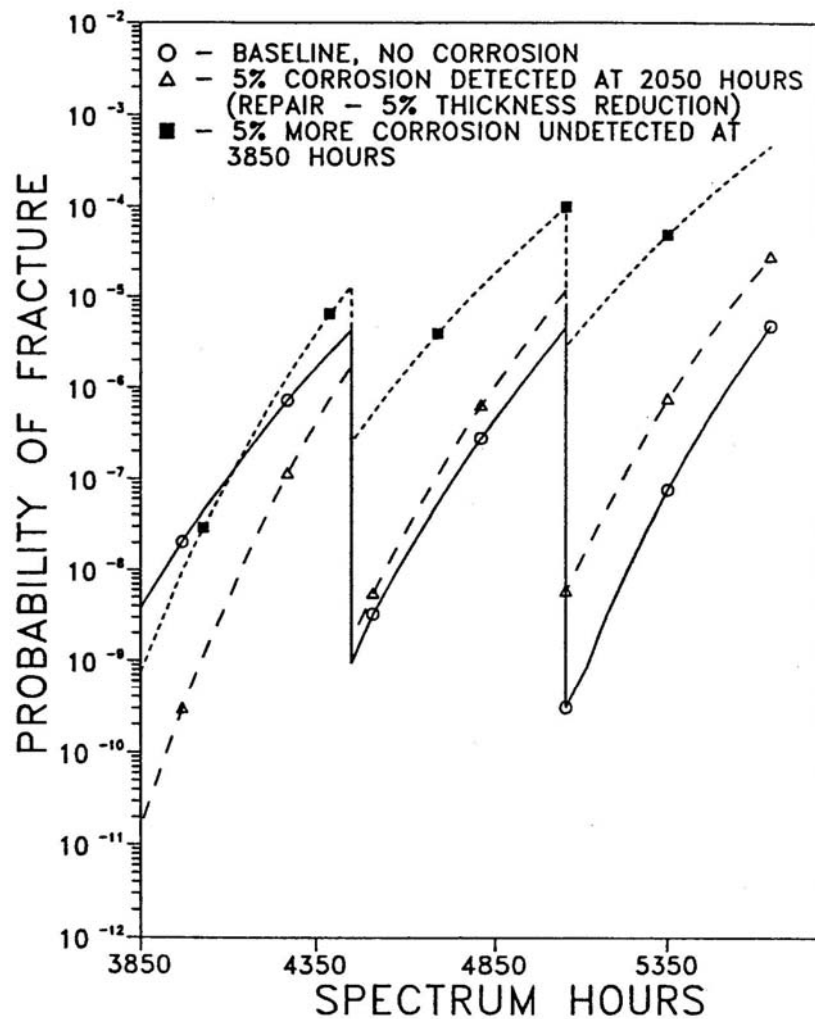
Figure 99. Fracture Risks for Baseline Conditions, 5 Percent Corrosion Detected at 2,050 Hours, and 5 Percent More Corrosion Undetected at 3,850 Hours

Case 6 The final case considered is that for which both episodes of corrosion thickness reductions were detected and repaired. The risks for this scenario, shown in Figure 100, are the smallest over the range of the analysis but would be expected to exceed those of the baseline over an extended analysis period.

86
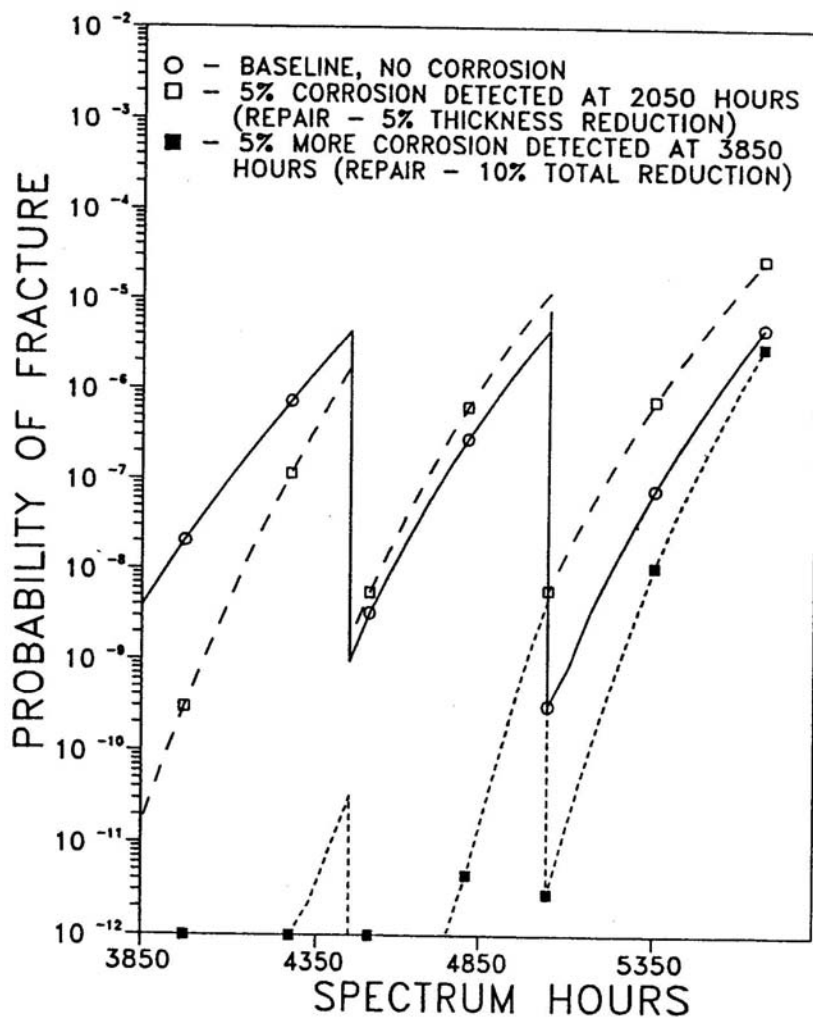
Figure 100. Fracture Risks for Baseline Conditions, 5 Percent Corrosion Detected at 2,050 Hours, and 5 Percent More Corrosion Detected at 3,850 Hours

5.3.1.4 Pitting Results

Reference 30 states that

> "Penetration of corrosive attack found in moderate to severely corroded metallic aircraft structures is comparable to, and often exceeds, the dimensions of fatigue life-limiting microfeatures commonly associated with failure in pristine element tests, typically 0.5 to 20 mils (12.7 to 508 μm) in the latter."

Interpreting these crack sizes as corrosion equivalent crack sizes provides a basis for a first order approximation to the effect of pitting damage in fracture mechanics terms. Since the corrosion equivalent crack size can be assumed to be the "weakest link" penetration depth, the equivalent

87

sizes are considered to be representative of the largest of the corrosion pits in the region. On this basis, it is reasonable to assume that the distribution of the equivalent corrosion cracks would be modeled by the Gumbel family of largest extreme values. This distribution is an asymptotic model for the extremes of the maximum of a large random sample from a broad family of continuous distributions.

The functional form of the Gumbel distribution is given in Equation (5.1) and has two parameters. Assuming that the corrosion equivalent crack sizes of 0.5 and 20 mils (12.7 and 508 μm) are low and high percentiles of the distribution of corrosion equivalent crack sizes for the detail, the parameters A and B can be easily calculated. In particular, it was assumed that the 5th percentile was 0.5 mil (12.7 μm) and the 95th percentile was 20 mils (508 μm), from which A=4.79 mils (121.7 μm) and B=5.76 mils (147 μm). The assignment of the percentiles is somewhat arbitrary but realistic considering the general statement defining the range of "observed" equivalent corrosion cracks.

Figure 86 shows a plot comparing the exceedance probabilities from the corrosion equivalent crack size distribution to distributions calculated by PROF immediately prior to inspections at 850, 1,450, and 2,050 hours. The PROF calculated distributions were obtained from the A-7D Weibull distribution of equivalent initial cracks sizes. Since POF is dominated by the large cracks, it is apparent from this figure that larger fracture probabilities will be obtained from the growing equivalent initial cracks than from the corrosive pitting. It was originally planned to define corrosion scenarios by imposing the corrosion equivalent crack sizes. Since this actually reduced the fracture probabilities even in the early life of the structure, this pitting scenario was abandoned. Note, however, that equivalent corrosion cracks are much more prevalent in the below-30-mils (762 μm) region and these could grow to be a durability problem, if not a fracture risk problem. Again, it must be emphasized that these distributions are only reasonable guesses of the actual situation and that the fracture probability is dominated by the extreme tail of these guesses.

88
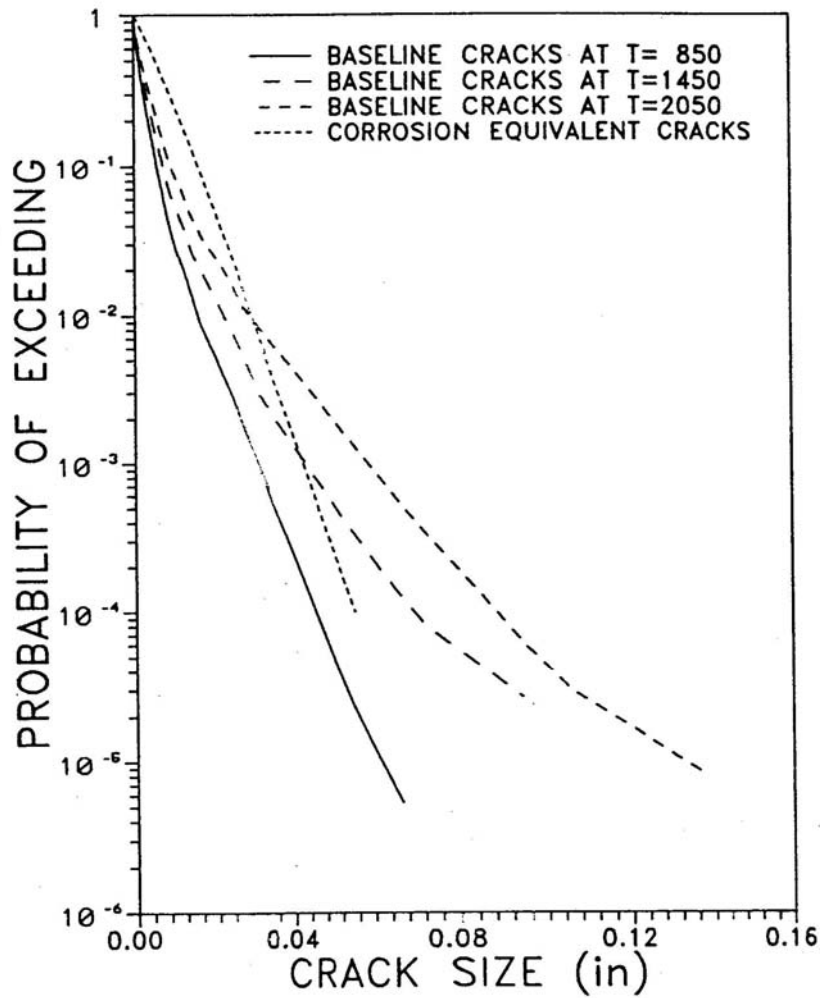
Figure 101. Comparison of Corrosion Equivalent Crack Size Distribution with Distributions of Growing Equivalent Initial Crack Size Distributions

6. DISCUSSION AND SUMMARY

The results of the research presented in this report indicate that preexisting corrosion can have a significant detrimental effect on the fatigue cracking behavior of aircraft aluminum alloys, depending on alloy composition, heat treatment, and grain orientation. To assess the effects of the different types and degrees of preexisting corrosion, and above-mentioned material parameters on the corrosion-fatigue interaction process, the three different phases that determine the fatigue life, namely corrosion, fatigue crack initiation, and fatigue crack propagation, were investigated in detail. The following sections will discuss the effects of each phase on the structural integrity of aluminum alloy aircraft components.

6.1 Corrosion

It is well known that the mode and severity of corrosion strongly depends on a combination of several factors, including alloy type, heat treatment, and grain orientation. In the present work, two widely used precipitation hardening alloys, namely 2024-T3 and 7075-T6, were exposed to various standard corrosive environments, which were designed to induce pitting and exfoliation corrosion.

Pitting corrosion is a form of localized surface corrosion. Aluminum owes its excellent resistance to general or uniform corrosion to a barrier oxide film that strongly adheres to the alloy substrate. However, in the presence of certain corrosive environments, particularly those containing chloride ions, the protective oxide film is broken down. Once a pit forms, oxygen inside the pit is depleted, the pH decreases, and the chloride ion concentration increases, resulting in a highly aggressive local environment, which does not allow the protective film to reform and thus, promotes pit growth independent of the composition of the outside or bulk environment. In pure aluminum, the pitting process is truly random process, depending primarily on point defects in the oxide film. Macdonald and Urquidi-Macdonald[46] have proposed a point defect mechanism for pitting and developed a pit initiation model based on the random occurrence of point defects.

In the case of aluminum alloys which are particularly susceptible to pitting corrosion, such as alloy 2024-T3, pitting corrosion is linked to the presence of constituent particles which are abundant in the alloy.[4,5] Wei and Coworkers[5] demonstrated that both Al-Cu-Mg containing particles (anodic with respect to the base alloy), and Al-Cu-Mn-Fe containing particles (cathodic with respect to the base alloy) act as nucleation sites for pitting. It was observed in the present study, that pits which formed on the surface of the 2024-T3 aluminum alloy, grow into the alloy for a limited depth, after which they start to grow laterally. Eventually, the pits coalesce, and form a shallow wide pit, at the bottom of which new pits nucleate at the freshly exposed constituent particles. This pitting process results in the characteristic scalloped appearance of pitted aluminum alloy 2024-T3. In Section 4.1.2.1, a method was described to characterize the random nature and typical morphology of pitting in this alloy.

The effect of pitting corrosion can be detrimental to the structural integrity of an aircraft component, by creating overall material loss, as well as stress concentrations. Both of these may have a significant effect on the residual strength of a critical component. The effect of corrosion on the residual strength of components was not addressed in the present work.

Although aluminum alloy 7075-T6 also contains constituent particles and is susceptible to pitting corrosion, the alloy is particularly susceptible to intergranular corrosion, and depending on the grain size and grain orientation, to exfoliation corrosion. The susceptibility of this alloy to intergranular attack is strongly dependent on the heat treatment process. When the alloy is heat treated to achieve peak strength or hardness, small coherent precipitates are homogeneously distributed throughout the grains. It is the presence of these small particles that provide the strength of the alloy. However, at the grain boundaries, larger particles form depleting the area adjacent to the grain boundary of the small precipitates, creating the precipitate free zone (PFZ). In the presence of a corrosive environment, and particularly when grain boundaries are exposed to that environment, galvanic cells are set up between the large grain boundary precipitates and the PFZ. In the 2000-series and the copper-bearing 7000-series alloys, the anodic side is a narrow band on either side of the grain boundary depleted of copper, while in the copper-free 7000-series alloys, the anodic sites are considered to be zinc- and magnesium-bearing precipitates on the grain boundary.

Because intergranular corrosion can occur in susceptible aluminum alloys without significant weight lossa and is generally involved in SCC of these alloys, it is often presumed to be more deleterious than general or pitting corrosion. In wrought and forged material, the grain morphology lends itself to a severe form of intergranular corrosion, namely exfoliation corrosion, where corrosion products that form on the elongated grain boundaries lift the grains. When end grains are exposed, such as in the case of fastener holes, exfoliation corrosion can grow several hole diameters before it can be detected by presently available nondestructive inspection (NDI) techniques. Since exfoliation corrosion is localized at the grain boundaries, the severity of attack can be readily characterized as the depth of penetration. For example, the extent of exfoliation corrosion of a test panel with the surface grains exposed to the EXCO solution can be plotted as a function of exposure time, and propagation rates can then be determined (see Figures 19 and 20).

Like pitting corrosion, intergranular and exfoliation corrosion can have a detrimental effect on the residual strength of aircraft structures by reducing the load-bearing cross-sectional area of a component or by creating stress concentrations. By reducing the residual strength, the structural integrity of the components can be jeopardized. No work has been performed under this program to evaluate the effect of exfoliation corrosion on the residual strength of aircraft components.

6.2 Fatigue Crack Initiation

The results of this work have demonstrated that preexisting corrosion, pitting and exfoliation corrosion, has a detrimental effect on the fatigue crack initiation in both 2024-T3 and 7075-T6 aluminum alloys. The corrosion was allowed to occur inside a semicircular hole, where the end

grains were exposed. This configuration was selected to provide a reasonable simulation of corrosion inside a fastener hole. It was found that even the smallest pits (≤ 10 µm) significantly decreased the time to fatigue crack initiation and the fatigue life of the test specimen. Fractography of both alloys indicated that when corrosion was allowed to grow beyond the small pits, the grain boundaries were attacked, which resulted in sharp penetrations in the fastener hole. In the case of exposure to the EXCO solution, corrosion was more severe, but appeared to be more general in nature.

The fractography of the fracture surfaces of the precorroded and subsequently fatigued specimens all showed cleavage-like areas indicating nucleation sites for fatigue cracking. Cleavage-like fracture is typical for transgranular SCC cracking in both the longitudinal or transverse direction. Since SCC of susceptible aluminum alloys is often attributed to some hydrogen embrittlement mechanism, the presence of cleavage-like features on the fracture surface strongly suggest some contribution of hydrogen to the fatigue crack initiation process. It is reasonable to assume that corrosion in the hole also provides a stress concentration, which promotes fatigue crack initiation. However, the amount each contributes to the initiation process, still remains to be answered.

The results of the fatigue crack initiation and short crack growth experiments on alloy 7075-T6 indicated a much greater sensitivity of the initiation process and initial fatigue crack growth to precorrosion than was found in the case of alloy 2024-T3. The fractography of fatigue cracked alloy 7075-T6, precorroded in the EXCO solution, further confirmed that hydrogen could play a significant role in the fatigue crack initiation process. In addition to the cleavage-like features, which were also seen on the alloy 2024-T3 fracture surfaces, secondary cracks perpendicular to the main fracture surface and extending far away from the corroded edge, were observed. The secondary cracks were identified as stress-corrosion cracks, which provided further evidence that hydrogen was present in the alloy lattice, and could have contributed to the fatigue cracking process. It is reasonable to assume that, as in the case of alloy 2024-T3, both the presence of hydrogen and the stress concentration created by corrosion contribute to the initiation process. Although there is some indication that the hydrogen contribution is greater for alloy 7075-T6 than for 2024-T3, the importance of the hydrogen effect with respect to the stress concentration effect remains unanswered.

6.3 Fatigue Crack Propagation

Fractography of the precorroded and fatigued modified CT specimens of both alloys 2024-T3 and 7075-T6 showed features which are characteristic of environmentally enhanced cracking such as so-called "mud" cracking and some intergranular cracking features.

6.4 Mechanisms of Interaction

As indicated in the previous sections, the mechanism of interaction between precorrosion and fatigue cracking may be a mixture of mechanical and hydrogen induced effects. In the case of alloy 2024-T3, it appears that the mechanical effects play a dominant role, although a possible

effect of hydrogen should not be ruled out. Doerfler et al.[41] and Bucci et al.[47] proposed to quantify corrosion by assigning a mechanical equivalent to corrosion damage, such that fracture mechanics can be applied to estimate fatigue crack initiation and crack growth rates. The proposed approach assumes that corrosion can be approximated by a geometric structural change consisting of a general reduction in thickness and a localized stress concentration.

The approach of assigning mechanical equivalents to corrosion damage is an acceptable initial approach to dealing with the effect of precorrosion on fatigue cracking. However, there are some issues that need to be addressed before proceeding with this particular approach. The present research has demonstrated that the application of a simple mechanical equivalency model may not be sufficient to adequately represent the effects of precorrosion on fatigue cracking. For example, the present work has shown that fatigue cracks do not necessarily nucleate from the tip of a corrosion pit or an exfoliated area. In fact, it was observed that constituent particles on the sidewalls of pits or exfoliated grains often act as preferential sites for crack nucleation.

This more complex geometry may be incorporated into a fracture mechanics model. However, there is evidence, although not yet conclusive, that hydrogen generated by the corrosion process, enters the alloy lattice and contributes to the fatigue crack initiation and propagation process.

If hydrogen indeed plays a detrimental role in the fatigue cracking behavior of precorroded aluminum alloys, particularly alloy 7075-T6, an understanding of the mechanism of corrosion-fatigue cracking interaction is needed. During the corrosion process, cathodically generated hydrogen adsorbs onto the alloy surface, and because of the high partial hydrogen pressure or fugacity, a driving force exists for hydrogen atoms to diffuse into the aluminum alloy lattice. Once the hydrogen atoms have diffused into the lattice, they can be trapped by inclusions such as Al-Zn precipitates at the grain boundaries or at stationary dislocations. When a fatigue crack propagates, the stationary dislocations near the crack tip become mobile, and move along with the propagating fatigue crack, stripping hydrogen atoms from the traps and transporting them in a solute atmosphere. Tien and coworkers[48] estimated the velocity of a dislocation transporting a hydrogen cloud to be: $\bar{V} = MF$, where M is the mobility of the hydrogen cloud and F is the driving force for dislocation motion.

This equation can further be developed to express the critical velocity of the dislocation above which the dislocation leaves the hydrogen cloud:

$$\bar{V}_C = \frac{D_H}{kT} \frac{E_B}{30b}, \tag{8}$$

where D_H is the coefficient for hydrogen diffusion , E_B is the binding energy, and b is the Burgers vector.

When comparing the time derivative of the critical velocity, or maximum diffusion distance:

$$\bar{X}_C = \frac{D_h}{kT} \frac{E_B}{30b} t_D, \tag{9}$$

93

with the diffusion distance resulting from random walk diffusion:

$$\overline{X}_D = 4\sqrt{D_h t_D} \ . \tag{10}$$

The equations suggest that moving dislocations may effectively transport hydrogen over a much larger distance than diffusion by random walk diffusion.

When the dislocations move at velocities less than X_C, the hydrogen atoms will move along with the dislocations. The aluminum alloy can be locally enriched with hydrogen when the dislocations lose their hydrogen cloud. This can occur, for example, when the dislocations speed up and exceed the critical velocity, or when the dislocations are annihilated or reach stationary sinks. Dislocation annihilation can occur within the lattice or at the grain boundaries or interfaces. In this manner, high concentrations of hydrogen can build up in the region ahead of a propagating fatigue crack, causing the crack to accelerate by a hydrogen mechanism. The effect of hydrogen should be the greatest at the crack tip where the local hydrogen concentration is increased by the effect of stress on the chemical potential of the hydrogen in solid solution.

Although evidence suggests that hydrogen contributes to the fatigue cracking process in aluminum alloys, the specific role of hydrogen in the fracture process can be subject to debate. In the literature, various hydrogen-based mechanisms for environmentally enhanced crack have been suggested, the three most viable mechanisms being the stress-induced hydride formation and cleavage, hydrogen-enhanced localized plasticity (HELP), and hydrogen-induced decohesion. The first of these mechanisms has definitely been established in metals which form stable or stress-induced hydrides such as titanium and zirconium. In the case that hydrides do not form, the second mechanism has shown to be operative in many systems including aluminum.[49-50] Thompson and Bernstein[51] demonstrated that for medium- and high-strength steels, hydrogen can degrade properties under conditions in which cracking proceeds by all microstructural modes, including quasi-cleavage, transgranular cleavage, brittle intergranular fracture, ductile tearing, and ductile rupture by microvoid coalescence. They stated that hydrogen tends to degrade the properties without changing the microstructure mode of fracture.

The results presented in this report on the interaction between preexisting corrosion and fatigue cracking in 2000-series, and more so in 7000-series aluminum alloys, are consistent with a hydrogen-induced failure mechanism. Although no detailed work was performed to investigate the specific mechanism of the hydrogen-induced failure in these alloys, the fractographic and metallographic results presented in this report showed a mix of transgranular and intergranular fracture modes that are consistent with hydrogen-assisted fracture.

6.5 Implementation

The results presented in this report indicate that the effect of preexisting corrosion on fatigue crack initiation and propagation may be a mixture of the formation of equivalent mechanical flaws and hydrogen-induced fracture. Although it is beyond the scope of the present program to determine the exact mechanism of corrosion-fatigue interaction, an initial approach to quantify

the effect of precorrosion can be made. It is proposed, as an initial approach, to consider precorrosion as equivalent mechanical damage such that linear elastic fracture mechanics (LEFM) can be applied to assess the structural damage introduced by corrosion.

If this approach is taken, the interaction between preexisting corrosion and fatigue cracking can also be evaluated in terms of POF. In Section 5.3.1, the interaction between the thinning effects of corrosion and fatigue cracking on the structural integrity of a representative airframe structure were evaluated in terms of single-flight probabilities of fracture as a function of flight hours. The first order methodology assumed that the effect of preexisting corrosion could be modeled by reduced structural thickness. Six simple corrosion damage scenarios were defined by introducing 5 percent increments of corrosion thickness loss at two times in the aircraft's history. Time histories of the POF were calculated using the PROF risk analysis computer code. The fracture risks from the corrosion scenarios were compared with those from a baseline condition which was the driver for the planning of the safety inspections for the critical location. Pitting due to corrosion was subjectively evaluated by comparing a distribution of corrosion equivalent crack sizes to the growing population of equivalent initial crack sizes.

In all but two of the thinning corrosion scenarios, the fracture risks associated with the reduced structural thickness exceeded those of the baseline condition by at least an order of magnitude. In the remaining two scenarios, the structure had been "renewed" at the second corrosion insertion, and was operating at stress levels that were 10 percent greater than the baseline. Although the fracture probabilities were less than those of the baseline at the end of the analysis, it was apparent that these scenarios would produce high risks in comparison with the baseline condition.

The equivalent corrosion crack size (pitting) distribution had significantly more cracks in the mid-and-small crack size ranges, but not in the large-crack size range, which dominates the fracture probability calculation. Consequently, introducing the corrosion equivalent crack sizes, as opposed to the growing initial cracks, would have had a beneficial effect on the fracture probability. Moreover, fractographic and metallographic analysis of the corroded areas have demonstrated the complex morphology of corrosion, which has not been addressed in the present analysis. Thus, a more realistic method for introducing the effects of corrosion, pitting as well as intergranular corrosion, will be needed.

In addition to the geometric effects of corrosion on the fatigue cracking behavior of aluminum alloys, the effect on the physical properties, particularly as a result of hydrogen entry into the lattice, needs to be taken into account, and further development work needs to be conducted to determine more accurately the contribution of hydrogen to the reduction in fatigue strength in each specific aluminum alloy.

The results of the preliminary probabilistic study support the results of the laboratory studies that preexisting corrosion decreases the fatigue life of aluminum alloy. The results of the probabilistic study further indicate that, when inspection intervals are set by damage tolerance analysis of cracks in a pristine structure, the effects of corrosion may be a safety issue, as well as

a durability issue. It was finally found that shortening inspection intervals could significantly lower the fracture risks.

7. CONCLUSIONS AND RECOMMENDATIONS

Based on the results and the discussion of the results, the following conclusions can be drawn:

1. Preexisting corrosion has a detrimental effect on the fatigue life of aluminum alloys 2024-T3 and 7075-T6. The results of the laboratory studies indicated that the effects depend on alloy composition and grain (boundary) orientation. The effect of pitting and intergranular corrosion is most pronounced in the initiation stage of cracking.

2. The corrosion morphology has a significant effect on the fatigue crack initiation in both alloys. Fatigue crack nucleation sites appear to be associated with constituent particles, which can act as stress concentrations or as trapping sites for hydrogen, generated during the corrosion process.

3. It was proposed that an initial approach needs to be taken to assign equivalent mechanical damage to the corrosion damage resulting from preexposure to corrosive environments. Based on the assumption that corrosion damage can be treated as a combination of thickness reduction and local stress concentration, fracture mechanics principles can be applied.

4. The interaction between thinning effects and pitting and fatigue cracking on the structural integrity of a representative airframe structure were evaluated in terms of single flight probabilities of fracture as a function of flight hours. The results of this preliminary study indicate that, when the inspection intervals are set by damage tolerance analysis of fatigue cracks in a pristine structure, the effects of corrosion may be a safety issue as well as a durability issue.

Based on the conclusions drawn from the results and analyses of the laboratory work, and the probabilistic analyses of the effect of corrosion on a representative airframe structure, the following recommendations are made.

1. It is recommended that, as an initial approach, the corrosion damage is quantified as simple, mechanical equivalent damage. This would be a first meaningful attempt to deal with the detrimental effects of preexisting corrosion on the structural integrity and durability of aircraft components.

2. In addition to the initial step (Item 1 above), it is recommended that more realistic corrosion geometries be characterized and that the effects of these complex geometries be incorporated into the geometric approach described above.

3. The possible role of hydrogen generated by the corrosion process, on the fatigue behavior of the aluminum alloys is not well understood, and it is recommended that at a minimum the hydrogen factor is taken into account by applying some safety factor. However, work needs to be conducted to develop a better understanding of the role of hydrogen, so that the effects of corrosion on structural integrity and durability of airframe components are better

97

understood and a more reliable assessment of the safety and life of corroded structures can be developed.

8. REFERENCES

1. W. R. Hendricks, "The Aloha Airlines Accident - A New Era For Aging Aircraft," Proceedings of Conference on <u>Structural Integrity of Aging Airplanes</u>, 1991 Eds., S. N. Atluri, S. G. Sampath, P. Tong, 1990, Atlanta, GA, p. 153.

2. E. H. Hollingsworth and H. Y. Hunsicker, "Corrosion Of Aluminum And Aluminum Alloys," Metals Handbook Ninth Edition, Volume 13, <u>Corrosion</u>, ASM International, Metals Park, Ohio, 1987, pp. 583-609.

3. M. L. Bauccio, "Corrosion In The Aircraft Industry," Metals Handbook Ninth Edition, Volume 13, <u>Corrosion</u>, ASM International, Metals Park, Ohio, 1987, pp. 1019-1057.

4. R. G. Buchheit, Jr., J. P. Moran, and G. E. Stoner, "Localized Corrosion Behavior Of Alloy 2029–The Role Of Microstructural Heterogeneity," Corrosion, Volume 46, 1990, p. 610.

5. G. S. Chen, M. Gao, D. G. Harlow, and R. P. Wei, "Corrosion And Corrosion Fatigue Of Airframe Aluminum Alloys," FAA/NASA International Symposium on <u>Advanced Structural Integrity Methods For Airframe Durability and Damage Tolerance</u>, Ed. Charles E. Harris, NASA Conference Publication 3274, pp. 157-173.

6. I. L. Mueller, J. R. Galvek, Corrosion Science Volume 7, 1977, p. 179.

7. A. Turnbull, "Chemistry Within Localized Corrosion Cavities," <u>Advanced Localized Corrosion,</u> NACE-9, Ed. H. Isaacs.

8. D. W. Siitari and R. C. Alkire, "Initiation Of Crevice Corrosion 1 Experimental Investigations On Aluminum And Iron," J. Electrochem Soc. 129 (1982), p. 481.

9. R. C. Alkire and D. W. Siitari, "Initiation Of Crevice Corrosion II Mathematical Model For Aluminum In Sodium Chloride," J. Electrochem Soc 129 (1982), p. 488.

10. K. Hebert and R. C. Alkire, "Dissolved Metal Species Mechanism For Initiation Of Crevice Corrosion Of Aluminum I Experimental Investigations In Chloride Solutions," J. Electrochem Soc 130 (1983), p. 1001.

11. K. Herbert and R. C. Alkire, "Dissolved Metal Species For Initiation Of Crevice Corrosion Of ALuminum II Mathematical Model," J. Electrochem Soc 130 (1983), p. 1007.

12. R. C. Alkire, T. Tomasson, and K. Herbert, "The Critical Geometry For Initiation Of Crevice Corrosion," J. Electrochem Soc 132 (1983), p. 1027.

13. A. Alavi and R. A. Cottis, "The Determination Of pH, Potential And Chloride Concentration In Corroding Crevices On 304 Stainless Steel And 7475 Aluminum Alloy," Corrosion Science 27 (1987), p. 443.

14. B. W. Lifka and D. O. Sprowls, Corrosion 20 (1966), p. 7.

15. M. G. Reboul and J. Bouvaist, "Exfoliation Corrosion Mechanisms In The 7020 Aluminum Alloy," Werkstoffe und Korrosion, 303, 11 (1979), p. 700.

16. M. J. Robinson, "Mathematical Modeling Of Exfoliation Corrosion In High Strength Aluminum Alloys," Corrosion Science 22, 8 (1982), p. 775.

17. M. J. Robinson, "The Role Of Wedging Stresses In The Exfoliation Corrosion Of High Strength Aluminum Alloys," Corrosion Science 23, 8 (1983), p. 887.

18. C. L. Harmsworth, "Effect Of Corrosion On The Fatigue Behavior Of 2024-T4 Aluminum Alloys," Aeronautical Systems Division Technical Report 61-121, July, 1961.

19. N. L. Person, "Fatigue Properties Of Prior-Corroded Aluminum Sheet Alloys," Materials Performance, Volume 14:12, December, 1975, p. 22.

20. E. Abramovici, P. Leblance, and B. Weaver, "The Influence Of Etch Pits On The Fatigue Life Of Anodized Aluminum Alloys: Fractographic Examination," Proceedings Of Conference 8-11, July 1991, ASM International, p. 21.

21. J. P. Chubb, T. A. Morad, B. S. Hockenhull, and J. W. Bristow, "The Effect Of Exfoliation Corrosion On The Fatigue Behavior Of Structural Aluminum Alloys," Proceedings of Conference on Structural Integrity of Aging Airplanes, 1991 Eds. S. N. Atluri, S. G. Sampath, P. Tong, 1990, Atlanta, GA, p. 87.

22. S. H. Smith, T. K. Christman. F. W. Brust, and M. L. Oliver, "Accelerated Corrosion Fatigue Test Methods For Aging Aircraft," 1991 SEM Spring Conference On Experimental Mechanics, The Society for Experimental Mechanics, June 10-13, 1991, Milwaukee, WI.

23. G. H. Koch, "Effect Of Preexisting Corrosion On Fatigue Of High Strength ALuminum Alloys," Durability of Metal Aircraft Structures, Proceedings of the International Workshop on Structural Integrity of Aging Airplanes, March 31 - April 2, 1992, Atlanta, GA.

24. R. J. Bucci, H. J. Konish, M. Kulak, and D. W. Hoeppner, "An Engineering Protocol For Evaluating Implications Of Metallic Corrosion Of Airframe Damage, Life And Risk Assessment," FAA/NASA International Symposium on Advanced Structural Integrity Methods For Airframe Durability and Damage Tolerance," Hampton, VA, May, 1994.

25. T. D. Burleigh, "The Postulated Mechanisms For Stress-Corrosion Cracking Of ALuminum Alloys–A Review Of The Literature 1980-1989," Corrosion Volume 7, No. 2 (1991), p. 89.

26.   W. Gruhl and Z. Metallkunde, Volume 75, No. 11, 1984, p. 819.

27.   E. F. Smith III, R. Jacko, and D. J. Duquette, "Hydrogen Assisted Fatigue Cracking Of High Strength Aluminum Alloys," Technical Report to the Office of Naval Research, Contract No. N00014-67-A-0117-0012, No. N00014-75-C-0466, NR036-093, August, 1975, (NTIS-AD-A014477).

28.   R. J. Jacko and D. J. Duquette, "Hydrogen Embrittlement Of A Cyclically Deformat High Strength Aluminum Alloy," Metallurgical Transactions A, Volume 8A, November 1977, p. 1821.

29.   E. F. Smith and D. J. Duquette, "The Corrosion Fatigue Behavior Of A High Purity Al-Zn-Mg-Cu Alloys," Technical Report to the Office of Naval Research Project No. N00014-75-C-0466, November, 1979, (NTIS-AD-A077-461).

30.   J. G. Burns, W. P. Johnson, and A. P. Berens, "Aging Aircraft Structural Damage Analysis," Fatigue Management, AGARD Conference Proceedings 506, May, 1991.

31.   ASTM E647-91, "Standard Test Method For Measurement Of Fatigue Crack Growth Rates," American Society for Testing and Materials, 1991.

32.   ASTM B386-85 "Copper Accelerated Acetic Salt Spray (Fog) Testing," American Society for Testing and Materials, 1985.

33.   ASTM B117-90, "Standard Method Of Salt Spray (Fog) Testing," American Society for Testing and Materials, 1990.

34.   ASTM G34-90, "Standard Test Method For Exfoliation Corrosion Susceptibility In 2XXX And 7XXX Series Aluminum Alloys (EXCO Tests)," American Society for Testing and Materials, 1990.

35.   T. Ohnishi and T. Ito, "Effects Of Cathodic Hydrogen Charging On The Mechanical Properties Of An Al-Li-Cu-Mg-Zr Alloy," Transactions of the Japan Institute of Metals, Volume 29, No. 8, p. 642, 1988.

36.   ASTM E 399-90, "Standard Test Method For Plane-Strain Fracture Toughness Of Metallic Materials," American Society for Testing and Materials, 1991.

37.   "The Slow Strain Rate Techniques," Eds. G. M. Ugianski and J. H. Payer, ASTM STP 665, Philadelphia, PA, 1979.

38.   J. A. Beavers and G. H. Koch, "Limitations Of The Slow Strain Rate Test For Stress Corrosion Cracking," MTI Publication No. 39, Materials Technology Institute of the Chemical Process Industries, Inc., 1995.

39.   "Corrosion Summary," Department of the Air Force, WR-ALCRP 400--1, WR-ALC/CNC, Robins Air Force Base, GA, March 1991.

40.   C. F. Tiffany, "Some Thoughts On Corrosion Research And Current USAF/Boeing Activities," presented at Corrosion Workshop, WL/FIBE, Wright-Patterson Air Force Base, OH, July 1994.

41.   M. T. Doerfler, A. F. Grandt, Jr., R. J. Bucci, and M. Kulak, "A Fracture Mechanics Based Approach For Quantifying Corrosion Damage," presented at <u>Tri-Service Conference on Corrosion</u>, Orlando, FL, June 1994.

42.   COSMOS/M User Guide, First Edition, Version 1.71, May, 1994.

43.   D. O. Sprowls and R. H. Brown, "Resistance Of Wrought High-Strength Aluminum Alloys To Stress Corrosion," Technical Paper, Aluminum Company of America, New Kensington, PA, 1962.

44.   F. J. Giessler, and P. C. Miedlar, "OV-10A Durability And Damage Tolerance Analysis Program Summary," UDR-TR-89-24, University of Dayton Research Institute, Dayton, OH, April 1991.

45.   J. L. Rudd and T. D. Gray, "Quantification Of Fastner-Hole Quality," Journal of Aircraft, Vol. 15, No. 3, March 1978.

46.   D. D. MacDonald and M. Urquidi-MacDonald, "Corrosion Damage Function - Interface Between Corrosion Science And Engineering," Corrosion, 48 Volume 5, pp. 354, 1992.

47.   R. J. Bucci, H. J. Konish, and B. J. Shaw, "A Technical Plan To Address Aircraft Structural Problems Arising For Corrosion/Corrosion Fatigue," USAF Corrosion/Fatigue Planning Meeting, Wright Laboratory, Wright-Patterson Air Force Base, OH, February 1995.

48.   J. K. Tien, A. W. Thompson, I. M. Barnstein, and R. J. Richards, "Hydrogen Transport By Dislocations," Metallurgical Transaction A, Volume 7A, p. 28, June 1976.

49.   H. K. Birnbaum, "Mechanisms Of Hydrogen Related Fracture Of Metals," <u>Hydrogen Effects On Material Behavior</u> Ed., N. R. Moody and A. W. Thompson, The Minerals, Metals & Materials Society, 1990, p. 639.

50.   P. Sofronis and H. K. Birnbaum, "Hydrogen Enhanced Localized Plasticity: A Mechanism For Hydrogen Related Fracture," AD-Volume 36, Fatigue and Fracture of Aerospace Structural Materials, p. 15,1993.

51.   A. W. Thompson and I. W. Bernstein, <u>Advanced Corrosion Science Technology</u>, Volume 7, pp. 53-175, 1979.

LIST OF ACRONYMS AND ABBREVIATIONS

ACRONYM	DESCRIPTION
ASIP	Aircraft Structural Integrity Program
CASS	Copper Accelerated Acetic Acid Salt Spray
CFC	corrosion-fatigue cracking
COD	crack opening displacement
CT	compact tension
ECT	extended compact tension
FEM	finite element model
HELP	hydrogen-enhanced localized plasticity
L	longitudinal
LEFM	linear elastic fracture mechanics
NDI	nondestructive inspection
PC	personal computer
PFZ	precipitate free zone
POD	probability of detection
POF	probability of fracture
PROF	Probability Of Fracture
RH	relative humidity
SCC	stress-corrosion cracking
SEM	scanning electron microscope or scanning electron micrograph
ST	short transverse